

Alma Mater Studiorum – Università di Bologna

DOTTORATO DI RICERCA IN
INGEGNERIA STRUTTURALE ED IDRAULICA

Ciclo XXIII

Settore scientifico-disciplinare di afferenza: ICAR09

Fiber beam-columns models with flexure-shear interaction for nonlinear analysis of reinforced concrete structures.

Presentata da: Filippo Cardinetti

Coordinatore Dottorato

Chiar.mo Prof. Erasmo Viola

Relatore

Chiar.mo Prof. Pier Paolo Diotallevi

Correlatore

Ing. Luca Landi

Esame finale anno 2011

Abstract

The aim of this study was to develop a model capable to capture the different contributions which characterize the nonlinear behaviour of reinforced concrete structures. In particular, especially for non slender structures, the contribution to the nonlinear deformation due to bending may be not sufficient to determine the structural response. Two different models characterized by a fibre beam-column element are here proposed. These models can reproduce the flexure-shear interaction in the nonlinear range, with the purpose to improve the analysis in shear-critical structures. The first element discussed is based on flexibility formulation which is associated with the Modified Compression Field Theory as material constitutive law. The other model described in this thesis is based on a three-field variational formulation which is associated with a 3D generalized plastic-damage model as constitutive relationship.

The first model proposed in this thesis was developed trying to combine a fibre beam-column element based on the flexibility formulation with the MCFT theory as constitutive relationship. The flexibility formulation, in fact, seems to be particularly effective for analysis in the nonlinear field. Just the coupling between the fibre element to model the structure and the shear panel to model the individual fibres allows to describe the nonlinear response associated to flexure and shear, and especially their interaction in the nonlinear field. The model was implemented in an original matlab[®] computer code, for describing the response of generic structures. The simulations carried out allowed to verify the field of working of the model. Comparisons with available experimental results related to reinforced concrete shears wall were performed in order to validate the model. These results are characterized by the peculiarity of distinguishing the different contributions due to flexure and shear separately. The presented simulations were carried out, in particular, for monotonic loading. The model was tested also through numerical comparisons with

other computer programs. Finally it was applied for performing a numerical study on the influence of the nonlinear shear response for non slender reinforced concrete (RC) members.

Another approach to the problem has been studied during a period of research at the University of California Berkeley. The beam formulation follows the assumptions of the Timoshenko shear beam theory for the displacement field, and uses a three-field variational formulation in the derivation of the element response. A generalized plasticity model is implemented for structural steel and a 3D plastic-damage model is used for the simulation of concrete. The transverse normal stress is used to satisfy the transverse equilibrium equations of at each control section, this criterion is also used for the condensation of degrees of freedom from the 3D constitutive material to a beam element. In this thesis is presented the beam formulation and the constitutive relationships, different analysis and comparisons are still carrying out between the two model presented.

Table of contents

Chapter 1 - Introduction

1.1	Sommario	1
1.2	Different approaches to the nonlinear analyses of reinforced concrete structures	1
1.2.1	Macroscopic approach	1
1.2.2	Microscopic approach	2
1.2.3	Global models	3
1.2.4	Fibre Models	10
1.3	Aim and objective of the thesis	13
1.4	Outline of the thesis	14

Chapter 2 - Fibre beam-column element with flexure-shear interaction: state of the art

2.1	Sommario	16
2.2	Fibre Beam-Column Element Using Strut-and-Tie Models	17
2.2.1	Guedes's Model	17
2.2.2	Martinelli's Model	20
2.2.3	Ranzo and Petrangeli's model	23
2.3	Fibre Beam-Column Element Using Microplane Model	27
2.3.1	Petrangeli's Model	27
2.4	Fibre Beam-Column Element Using Smearred Crack Models	29

2.4.1	Vecchio and Collins's model	29
2.4.2	Bentz's Model	33
2.4.3	Remino' Model.	35
2.4.4	Bairan's Model	37
2.5	Fibre Beam-Column Element Using Damage Models.	41
2.5.1	Modello di Mazars	41

Chapter 3 - Fibre beam-column beam formulation

3.1	Sommario	44
3.2	Definition of the vectors involved	45
3.3	Formulation of the element starting from mixed method	46
3.4	Element state determination	48
3.4.1	Description of the procedure	49
3.4.2	Element state determination algorithm.	50

Chapter 4 - Constitutive Relationship: Section state determination

4.1	Sommario	55
4.2	Modified compression field theory	56
4.2.1	Introduction	56
4.2.2	Compatibility condition	56
4.2.3	Equilibrium Condition	57
4.2.4	Constitutive relationship	59
4.2.5	Transmitting loads across the cracks	60
4.3	Disturbed stress field model	63

4.3.1	General overview	64
4.3.2	Equilibrium equation	65
4.3.3	Compatibility relations	67
4.3.4	Constitutive Relations	69
4.3.5	Shear slip model	71

Chapter 5 - Implementation of the model

5.1	Sommario	74
5.2	Definition input vectors and matrices	75
5.3	Algorithm steps	77
5.3.1	Structure state determination	80
5.3.2	Element state determination	81
5.3.3	Section state determination	83
5.4	Solution strategies	89
5.5	Flow Chart	91
5.5.1	Structure state determination	91
5.5.2	Element state determination	92
5.5.3	Section state determination	93

Chapter6 - Numerical analysis and validation

6.1	Sommario	97
6.2	Comparisons between numerical and experimental results	98
6.2.1	Geometry of specimen B4 and modeling criteria	98
6.2.2	Results of the comparison	101

6.3	Numerical comparison with VecTor2	106
6.4	Investigation on the influence of flexure-shear interaction	107
6.4.1	Parametric analysis on bridge pier	107
6.4.2	Parametric analysis on a shear wall	111
6.4.3	Analysis with the ratio (slender shear wall) $L/D=10$.	111
6.4.4	Analysis with the ratio $L/D=2$.	116
6.4.5	Analysis with the ratio $L/D=1$.	118

Chapter 7 - Alternative formulation for the shear critical beam-column element (developed in University of California Berkeley)

7.1	Sommario	121
7.2	Finite element formulation	122
7.2.1	Kinematic assumptions	122
7.2.2	Hu-Washizu Functional	122
7.2.3	Force interpolation matrix	126
7.2.4	Description of the shear forces	126
7.2.5	Section deformation and stiffness matrix	127
7.3	Constitutive relationships.	128
7.3.1	Steel material model	128
7.3.2	Concrete material model	130
	Conclusion	134
	References	137

CHAPTER 1

Introduction

1.1 Sommario

In questo capitolo introduttivo verranno trattati i criteri di modellazione della risposta sismica non lineare di strutture in c.a. Si riporta sia una classificazione delle diverse tipologie di modelli, sia una descrizione degli aspetti che sono stati sviluppati e perfezionati nel corso degli ultimi decenni. Vengono poi richiamati alcuni modelli e, senza entrare nel dettaglio, se non evidenziando le caratteristiche salienti. In questo modo è possibile inquadrare meglio le proprietà e le assunzioni su cui si basano i modelli proposti.

1.2 Different approaches to nonlinear analysis of reinforced concrete structures

The study of reinforced concrete structures under strong seismic actions requires the formulation of analytical models capable of describing the behaviour of structural elements subject to cyclic loading in the non-linear fields, taking into account the typical phenomena of progressive deterioration of stiffness and strength. the following approaches can be distinguished in relation to the complexity and the model scale.

1.2.1 Macroscopic approach

Structural modeling of the is made trying to achieve a correspondence between the structural members and the elements of the analytical model. To this end, the one-dimensional elements are used to simulate the response of a beam, columns, or a wall portion between two floors. Following a macroscopic approach the effects of geometry details can be lost, such as the exact form of longitudinal and transverse reinforcement, but the main aspects of structural behavior can be reproduced quickly and the spread inelastic deformations along the element can be considered.

A typical example of the macroscopic approach are the global models. The constitutive laws for this kind of modes, are introduced in terms of section forces-section deformation such as moment-curvature relations. These approximation are sufficiently accurate to describe the aspects that characterize the cyclic loading response, defined through

hysteretic model. The reduced computational time and accurate simulation of the global hysteretic behavior, makes these models the most efficient method for the analysis of complex structures, consisting in a large number of elements.

The class of fiber models can be set in a macroscopic approach, indeed each structural element can be described by a single finite element, and the equilibrium and compatibility conditions are expressed in global terms. The sections behavior is studied through a discretization into finite areas, or, for planar elements, in strips. The constitutive relationships are locally defined, in terms of stress-strain relation for each fiber. Therefore, the fiber models are considered as intermediate between local and global formulation. At one side fiber model are based on simplified kinematic assumptions that allow to reduce the number of equations, to the other hand the global behaviour is derived from the materials constitutive laws. However fiber models requires remarkable computational effort, especially in complex structures analysis.

1.2.2 Microscopic approach

The structure is discretized with a large number of two or three-dimensional finite elements, using different elements for concrete, reinforcement and the bonds between the two materials. It's much more accurate in describing the local behavior, but requires an excessive computational time. The use of microscopic models allows, at the most, to run analysis of individual elements or portions of structures, such as walls, beam-column or nodes.

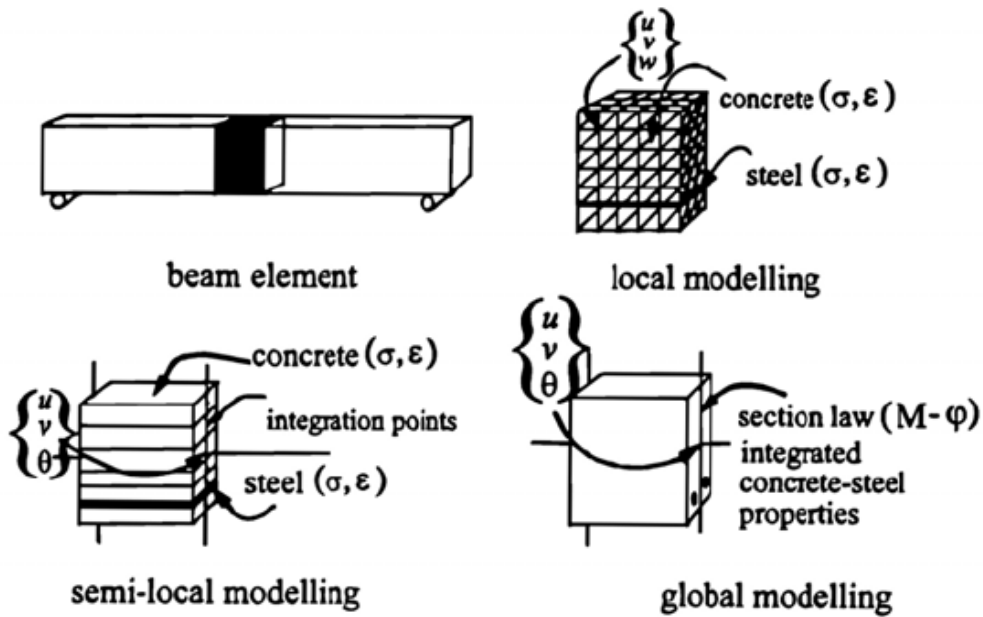


fig. 1.2-1

1.2.3 Global models

The modeling of seismic behavior of reinforced concrete structures in the last forty years' was the focus of many researchers and led to the development of multiple types of global models. Since the late 60s were proposed simple models, which over the years have been improved and expanded.

This introduction it is focused on the elements for non linear analysis of structures, in which the shear strength is enough to ensure the development of inelastic deformation. In this context, global models can be classified in relation to the inelastic deformation distribution, with this criteria may have lumped plasticity elements and distributed plasticity elements.

The nonlinear behavior of frame structures of usually concentrated in critical areas corresponding to the beams-columns ends. So one of the first approaches to modeling this behavior has been carried out assuming a zero-length plastic hinges as a rotational springs located at the ends of the beam-column elements, and connected in series or in parallel, depending on the type of connection may have series or parallel models as shown in fig. 1.2-2

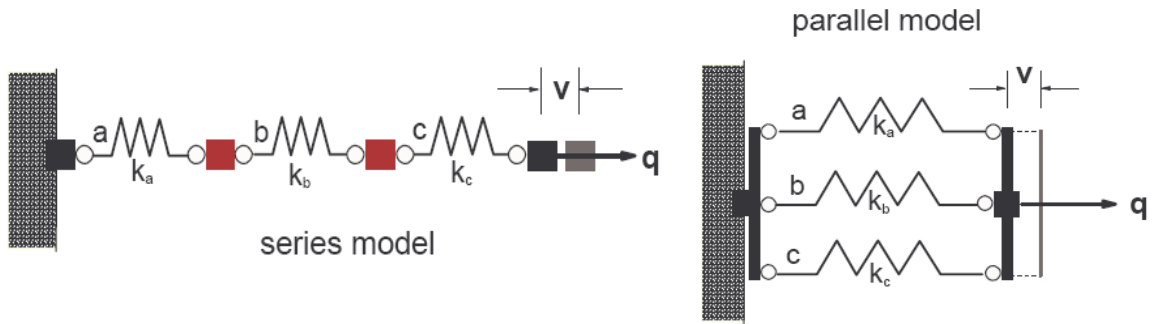


fig. 1.2-2

The first component model was introduced in parallel by Clough et al. (1965), and is shown in fig. 1.2-3. The model consists of two elements in parallel, one elastic-perfectly plastic, to represent the yield strength, and the other elastic with a reduced stiffness to reproduce the hardening. The element stiffness matrix is the sum of those of the two parallel elements. The advantage of these models, also called "two component model", lies in the independence of the formulation from the moments diagram, while the problem arise from the fact that this kind of elements allow to use only a bilinear moment-curvature relation, so it is incapable of represent the typical degradation of reinforced concrete elements. These models, overestimate the energy dissipation capacity of reinforced concrete structural elements.

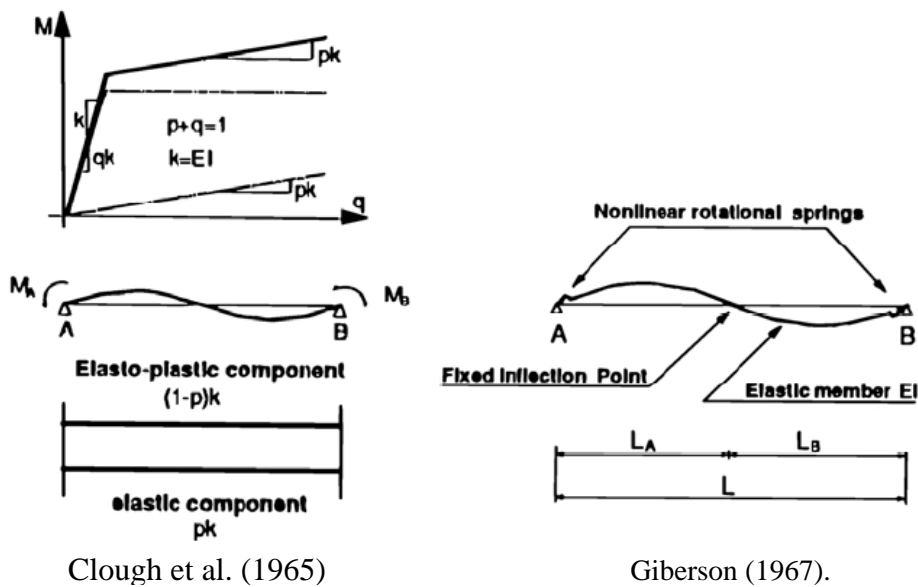


fig. 1.2-3

Series models were introduced to overcoming the limitations inherent in the parallel models. They were formally introduced by Giberson (1967), the model (fig. 1.2-3) consists of two non-linear rotational springs and end of an elastic beam. For each spring is introduced a moment-rotation relationship assuming an antisymmetric linear distribution of moments along the element. In series models the flexibility matrix of each spring is summed with the flexibility matrix of the linear elastic beam. This type of models are much more versatile than the parallels, with series models is possible to describe a more complex hysteretic behavior, selecting an appropriate moment-rotation relationship for springs, but they are limited by the assumption of a constant moments distribution along the element. Suko and Adams (1971), proposed to take the contraflexure point from the initial elastic analysis instead of the center of the beam. Otani (1974), proposed a more sophisticated model, shown in fig. 1.2-4. The Otani's model consists of two deformable parallel elements, one linear elastic and the other non-linear, two rotational springs and two rigid connection at the ends to take into account the finite size of the beam-column node. The rotational springs are used to consider the effects of the reinforcement slip at the nodes. The construction of the flexibility matrix is based on the calculation of the contraflexure point step by step. The element is treated as two cantiliver beams, with a free end at the contraflexure point. With this assumption the element is equivalent to two inelastic rotational springs at the ends, whose properties are related to the current position of the contraflexure point. The Otani's model, however, is not capable to evaluate the actual spread inelasticity along the element, depending not only on the current state of the element, but also on the load history.

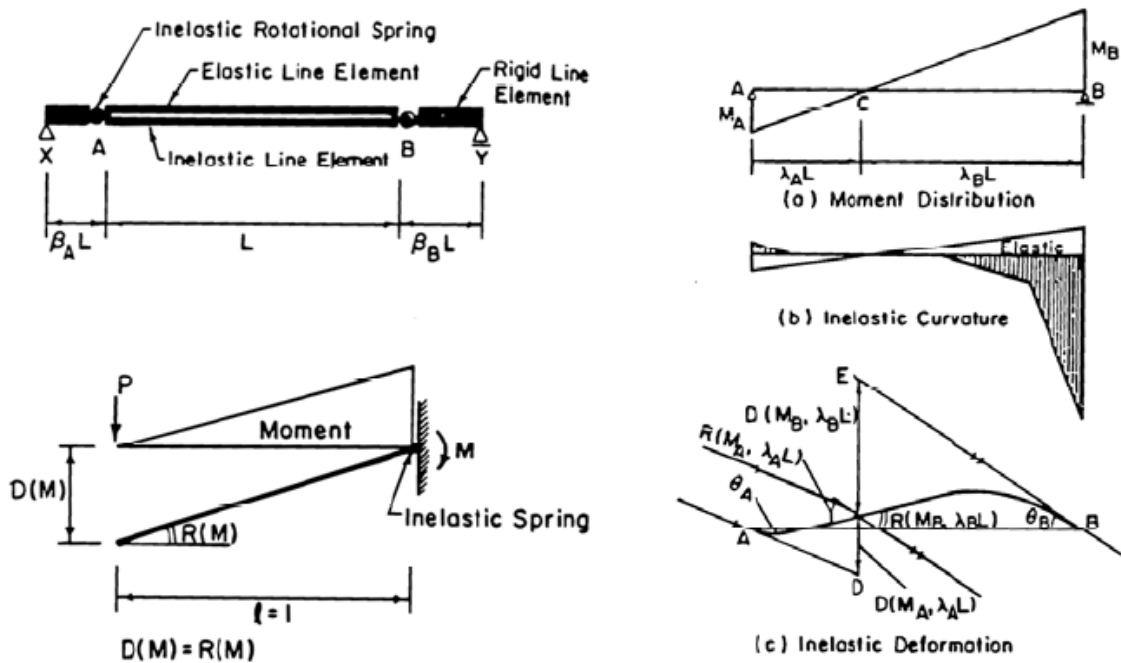


fig. 1.2-4

Concentrated plasticity models have been formulated neglecting the phenomena of axial force-moment interaction. The moment-rotation relationships are defined referring to a constant value of axial force, usually the gravity loads. Actually, the normal stress in the columns due to seismic action can vary significantly, affecting both the resistance and the stiffness properties of structural elements. Considerable efforts have been made to include the effects induced by the variations of normal stress in simplified models, but this kind of models are not applied extensively. Saatcioglu et al. (1983) introduced a concentrated plasticity model, in which the moment-rotation relationship of the springs is characterized by a family of curves, each corresponding to a different value of normal stress.

An important step in the modeling of axial force-bending moment interaction, was made with the introduction of multispring models, which are classified between as concentrated plasticity, but actually these differ considerably from those described above, and in some way are similar to simplified fibers models. The first multispring model was proposed by Lai et al. (1984), it was constituted by a central elastic element, and a series of axial springs at the end zones to simulate the inelastic response (fig. 1.2-5). The non-linear deformations are concentrated in the end zone, although their behavior is not defined by

the moment-rotation relation, but through a discretization of such zones in areas that represent the springs.

In the Lai's model each inelastic element consists of five spring for concrete, four for corners and a central one, and four for steel. The force-displacement relationship for the steel springs follows an hysteretic model with degradation similar to that assumed on the moment-rotation relationship viewed for others concentrated plasticity models. The elongation of each spring is correlated with the average axial displacement and the section rotation, through the assumption of plane sections remain plain.

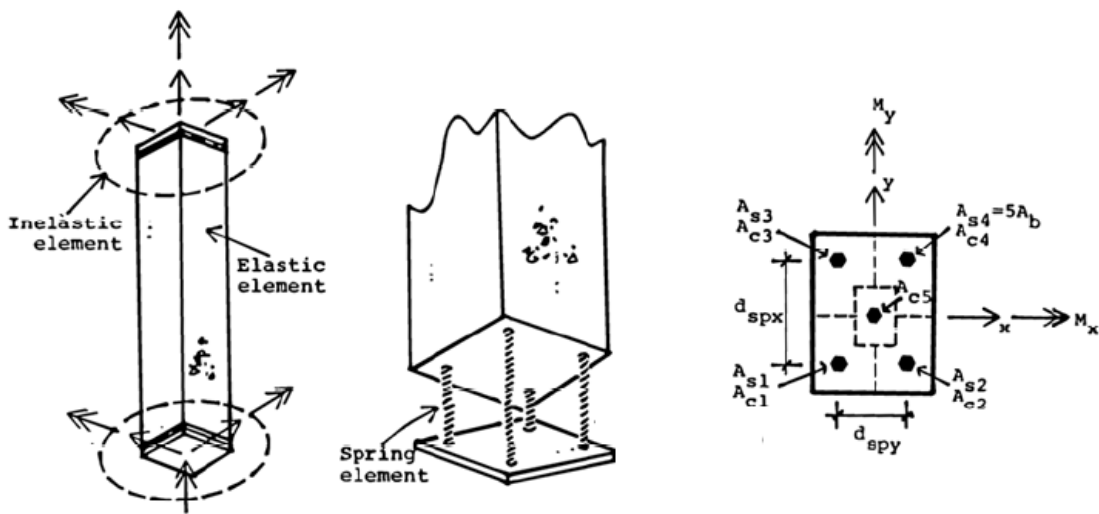


fig. 1.2-5

Saiid et al. (1989), proposed a multispring model with five springs based on Lai et al. (1984). One spring is central to simulate concrete core, while four springs are placed at sides to simulate the behavior of a reinforced concrete element subjected to axial elongation, corresponding to the area represented by each spring. With this model the authors overcame some inherent inconsistencies in the Lai's model, and have performed good comparison with experimental tests.

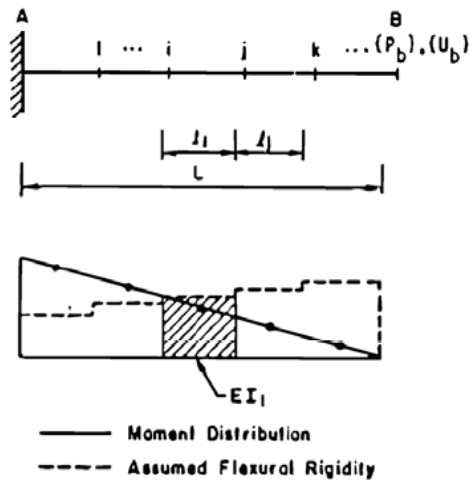
The best feature of multispring models is the ability to simulate with good accuracy the nonlinear behavior of spatial columns, requiring much lower computational effort than fiber models.

The concentrated plasticity models, as seen above, are not able to take into account the gradual spread of inelastic deformation within the elements. A more accurate description of the nonlinear behavior of reinforced concrete elements is possible by using distributed plasticity models. These kind of models assumes that the inelastic deformation may occur in any section, the element response is derived through an integration of sections response along the element.

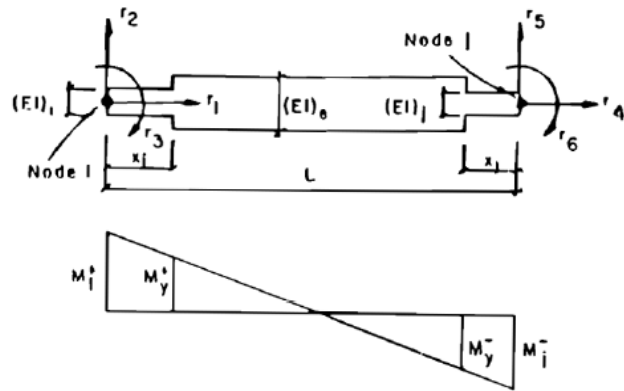
Schnobrich and Takayanagi (1979), have proposed to divide the element into a finite number of segments (fig. 1.2-6), each with constant properties dependent on the bending moment at the midpoint. Each segment is studied through a moment-curvature relation including the effects of degradation due to cyclic loading. Also in this model a proposal to take account the axial-bending interaction is made. The section stiffness is defined, including axial effects, as resulting from predefined interaction diagrams.

Analyze the sections response along the element leads to various difficulties, for the greatest calculation time and for the numerical problems related to the arise of unbalanced moments within the element. Equilibrate these moments requires the introduction of complex procedures not necessary when are studied only the end sections. Therefore, several authors have developed concentrated plasticity models able to take into account the gradual spread inelasticity. These models, also called distributed inelasticity have been widely used, and many computer codes have been based on them.

In fig. 1.2-6 is shown the Meyer's model, Meyer et al. (1983) and the later one improved by Roufaiel and Meyer (1987). The element is divided into three zones, one central elastic and two inelastic ends, varying in length depending on the load history.



Schnobrich and Takayanagi (1979)



Roufaiel e Meyer (1987).

fig. 1.2-6

This formulation is independent from the position of contraflexure point, and take into account the coupling of the inelastic deformation in the two non linear segments. The properties of these segment are derived by simplified assumptions on the end sections, carried out through hysteretic moment-curvature models

Schnobrich and Keshavarzian (1985), have adopted the same element, but taking into account axial-flexure interaction. To consider these effects they followed a similar approach to that proposed by Takayanagi and Schnobrich (1979).

The criteria used by Meyer et al. (1983) is part of the formulation of Filippou and Issa (1988), and Mulas and Filippou (1990), which added to the element, two rotational springs at the extremities, for take into account the fixed end rotation at the beam-column joint, due to bar pull-out.effects. These authors have attempted to define more accurately the moment-rotation relationship of the springs, which was independent from the assumed moment-curvature relationship at the end sections. Filippou Ambrisi (1997) have included more non-linear springs to account for translational non-linear deformations due to shear. This model is made up of several sub-elements connected in series to distinguish the various aspects that affect the nonlinear behavior of the structural element.

A further evolution was carried out by Aredia and Pinto (1998) dividing the element into three zones. They have developed a method to identify, in the elastic part of the element, cracked and uncracked zones. Their model is based on the assumption that the elastic limit

may be exceeded only in the end zone, and that the cracked areas can be developed at both of them, both from the central section of the element, where it is possible to apply a concentrated load. Both areas, cracked and plasticized have variable length depending on the loading history, determined by taking a linear progression of bending moment from each end to the center of the beam.

A common plasticity model that differs from those just described was carried out by Kunnath et al. (1990), this model can perform local and global damage evaluation as well as non-linear seismic analysis of reinforced concrete structures. Kunnath et al. (1990) did not directly assess the length of the plasticized hinges. The element characteristics will be deducted from the sections by integration, assuming a flexibility distribution piecewise linear (fig. 1.2-7).

This distribution is identified by the beam ends flexibility, that come from the moment-curvature relationship, and from the flexibility of the contraflexure point, which is assumed to be equal to the elastic value.

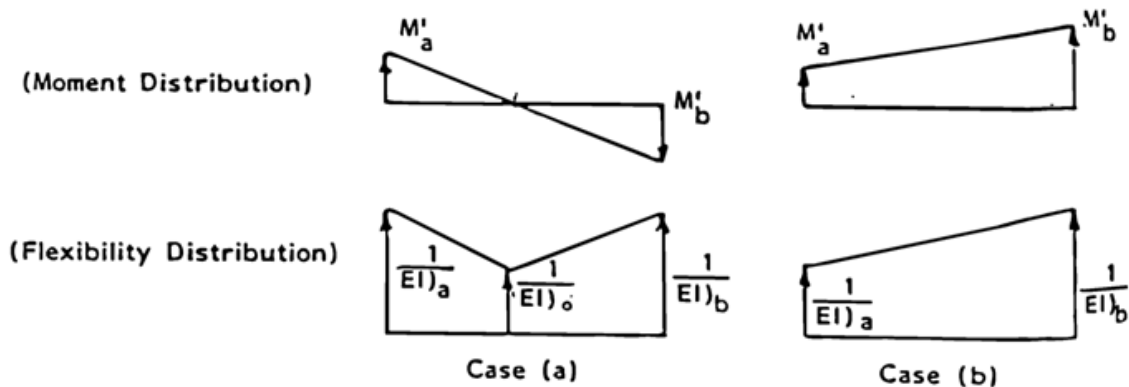


fig. 1.2-7

1.2.4 Fibre Models

In Fibres models is carried out a double discretization, in the longitudinal direction defining a predetermined number of sections and in the transverse direction, discretizing in small finite areas the element cross sections. In case of simple planar bending model is sufficient to subdivide the sections into strips perpendicular to the axis of flexion, in the more general spatial cases a double subdivision into small rectangular areas is required

(fig. 1.2-8). Each fiber, represent a corresponding portion of elementary concrete or reinforcement area , by integration over the cross section is possible to obtain moment-curvature relationship, and thus determines the overall response of the whole element. By the hypothesis of plane sections remain plane, axial deformation of each fiber $\varepsilon(x, y)$ can be obtained, once knowing curvature χ_x, χ_y and axial deformation ε_0 referred in section centroid.

$$\varepsilon(x, y) = \varepsilon_0 + y \cdot \chi_z - z \cdot \chi_x \quad (1.3.1)$$

The characteristics described above are common to all models, so that not changes in different element formulations. What really change in different fibre models is essentially the state determination procedures that depend on different formulation. In fact fiber models, as distributed plasticity models, has the problem, highlighted in previous paragraph, about the arise of unbalanced section forces within the element. After a load step application, nodal displacement are calculated and from these the section forces can be evaluated, but because of the materials nonlinear behavior in all control sections, resisting forces doesn't match section forces.

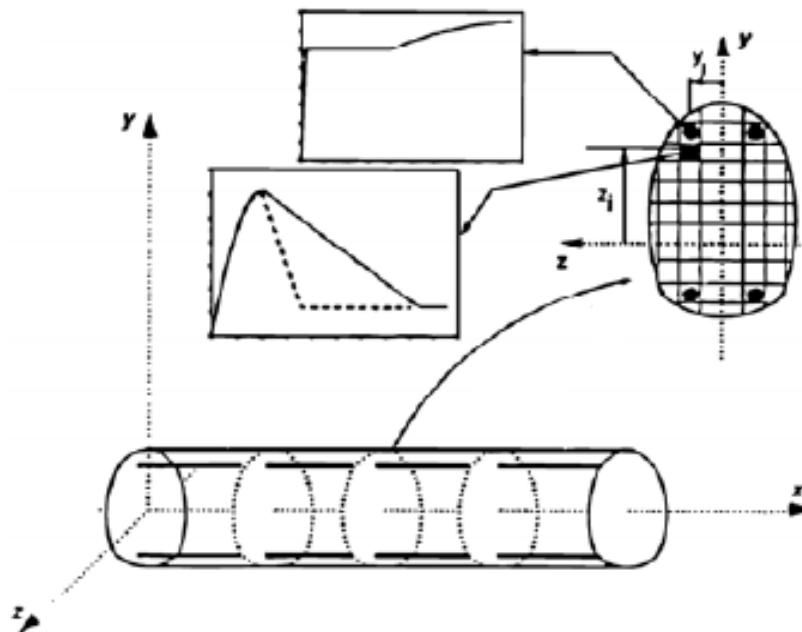


fig. 1.2-8

In global models, especially those with concentrated plasticity this problem is not treated because only the end sections are taken into account. Fibre models differ therefore in the process used to determine the section resisting forces. Different procedure has been proposed depending on the element formulation, in particular can be found procedure for stiffness based, flexibility based or mixed elements.

The early models have been developed on a stiffness based approach, using classical shape functions. A model that use this approach is due to Aktan et al. (1974), in which nodal resisting forces are obtained directly from section resisting forces by applying the virtual work principle. The formulation is compatible, however, it is shown that is inadequate in nonlinear cases because it involves a linear curvature distribution over the length. This assumption is unrealistic for reinforced concrete elements in nonlinear field.

The latter models become increasingly based on a flexibility approach, this class of models uses forces interpolation functions, thus a balanced element is achieved while in stiffness models the compatibility was the basic assumption. One of the first balanced element is proposed by Kaba and Mahin (1984), based on Aktan (1974), this model introduce the displacements interpolation functions updated for each load increment through the flexibility matrix. In this model, however, the numerical problems discussed above have not been solved because the theoretical formulation is not totally consistent with the flexibility approach.

Essentially the flexibility approach is more realistic than the stiffness based one, but involves significant problems in determining the nodal resisting forces. Many studies, therefore, have attempted over the years to overcome these problems. Zeris and Mahin (1988, 1991), developed a complex iterative procedure to investigate the cross section deformation associated with internal balanced forces, with a shape coincident with forces interpolation functions. Taucer et al. (1991) have proposed a model that is part of a more general mixed approach. The nodal resisting forces are calculated for each element through an iterative procedure. At each iteration, are calculated the residual nodal displacements associated with the unbalance section forces along the element. The main characteristic of this model is that, at each iteration, compatibility and equilibrium are satisfied within the element. Taucer et al. (1991) show that the proposed algorithm is effective even if the structural response is characterized by "softening" as in concrete structures.

Finally some recent developments in fiber models are oriented in the attempts to develop extensions in classical elements including other sources of nonlinear deformation, such as those related to shear stress. In this class of models, widely described in chapter two, the section state deformation is characterized not only by the axial deformation and the curvature in the centroid, but also by the shear deformation evaluated in nonlinear field. Besides the hypothesis of plane sections remain plane, a given distribution of shear deformation is assigned in order to detect the state of deformation of each fiber. Generally a biaxial stress-strain relationships is associated to these elements. This model is very close to a microscopic approach, but compared to the that has the same degrees of freedom of beam element type.

In conclusion, fibre models requires a large number of operations to evaluate the element stiffness matrix, the stress and strain state in each section. In other words fibre models are really time consuming in state determination procedures. Although sometimes it incurs in numerical stability problems, many advantages can be identified using these models as:

- Catch the actual evolution of plasticization along the element
- Are able to reproduce realistically pinching phenomena
- Describe in detail geometry and position of transverse reinforcement
- Can reproduce the interaction between axial forces and bending moments
- Can be easily implemented spatial elements.

Also the constitutive relationship are more easy to implement because the singles materials are considered instead of moment-curvature relationship.

In this thesis a fibre model able to take into account the coupling between moment, axial forces, and shear in non-linear field is presented. It is based on the flexibility approach to take advantage of the benefits attributed to this class of fiber model, in particular between all fibre modes has been chosen Taucher et all. (1991) because it seemed to respond better to requests features.

1.3 Aim and objectives of the thesis

The main purpose of the thesis is to propose a finite element able to model structures, where the shear deformation appears predominant. The category of models chosen to attain this goal are the fiber models, treated in the previous chapter. As highlighted in the

overview in this introduction, the shear deformation and in particular the shear-flexure coupling in nonlinear field is still an open research topic, in particular, in global models as beam-column elements.

This aim will be achieved through the following enabling objective:

- To gather information on existing knowledge about flexure- shear interaction in fibres models, through a comprehensive literature review.
- To develop and implement an efficient fibre model, capable of predicting the behaviour of concrete squat structures, which include a bidimensional theory for concrete (Modified Compression Field Theory) as constitutive relationship.
- To validate the model by comparing the predicted behaviour with the behaviour observed in experimental results, in particular the model must reproduce the global response of the structure with reasonable agreement with experimental evidence.
- To validate the model by comparing the results with another code with different approach and carrying out a parametric analysis with the aim of study the influence of flexure-shear interaction by varying the slenderness.
- To illustrate a different model proposed, based on a different formulation and a different constitutive relationship , with the aim of proposing an alternative model with which, will carry out future comparison and mutual improvement.

1.4 Outline of the thesis

The contents of the thesis will be divided into different chapters as follows:

- The first chapter is introductory, recalls some basic concepts of nonlinear analysis and models categories. In this chapter can be found descriptions of concentrated plasticity elements (one component and two components model) , distributed plasticity elements and fibres models, focusing on the stiffness and flexibility formulations highlighting the benefits and the deficiency of each approach.
- The second chapter is entirely dedicated to the state of the art of fibres beam-column element, in which some author tried to introduce shear deformation. In this chapter will be discussed in detail each of these models, from the strut and ties, to Microplane and smeared crack to finish with damage models.

- In the third chapter will be treated the finite element formulation, will be described in detail the derivation of the flexibility based element, starting from the two-fields mixed method. This chapter describes how numerical procedures for structural and element determination have been carried out.
- The fourth chapter is entirely dedicated to section state determination, through the description of MCFT (modified compression field theory) and DSFM (disturbed stress field model) that are the basis of the constitutive law implemented in the model. For each theory will be analyzed compatibility, equilibrium and constitutive relationships for the average quantities between the material cracks, will be explained the equilibrium problem on cracks location and shear slip over the cracks.
- In the fifth chapter will be explained the implementation of the model, this chapter will show the vectors and matrices involved in the program and the flow charts of the code. Furthermore will be explained in detail how the theories on which the model have been based are unified in a single computer code.
- The sixth chapter will report all tests and comparisons performed with the computer code. First of all will be presented the reproduction of the experimental test conducted by Osterle et al. (1979). Then will be shown the numerical comparison between the computer program Vector2, developed at University of Toronto, and the code proposed in this thesis. Finally, two parametric analysis conducted on a bridge pier and on a shear wall, show how the nonlinear flexure-shear interaction actually affect the response in squat structure. Different analysis are carried out with the aim of evaluate this influence varying the structural slenderness.
- The seventh chapter describe the formulation the constitutive relation and the implementation of the model studied at University of California Berkeley. This model represent an alternative solution to the presented problem, some comparison between the two models are in progress. For the element formulation has been used a three-field variational formulation while for constitutive relationship a three-dimensional material model. For concrete has been implemented a damage model with two parameters, one for tension and one for compression Lee and Fenves (1998), while for steel structures has been implemented a classical plasticity model.

CHAPTER 2

Fibre beam-column element with flexure-shear interaction: state of the art

2.1 Sommario

Tra i vari approcci adottati per eseguire delle analisi non lineari di strutture in c.a. gli elementi a fibre hanno mostrato una grande capacità di riprodurre l'interazione tra sforzo assiale e momento flettente, mentre l'accoppiamento di sforzi normali, flessionali e taglianti è un fenomeno ancora poco chiaro.

La soluzione al problema della modellazione taglio-flessione è stata affrontata in molti studi con approcci diversi. Un aspetto che caratterizza molti dei modelli proposti è il disaccoppiamento di flessione e taglio. Ad esempio, nei modelli "strut and tie" il classico elemento trave è associato ad un traliccio che simula il meccanismo resistente a taglio. In alcuni casi i modelli "strut and tie" sono stati combinati con elementi a fibre, come nei modelli proposti dalla Guedes e Pinto (1997), Martinelli (2002) e da Ranzo e Petrangeli (1998). Un altro metodo seguito per predire la risposta taglio-flessione si basa sulla teoria Microplane studiato da Bazant e Oh (1998), Bazant e Prat (1998) e da Bazant e Ozbolt (1990). L'approccio Microplane permette la descrizione della risposta multiassiale attraverso la combinazione di relazioni costitutive monoassiali. Petrangeli et al. (1999) usarono la teoria Microplane all'interno di un elemento a fibre.

Un altro approccio si basa sui modelli a fessurazione diffusa Vecchio e Collins (1988). In questo approccio, il calcestruzzo fessurato è modellato come un materiale ortotropo, in cui equilibrio e di compatibilità sono formulati in termini medi di tensione e deformazione.. Remino (2004) ha sviluppato un elemento a fibre con un legame costitutivo basato su Rose (2001). Ceresa et al. (2008) hanno realizzato un modello a fibre basato su una formulazione in rigidità considerando la modified compression field theory (Vecchio e Collins (1996)) come legame costitutivo. Una particolare tipologia di modelli, come quella presentata da Mazars et al. (2006), implementano anche la teoria del danno.

In questo capitolo saranno illustrati nel dettaglio questi modelli sottolineandone le caratteristiche ed i punti deboli.

2.2 Fibre Beam-Column Element Using Strut-and-Tie Models

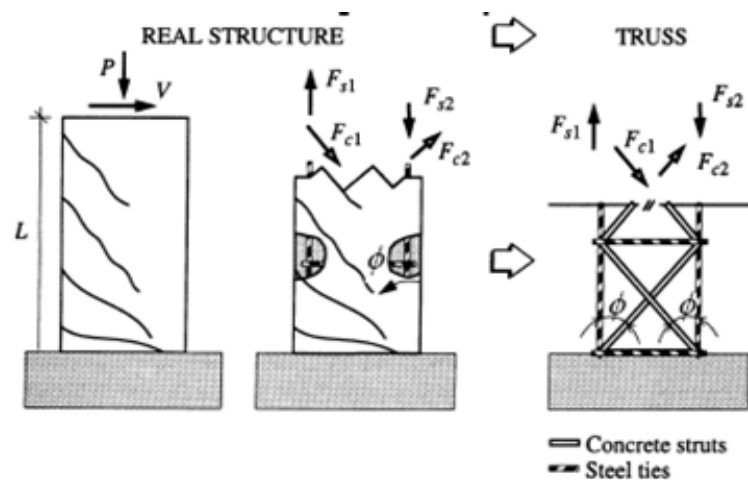
This approach considers a Timoshenko fibre beam-column element, which is coupled with a truss structure. All the shear action is carried by the truss members. There are several models that adopt this technique, these models are presented below.

2.2.1 Guedes's Model

Guedes et. al. (1994-1997) proposed a two-node 3D beam-column element based on a displacement formulation, with linear shape functions for axial displacement and rotation. The degrees of freedom per node are six, three displacements and three rotations::

$$\mathbf{u}(x) = [u(x) \quad v(x) \quad w(x) \quad \theta_x(x) \quad \theta_y(x) \quad \theta_z(x)] \quad (2.2.1)$$

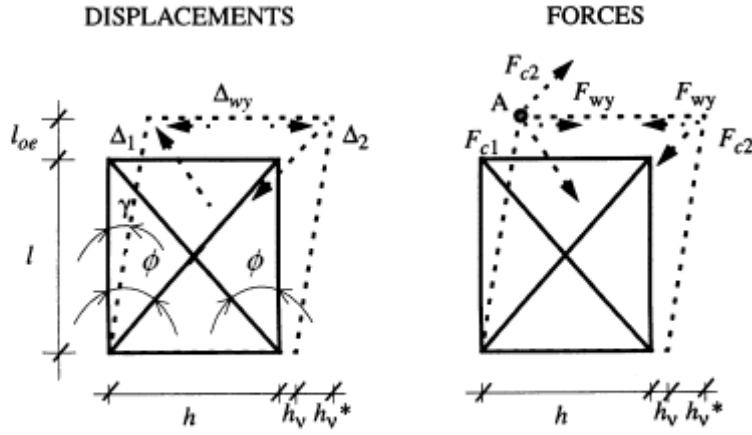
On section, the axial components are obtained through a classical fibre model, while the shear components are obtained independently by a truss model (fig. 2.2-1).



Truss analogy [Guedes and Pinto, 1997]

fig. 2.2-1

The truss consists in two concrete struts whose slope represents the direction of principal stresses and strains, and longitudinal and transverse steel beam. The equilibrium and compatibility are shown in fig. 2.2-2



Compatibility of displacements, and equilibrium of forces [Guedes and Pinto, 1997]

fig. 2.2-2

Referring to fig. 2.2-1 and fig. 2.2-2, the equilibrium between internal and external forces must be satisfied according to the equations:

$$F_{wy} + (F_{c1} + F_{c2}) \cdot \sin \theta = 0 \quad (2.2.2)$$

$$V + (F_{c1} - F_{c2}) \cdot \sin \theta = 0 \quad (2.2.3)$$

The iterative procedure begins by estimating the value of ε_{wy} , the principal strains are calculated using the following:

$$\varepsilon_i = \frac{\Delta_i}{l / \cos \theta} = \varepsilon_{0e} \cdot \cos(\phi)^2 + \varepsilon_{wy} \cdot \sin(\phi)^2 \pm \frac{\tan \gamma}{2} \cdot \sin(2\phi)^2 \quad (i = 2,1) \quad (2.2.4)$$

Where $\varepsilon_{0e} = l_{0e} / l$ e γ are the kinematic parameters derived from Timoshenko beam theory and $\varepsilon_{wy} = \Delta_{wy} / h$ is the deformation in the stirrups calculated iteratively by the equilibrium in the cross section. The forces in the principal direction can be calculated as follow:

$$F_{ci} = f_c(\varepsilon_i) \cdot A_{strut} = \sigma_c(\varepsilon_i) \cdot (1 - D_i) \cdot b_w \cdot h \cdot \cos(\phi) \quad (i = 1,2) \quad (2.2.5)$$

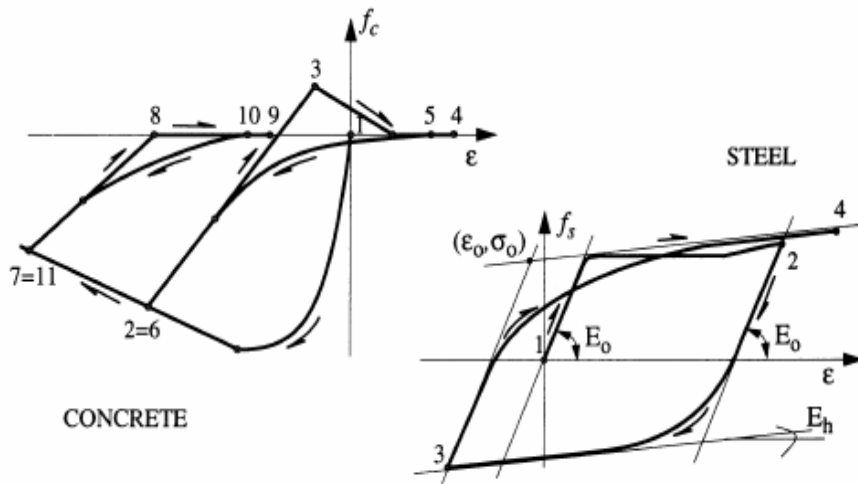
Where D_i is a damage parameter, $b_w \cdot h$ is . Knowing F_{c1} F_{c2} e ϕ the force F_{wy} can be calculated from (2.2.2) and used to find ε_{wy} from the following equation:

$$F_{wy} = f_{sw}(\varepsilon_{wy}) \cdot \frac{h}{\tan(\phi) \cdot s} \cdot (2 \cdot A_{sw}) \quad (2.2.6)$$

If the two subsequent values of ε_{wy} match with a predetermined tolerance, the solution is found, otherwise the iterative procedure continues. At the end of each iteration shear resisting forces V are estimated for each cross section.

The stiffness matrix, which the authors suggest to use, is derived from classic Timoshenko beam element keeping uncoupled flexure and shear. The following consideration can be made:

- The nonlinear behavior is derived from the use of the uniaxial constitutive relationship $\sigma - \varepsilon$, the tangent modulus is obtained step-by-step. The constitutive relationship used by the author is shown in fig. 2.2-3
- A simple linear elastic relationship can be used to represent the relation between the shear forces V and the shear deformation γ in the truss model.



Numerical models for concrete and steel under cyclic loading used by Guedes and Pinto [1997]

fig. 2.2-3

This was one of the first attempts to model the shear behavior in a fiber element. The model presented is a 3D beam-column element, but the shear is modeled with a 2D mechanism. Furthermore, the truss model is not able to take into account other shear resistance mechanisms such as dowel action, arch action, aggregate interlock, compressive concrete that contribute to increase the beam-column shear capacity.

Questo fu uno dei primi tentativi nel quale si cercò di modellare il comportamento a taglio in un elemento a fibre.

Another limitation is represented by the inclination of the cracks that is fixed, equal to 30° or 45° , further the truss model is not able to catch the coupling between axial flexure and

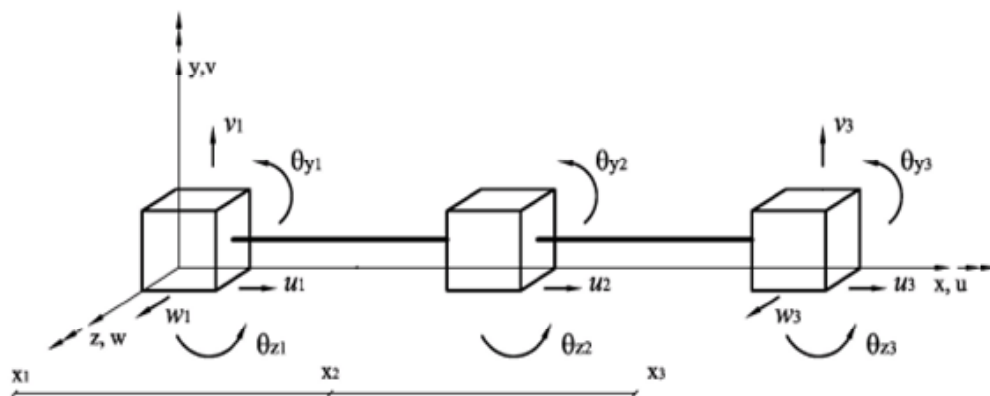
shear, in other words, the shear force has no effect on flexural response. The numerical verification highlight that the model did not represent the crack-closing phenomenon, so the pinching effect is amplified.

2.2.2 Martinelli's Model

Martinelli (1998-2002) developed a model fibre beam-column element with the aim of evaluating the cyclic response of squat bridge piers. The author proposed a finite element superimposing a classical fibre model for the flexural deformations to a truss for shear deformations. The model is a classic 3D fibre element, based on a Timoshenko beam theory, formulated using a displacement-based approach. The element is a three-node beam with the intermediate node with only two degrees of freedom, rotations and axial displacement. The shear-locking phenomenon is avoided by keeping a mean constant shear deformation along the element and a linear curvature variation Crisfield (1986).

The displacement vector $\mathbf{u}(x)$ is represented as follow (fig. 2.2-4).

$$\mathbf{u}(x) = [u(x) \quad v(x) \quad w(x) \quad \theta_y(x) \quad \theta_z(x)]^T \quad (2.2.7)$$

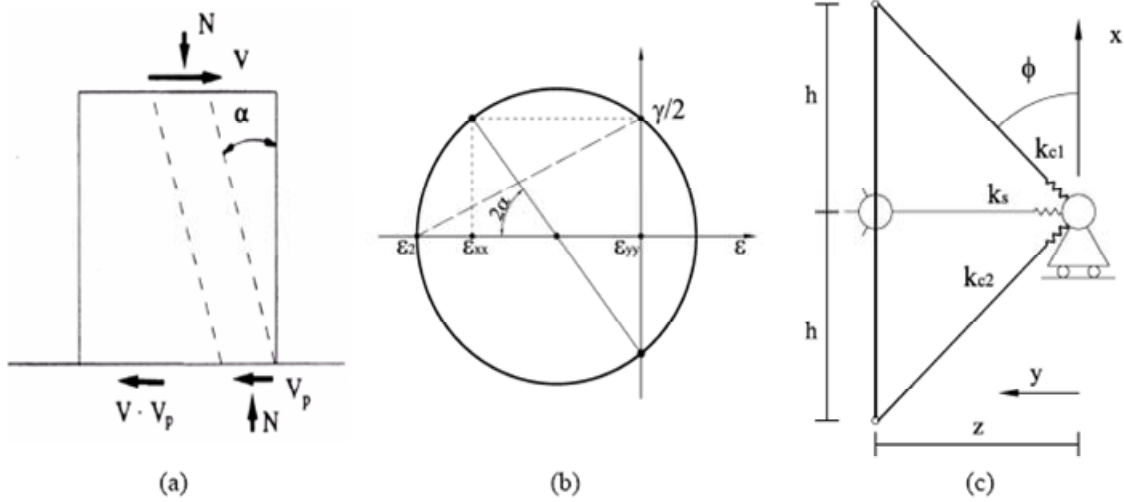


Nodal degrees of freedom of Martinelli's fibre element [adapted from Martinelli, 1998]

fig. 2.2-4

The shear resultant over the cross-section is the results of many different resisting mechanisms as the arch action, the truss mechanism, the compression concrete above the neutral axis, and the aggregate interlock, each of which considered independently.

The *arc mechanism* is shown in fig. 2.2-5 (a) where it's observed that an inclined strut transfers a shear force proportional to the axial force $V_p = N \cdot \tan(\alpha)$.



(a) Inclined strut, (b) Mohr's circle used in arch action mechanism, and (c) assemblage used to model truss mechanism [Martinelli, 1998]

fig. 2.2-5

The fibres are aligned with the strut, the inclination α , is calculated from the nodal moments $(M_{zi}, M_{yi}, M_{zf}, M_{yf})$, and the centre of compressive stresses. Known α e ϵ_{xx} , assuming $\epsilon_{yy} = 0$, the principal direction ϵ_2 and the shear deformation $\frac{\gamma}{2}$ can be calculated by the Mohr circle fig. 2.2-5 (b). An uniaxial constitutive relationship is used to deduce σ_2 from ϵ_2 (with the assumption of zero tensile principal stress $\sigma_1 = 0$). Known σ_2 and γ σ_{xx} and τ_{xy} are derived from Mohr's circles. The tensions thus obtained are integrated on the cross section to get the resisting forces.

$$\begin{aligned}
 N &= \int_A \sigma_{xx} dA & M_y &= \int_A \sigma_{xx} \cdot z dA & M_z &= \int_A \sigma_{xx} \cdot y dA \\
 V_{pxy} &= \int_{A_{cc}} \tau_{xx} dA & V_{pxz} &= \int_A \tau_{xz} dA
 \end{aligned}
 \tag{2.2.8}$$

An Iterative procedure is required to calculate α . the authors suggest to take α as the value at the end of the previous step in a step-by-step dynamic analysis.

The *truss mechanism* is based on a 2D structure composed by the transverse reinforcement and the concrete diagonals in tension and compression as shown in fig. 2.2-5 (c). The diagonals are inclined by an angle ϕ assumed equal to the cracks inclination. The deformation of the truss is obtained from the kinematic parameters of the Timoshenko

beam ε_{xx} and γ_{xy} where ε_{yy} it is assumed equal to the strain in the stirrups and is calculated by imposing the equilibrium of the truss along y $\sigma_{yy} = 0$.

Using the Mohr circles of the principal directions are simply calculated, and τ_{xy} can be deduced by knowing the principal stresses. The shear transferred by the truss is calculated by integrating the shear stress over the tensioned concrete in the cross section $V_t = \tau_{xy} \cdot A_t$. concrete tangent modulus E_1 and E_2 in principal direction and steel tangent modulus E_s can be also evaluated. By the tangent modulus is possible to calculate the stiffness matrix K_{shear} associated with the contribution of the truss.

The *interlocking mechanism*, is taken into account assuming a set of diagonal cracks with constant spacing s (s a model parameter), inclined by an angle ϕ kept constant, respect to the beam axis. The shear component τ_{xyIN} on the cross section are derived from the stresses arising at crack faces, due to the relative displacement. These stresses are calculated from the strains ε_{xx} , γ_{xy} e $\varepsilon_{yy} = \varepsilon_s$ derived from the truss mechanism. The shear force associated to the interlocking mechanism is derived from the integration of the shear stresses τ_{xyIN} over the tensioned concrete area: $V_{IN} = \tau_{xyIN} \cdot A_t$

The shear resistance force is given by the sum of the contribution of V_p , V_t e V_{IN} and the stiffness matrix of the section is the following:

$$\mathbf{K}_s = \begin{bmatrix} \int_A EdA & -\int_A y \cdot EdA & \int_A z \cdot EdA & 0 & 0 \\ -\int_A y \cdot EdA & \int_A y^2 \cdot EdA & -\int_A y \cdot z \cdot EdA & 0 & 0 \\ \int_A z \cdot EdA & -\int_A y \cdot z \cdot EdA & -\int_A z^2 \cdot EdA & 0 & 0 \\ 0 & 0 & 0 & \mathbf{K}_{shear} & 0 \\ 0 & 0 & 0 & 0 & \mathbf{K}_{shear} \end{bmatrix} \quad (2.2.9)$$

where E is the elastic tangent modulus and K_{shear} is obtained by the truss mechanism.

A positive characteristic of this model is that it takes into account different shear resisting mechanisms. In particular, the arch effect and the flexural behavior are formulated in 3D, while other mechanisms are studied separately in planes xy and xz .

This means that the actual spatial behavior of the model is sometimes lost. It is also noted that in the arch effect the contribution of the shear depends on α and ε_{xx} , that are flexure-dependent parameter, so flexure and shear in the truss mechanism are actually coupled.

In the truss mechanism the inclination of the cracks and the crack spacing are assumed constant, thus the effect of the longitudinal reinforcement is not taken into account.

The deformation involved are γ_{xy} and ε_{yy} (neglected in the arch mechanism) are calculated iteratively until the equilibrium in y direction is reached.

The solution of the aggregate interlock is derived from the truss mechanism, in terms of strains, thus the aggregate interlock is not able to influence the other mechanisms, in particular, is not able to affect the principal stresses directions.

In the sectional stiffness matrix the shear contribution is given only by the truss mechanism and it is uncoupled from the flexural term. It could imply low convergence rate.

The comparisons with experimental results highlight some lacks of the model: first of all the capability to capture some specimen collapse, furthermore it tends to exaggerate strength degradation in cycles.

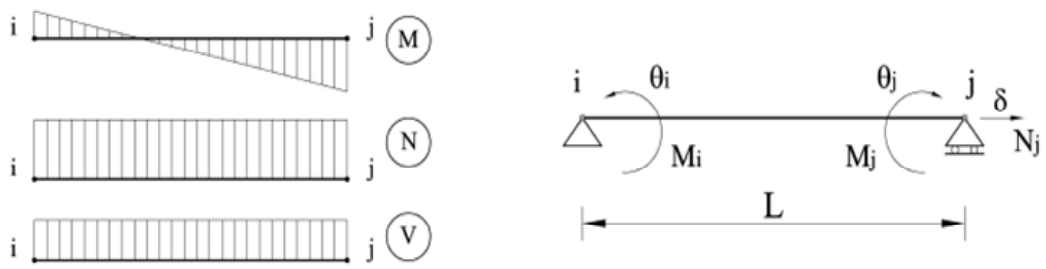
The model proposed by Martinelli [1998, 2002] is able to take into account different shear resistance mechanisms studied independently. While failing to capture a full coupling between axial, flexure and shear forces, it still can capture the behaviour of reinforced concrete with shear-influenced response with a very reasonable accuracy.

2.2.3 Ranzo and Petrangeli's model

Ranzo and Petrangeli (1998) proposed a 2D fibre beam column element based on flexibility approach, in which the bending-axial behaviour is modelled by a classical fibre discretisation whilst the shear response is represented by a nonlinear truss model in which is applied an hysteretic stress-strain relationship. The two different behaviours are coupled by a damage criterion at section level and then integrated along the element.

Stress shape functions are introduced for the 2-node element (fig. 2.2-6), so that the moment, axial and shear forces can be given by the following equations:

$$N(x) = N, \quad M(x) = -\left(1 - \frac{x}{l}\right) \cdot M_i + \left(\frac{x}{l}\right) \cdot M_j, \quad V(x) = \frac{M_i + M_j}{l} \quad (2.2.10)$$



Stress shape functions and element forces and deformations [adapted from Ranzo and Petrangeli, 1998]

fig. 2.2-6

Three are the degrees of freedom, two rotation θ_i, θ_j and an axial elongation δ , the displacements vector is:

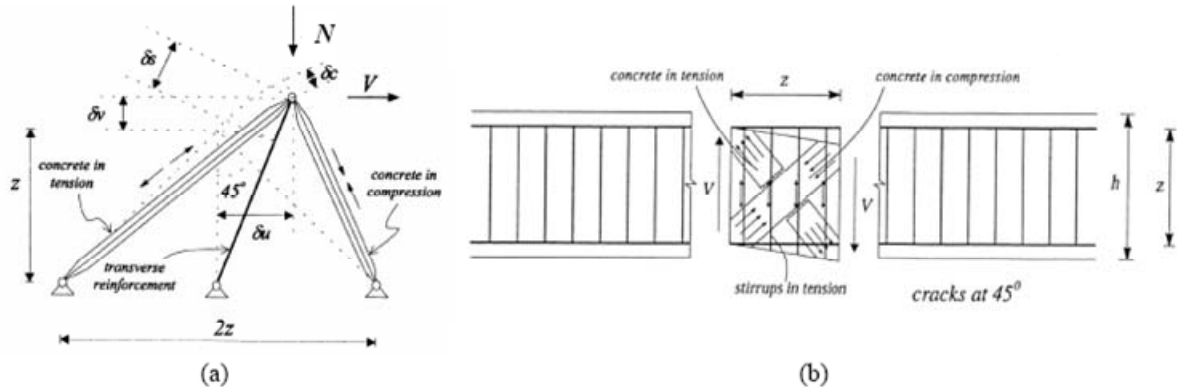
$$\mathbf{u}(x) = [u(x) \quad \theta_z(x)] \quad (2.2.11)$$

In terms of compatibility, curvature χ , axial deformation ε and shear strain γ of the section are defined. Axial force and moment are functions of (ε, χ) , while the shear force depends on axial and shear strains (ε, γ) .

The resulting section stiffness matrix is the following:

$$\mathbf{k}_s = \begin{bmatrix} \sum_{i=1}^{nfib} E_i A_i & \sum_{i=1}^{nfib} E_i y_i A_i & 0 \\ \sum_{i=1}^{nfib} E_i y_i A_i & \sum_{i=1}^{nfib} E_i y_i^2 A_i & 0 \\ 0 & 0 & \frac{\partial [v(\gamma, \varepsilon_{\max})]}{\partial \gamma} \end{bmatrix} \quad (2.2.12)$$

the stiffness matrix highlights the lack of coupling between shear and bending at the section level.



Beam segment truss idealisation [adapted from Ranzo and Petrangeli, 1998]

fig. 2.2-7

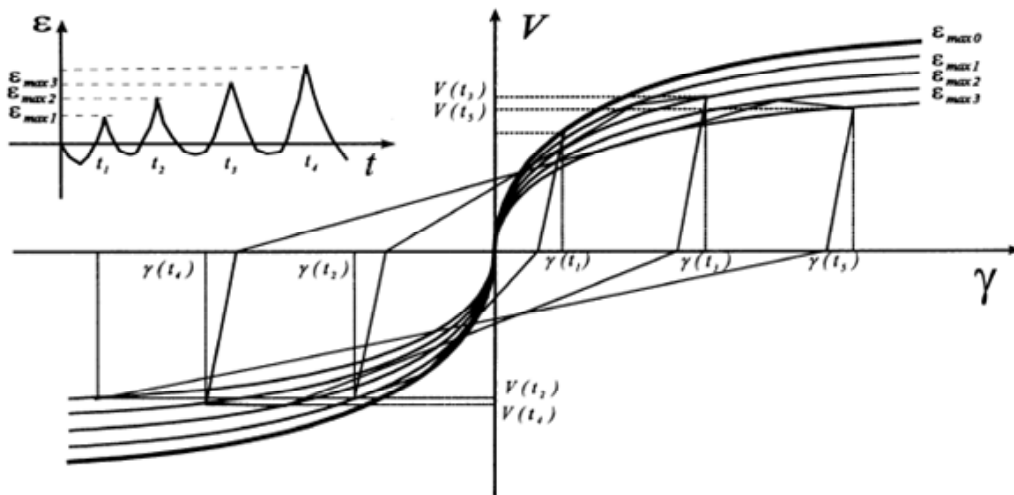
In fig. 2.2-7 can be observed the schematization of the model, concrete is represented as a single truss element whose area is a percentage of the total section. This percentage depend on the neutral axis at the flexure cracking point. The shear reinforcement, is equivalent to a chord whose area is equal to the sum of shear reinforcement plus a percentage of the longitudinal bars. Solving the strut-and-tie model, the $V - \gamma$ curve is found, having assumed a constant value for the inclination of the cracks ϕ . $V - \gamma$ curve is defined as a function of the applied load N , shear reinforcement and diagonal concrete struts. This curve is obtained by applying small increments $\Delta V_{(i)}$ until the failure is reached, with the

distortion $\gamma = \frac{\partial u}{(z + \partial v)} \cong \frac{\partial u}{z}$. To obtain a continue curve, an analytical function is used to

interpolate these points. This procedure leads to the determination of the cracking, yielding and ultimate shear force and distortion.

To relate the shear strength to the ductility, there are many branches of the hysteretic relationship $V - \gamma$ incorporates a degradation criterion, the primary curve is function of the axial strain, chosen as damage indicator

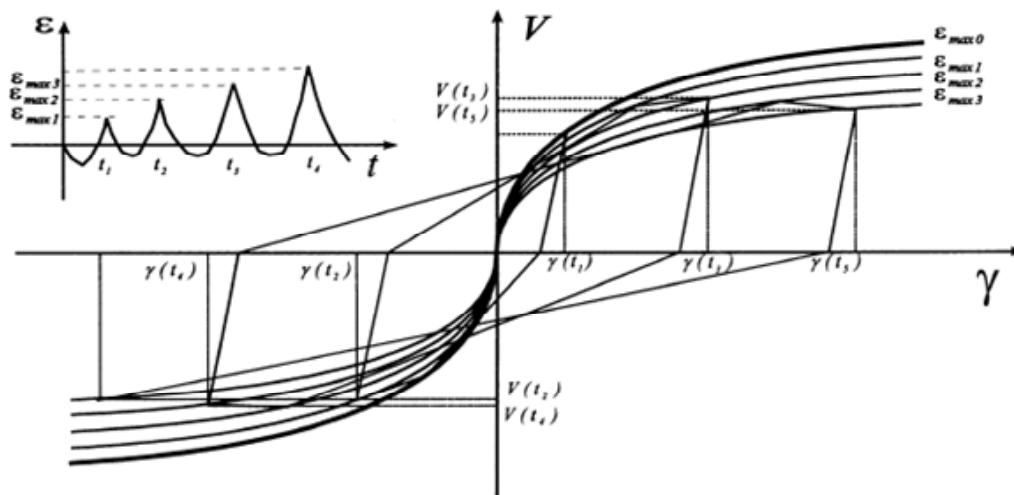
(



Section shear hysteretic model – Skeleton and degraded curves [Ranzo and Petrangeli, 1998]

fig. 2.2-8).

Like other models based on a truss mechanism, the shear strength is the resultant of different mechanisms (ductility-dependent concrete contribution and truss mechanism formed by the transverse reinforcement).



Section shear hysteretic model – Skeleton and degraded curves [Ranzo and Petrangeli, 1998]

fig. 2.2-8

In this model flexural and shear behaviour works in series without any specific coupling between axial, flexure and shear components, this characteristic is underlined in the stiffness matrix components.

Some of the assumptions are based on empirical considerations that are not necessarily theoretically-based nor experimentally-validated. First of all the location of the equivalent struts is given by the assumption that the axial force N is parallel to the transversal steel, in this way the proposed system configuration is able to reproduce the correct damage

sequence. Further, the cracking angle ϕ is assumed constant, with an average value (30° or 45°), whilst the contribution of the longitudinal bars in the truss mechanism is simply estimated by the author.

The primary $V - \gamma$ skeleton curve of the hysteretic shear relationship has been calibrated using a nonlinear truss model, whilst a simplified damage criterion has been used to take into account the degradation of the curve due to flexure-shear interaction]. A calibration procedure is required for each analysis and for each structural element to be studied. This mean that this model is very limited in general applications.

2.3 Fibre Beam-Column Element Using Microplane Model

The Microplane model family Bazant and Oh (1985), Bazant and Prat (1988) Bazant and Ozbolt (1990), Ozbolt and Bazant (1992) is based on a kinematic constraint that links the external deformation with slected internal planes, and the simple monitoring of the stress - strain relations on these planes. The state of each Microplane is characterized by axial and shear strains which makes it possible to match any Poisson ratio value.

This approach allows to describe a multi-axis response through a combination of uniaxial constitutive laws.

2.3.1 Petrangeli's Model

Petrangeli et al. (1996.1999) developed a fiber element based on flexibility approach to model the shear behavior and its interaction with the bending moment and axial force in reinforced concrete columns. The element is a 2D beam with two nodes and three degrees of freedom per node:

$$\mathbf{u}(x) = [u(x) \quad v(x) \quad \theta_z(x)] \quad (2.3.1)$$

Tension and deformation vectors are the following:

$$\mathbf{q}(\xi) = [\varepsilon_0 \quad \chi \quad \gamma], \quad \mathbf{p}(\xi) = [N, M, V] \quad (2.3.2)$$

Where ξ is the normalized abscissa, the beam forces \mathbf{p} are related to the nodal forces N_j, M_j, M_i , and plane sections remain plane in order to determine the longitudinal strain ε_{xx} . To evaluate the transverse strains are assumed several shape functions Vecchio Collins (1988). In addition to the classical assumption derived by the Timoshenko beam theory, that keep the shear strain constant along the depth of the section, the authors have

also introduced a parabolic distribution obtaining equally acceptable results in both cases. To determine the deformations in the transverse direction ε_{yy} , the equilibrium in y direction between concrete and steel is imposed in this way an iterative procedure begin in order to determine a complete deformation vector $[\varepsilon_{xx} \ \varepsilon_{yy} \ \varepsilon_{xy}]$ associated with each layer. Once known the deformation vector a biaxial constitutive law is applied in order to determine the tension vector. For each fibre an incremental constitutive relationship is derived from the static condensation of the degrees of freedom in y direction.

$$\begin{bmatrix} d\sigma_{xx}^i \\ d\sigma_{xy}^i \end{bmatrix} = \begin{bmatrix} K_a^i & K_{as}^i \\ K_{sa}^i & K_s^i \end{bmatrix} = \begin{bmatrix} d\varepsilon_{xx}^i \\ d\varepsilon_{xy}^i \end{bmatrix} \quad (2.3.3)$$

The stiffness coefficient are calculated as follow:

$$\begin{aligned} K_a^i &= (D_{11}^i - D_{21}^i \cdot D_{12}^i \cdot \alpha^i), & K_s^i &= (D_{33}^i - D_{23}^i \cdot D_{32}^i \cdot \alpha^i) \\ K_{as}^i &= (D_{13}^i - D_{23}^i \cdot D_{12}^i \cdot \alpha^i), & K_{sa}^i &= (D_{31}^i - D_{32}^i \cdot D_{21}^i \cdot \alpha^i) \end{aligned} \quad (2.3.4)$$

α^i is a percentage of the transverse reinforcement and D_{mn}^i are the coefficient of the material matrix in the i-th fibre .

As constitutive relationship for concrete, the authors chose a modified microplane model " which links together and an equivalent uniaxial rotating model. In particular, in the modified model, only microplane normal components are monitored. Strains are subdivided into “weak” and “strong” components along the principal strain directions, therefore, tensions are found for the two directions w (weak) s (strong)

$$s_k^w = s(e_k^w); \quad s_k^s = C_k^s \cdot e_k^w \quad (2.3.5)$$

For each k-th micoplane. Regarding weak microplane, the constitutive model is based on Mander et. al (1988), while for the stroger one, a linear elastic relationship is used. Stresses and strains are calculated as follow:

$$\varepsilon_k = e_k^w + e_k^s; \quad \sigma_k = s_k^w + s_k^s \quad (2.3.6)$$

Tension vector $\boldsymbol{\sigma} = [\sigma_{xx} \ \sigma_{yy} \ \tau_{xy}]$ is derived by the virtual work principle, while the material matrix \mathbf{D} can be obtained using an incremental form of constitutive relationship. Both $\boldsymbol{\sigma}$ and \mathbf{D} are numerically evaluated, by monitoring a suitable number of microplanes. (generally eight).

Stress-strain relationship for steel is described by Menegotto and Pinto (1977).

The originality of this model compared to the strut and tie is the introduction of a biaxial constitutive law based on a "Microplane. The biaxial approach of this formulation lead toward an advanced model, able to describe in a more accurate manner the behaviour of reinforced concrete structure without superimposition of different models.

On the other hand is difficult to get the influence of the different contributions to the shear resistance. Indeed, the author reports deficiencies in the introduction of the dowel effects as well as the relative displacement of the concrete surfaces across large cracks.

Further this model tend to underestimate the shear resistance in some areas of the beam where the shear resistant mechanism is well represented with a strut and tie, since the local effects caused by support and loading details cannot be predicted with the proposed formulation, according to the author. The computational complexity of the model is similar to the others analyzed so far while no deterrent effect are taken into account in this element. Particularly considering that the macro stress tensor σ and the concrete fibre constitutive matrix \mathbf{D} must be numerically evaluated for each fibre and for each load step.

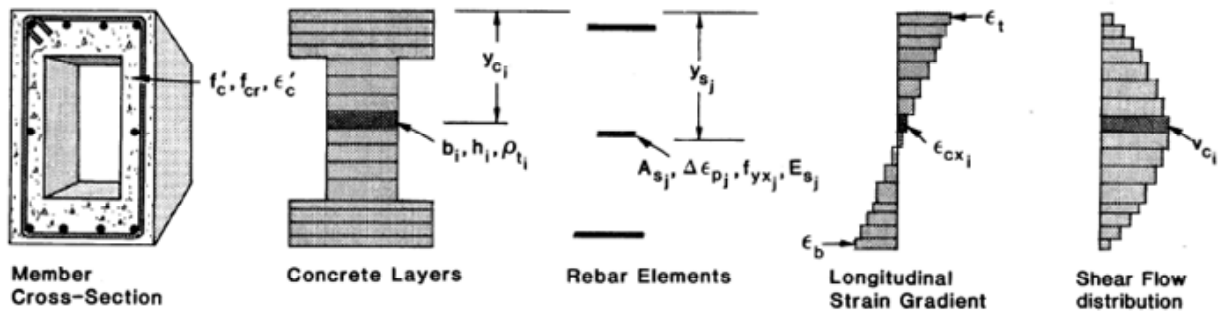
2.4 Fibre Beam-Column Element Using Smeared Crack Models

In this approach, the cracked concrete is modeled as an orthotropic material, continuous, in which compatibility, equilibrium and constitutive relationship are formulated in terms of average stresses and strains. This approach is particularly suitable for the analysis of a single section under combined loads as shown in the following paragraph.

2.4.1 Vecchio and Collins's model

Vecchio e Collins (1988) introduced the "dual-section analysis" to predict the response of a reinforced concrete beam subject to shear, the authors developed a sectional model only, without introducing it within a finite element.

The beam is a 2D plane and the section is discretized by layers as shown in fig. 2.4-1, the only compatibility relationship required is the plane section remain plane after deformation, The shear stresses calculation is carried out by finite differences between normal stresses evaluated at each end of the fibre.



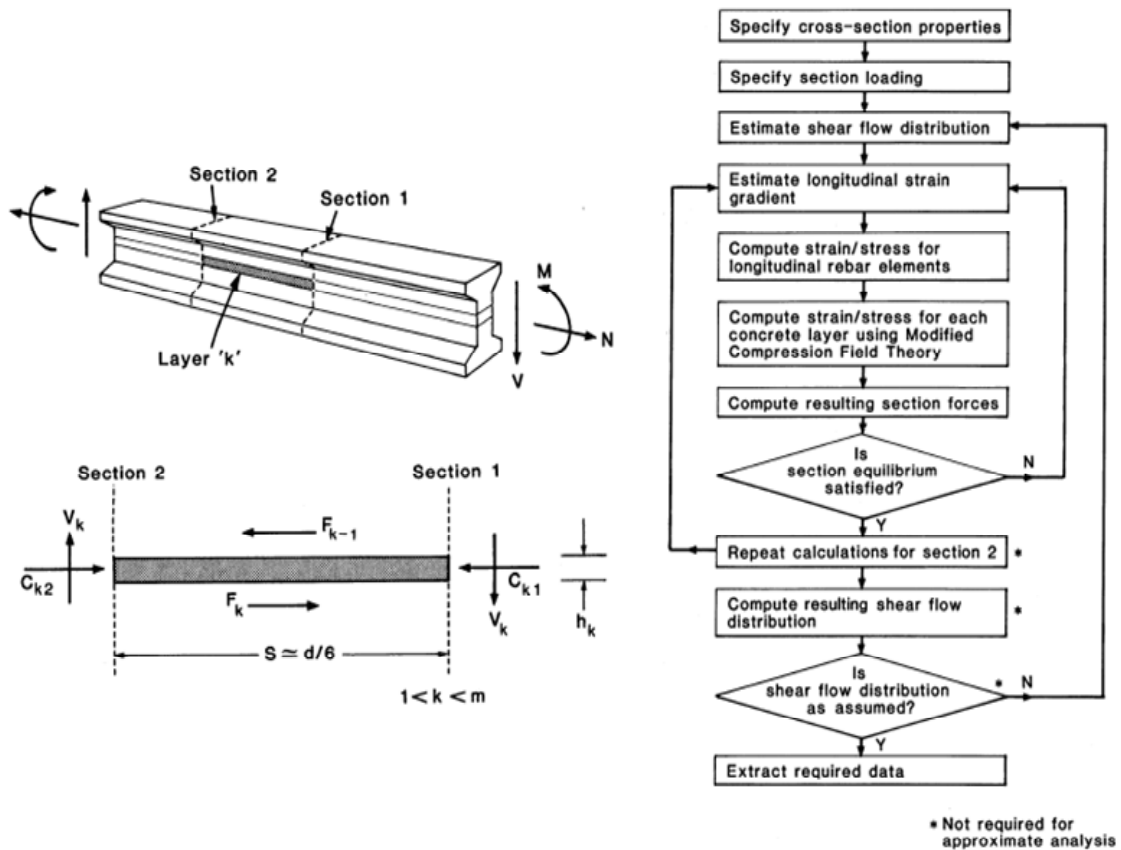
Beam section discretisation. Estimates of longitudinal strain gradient and shear flow distribution are required across section [Vecchio and Collins, 1988]

fig. 2.4-1

$$\tau_{xy}(x) = -\frac{1}{b(y)} \cdot \int_{-y_b}^y \frac{\partial \sigma_{xx}}{\partial x} \cdot b(y) dy \quad \text{dove} \quad \frac{\partial \sigma_{xx}}{\partial x} \approx \frac{\sigma_{xx}(x_2) - \sigma_{xx}(x_1)}{S} \quad (2.4.1)$$

y_b is the coordinate of the last fibre, $\sigma_{xx}(x_2)$ e $\sigma_{xx}(x_1)$ are the normal tension in fibres evaluated in two section separated by a distance S (this distance is assumed $d/6$ with $d =$ beam depth).

The iterative procedure for the analysis of the section is represented in the follow flow chart fig. 2.4-2.



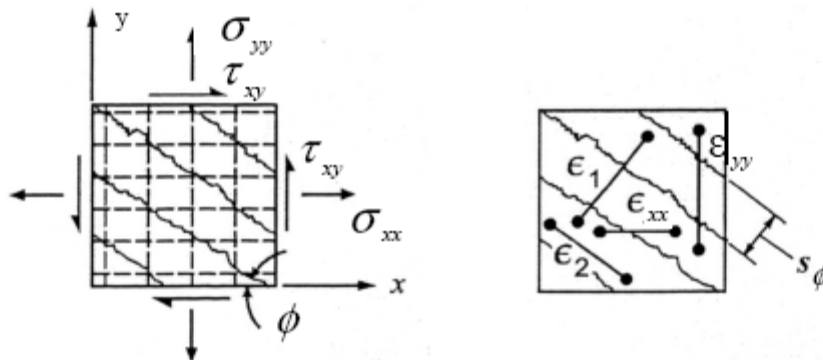
Dual section analysis: (a) scheme and free-body diagram for concrete layer k , and (b) solution procedure for beam analysis model [Vecchio and Collins, 1988]

fig. 2.4-2

The analysis starts with the estimation of shear and axial strains. The equilibrium for each one of the two sections at distance S is satisfied by an inner loop. Outer loop checks if the shear stress calculated are equal (within an acceptable tolerance) to the initially assumed one. Vecchio and Collins (1988) proposed two alternative and approximate solutions based on a constant or a parabolic shear strain with the aim of simplifying the procedure. This improvement eliminate the iterations on shear strains estimates (indicated with an asterisk in the flowchart of fig. 2.4-2.). Generally the approximate procedures is close to more accurate full dual-section analysis approach in terms of global behaviour.

The constitutive relationship adopted was the modified compression field theory (MCFT), which in its first formulation (Vecchio Collins (1986)) was able to reproduce only monotonic loadings. In twenty years, some improvement of the theory where carried out in order to pass these limitation.

According to MCFT theory, the cracked concrete is considered as an orthotropic material along the two principal stress and strain direction as shown in fig. 2.4-3.



Stresses, strains and smeared cracks in MCFT [adapted from Vecchio and Collins, 1988]

fig. 2.4-3

Vecchio and Collins's sectional model use an iterative procedure in order to calculate the shear distribution over the section. This approach give accurate results for beam subjected to monotonic loading while the procedure is really time-consuming if implemented in a finite element program. The dual-section analysis features also inherent difficulties in accurately evaluating the shear stress profile on the two sections in a numerical stable manner Benz (2000).

Indeed, the two sections must be evaluated to the same value of shear and axial load, in order to avoid numerical instabilities. Even a small difference in axial force between the two sections implies inaccuracy in shear stress profile. Discontinuities in shear stress profile could be predicted for different depths of cracking subjected to different moments. This problem, was overcome by Vecchio and Collins [1988] using a kinematics constraint, or rather the introduction of a shear strain or shear stress distribution, in the definition of the shear profile. This makes the procedure more stable and simple, and even if in this way the shear stress cannot satisfy section equilibrium (because of open shear stress profile), the approximation is considered by the author consistent with the approximation of the model. The model can predict shear strength very well compared with the experimental results, an exception are those beams lightly shear reinforced. This limitation (reduced accuracy in shear-critical beams containing very little or no transverse reinforcement), Vecchio (2000) introduced a new conceptual model for describing the behaviour of cracked reinforced concrete – the Disturbed Stress Field Model DSFM.

Finally, since the analytical procedure is a sectional model based on the assumption that plane sections remain plane, it is not capable of predicting the local effects present in the loading and support zones.

2.4.2 Bentz's Model

To overcome the limitations of the dual section analysis, Benz (2000) proposed an approach called Longitudinal sectional stiffness method. This approach was formulated for predicting the load-deformation response of RC sections subjected to bending moments, axial loads and shear forces. The assumption of this procedure are plane sections remain plane and the distribution of shear stresses across the section is defined by the rate of change of flexural stresses. An initial shear strain profile is required as function of the mean sectional shear deformation $\bar{\gamma}$ (for the first load step, the elastic Jourawski solution is assumed):

$$\gamma_{xy} = \frac{A \cdot Q(y)}{I \cdot b(y)} \cdot \bar{\gamma} \quad \text{con} \quad \bar{\gamma} = \frac{V}{A} \quad (2.4.2)$$

Once calculated the axial deformation of the beam with the classic Eulero Bernoulli theory and shear deformation with (2.4.2), the relationship between the section's elongation, curvature and mean shear strain and the fibre strains can be derived :

$$\hat{\boldsymbol{\varepsilon}}(x) = \mathbf{B} \cdot \boldsymbol{\varepsilon}_s \quad (2.4.3)$$

Where $\hat{\boldsymbol{\varepsilon}}(x) = \begin{bmatrix} \varepsilon_{xx} & \gamma_{xy} \end{bmatrix}$ e $\boldsymbol{\varepsilon}_s = \begin{bmatrix} \varepsilon_0 & \chi & \gamma \end{bmatrix}$.

At each fibre, the differential increment of stress along the beam axis can be computed as follows

$$d\boldsymbol{\sigma} = \mathbf{D}_{nt} \cdot d\boldsymbol{\varepsilon} \quad (2.4.4)$$

In which \mathbf{D}_{nt} is the nodal tangent stiffness matrix, $\boldsymbol{\varepsilon} = \begin{bmatrix} \varepsilon_{xx} & \varepsilon_{yy} & \gamma_{xy} \end{bmatrix}$ and $\boldsymbol{\sigma} = \begin{bmatrix} \sigma_{xx} & \sigma_{yy} & \tau_{xy} \end{bmatrix}$.

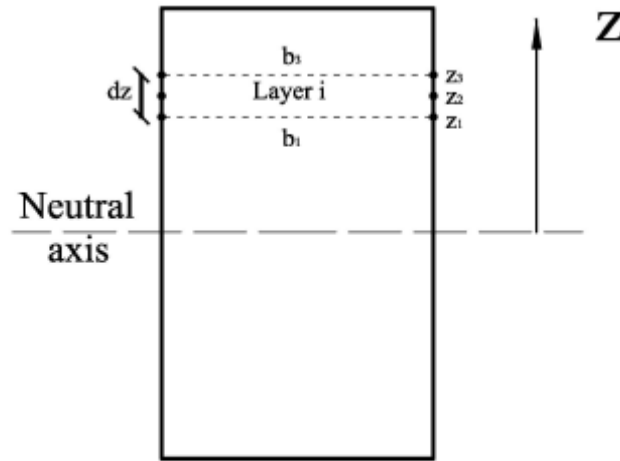
For the equilibrium in the transverse direction, the component $\sigma_{yy} = 0$ at each fibre.

From this equilibrium equation a static condensation of the DOF in the y-direction is obtained, and an incremental constitutive relation is derived:

$$d\hat{\boldsymbol{\sigma}} = \begin{bmatrix} d\sigma_{xx} \\ d\tau_{xy} \end{bmatrix} = \hat{\mathbf{D}}_{nt} \cdot \begin{bmatrix} d\varepsilon_{xx} \\ d\gamma_{xy} \end{bmatrix} = \hat{\mathbf{D}}_{nt} \cdot d\hat{\boldsymbol{\varepsilon}} \quad (2.4.5)$$

In which $\hat{\mathbf{D}}_{nt}$ is the condensed nodal stiffness matrix, this include spread reinforcement. Both the tangent stiffness matrices $\hat{\mathbf{D}}_{nt}$ e \mathbf{D}_{nt} are non symmetric. These matrices are integrated along the section in order to generate the section stiffness matrix \mathbf{K}_s , for each layer tree point of integration are considered z_1 z_2 e z_3 at different depth(fig. 2.4-4). At each depth z_1 , z_2 , and z_3 , a width b_1 , b_2 , and b_3 of the section is associated as well as three local nodal stiffness matrices $\hat{\mathbf{D}}_{nt}$ with coefficients:

$$\begin{bmatrix} j & k \\ m & n \end{bmatrix}_p \quad \text{con } p=1,2,3 \quad (2.4.6)$$



Parameters for global stiffness matrix calculation [adapted from Bentz, 2000]

fig. 2.4-4

This mean that for each point of integration p, the equations (2.4.5) became:

$$\begin{bmatrix} d\sigma_{xx} \\ d\tau_{xy} \end{bmatrix} = \begin{bmatrix} j & k \\ m & n \end{bmatrix} \cdot \begin{bmatrix} d\varepsilon_{xx} \\ d\gamma_{xy} \end{bmatrix} \quad (2.4.7)$$

By integrating this differential system, stiffness matrix \mathbf{K}_{s_layer} for each layer is obtained, while stiffness matrix \mathbf{K}_s for the whole section is calculated by the simple sum of each layer.

Once known \mathbf{K}_s , the following relationship can be wrote as follow:

$$\begin{bmatrix} dN \\ dM \\ dV \end{bmatrix} = \mathbf{K}_s \cdot \begin{bmatrix} d\varepsilon_0 \\ d\chi \\ d\gamma \end{bmatrix} \quad (2.4.8)$$

Since the deformation increments s given by the following equation:

$$\frac{d\boldsymbol{\varepsilon}_s}{dx} = \mathbf{K}_s^{-1} \cdot \begin{bmatrix} \frac{dN}{dx} = 0 \\ \frac{dM}{dx} = v \\ \frac{dV}{dx} = 0 \end{bmatrix} \quad (2.4.9)$$

Using the (2.4.5), (2.4.3) and the (2.4.9) and changing the variable the following relationship can be reached:

$$\frac{d\hat{\boldsymbol{\sigma}}_s}{dx} = \frac{d\hat{\boldsymbol{\sigma}}}{d\hat{\boldsymbol{\varepsilon}}} \frac{d\hat{\boldsymbol{\varepsilon}}}{d\boldsymbol{\varepsilon}_s} \frac{d\boldsymbol{\varepsilon}_s}{dx} = \hat{\mathbf{D}}_{nt} \cdot \mathbf{B} \cdot \mathbf{K}_s^{-1} \cdot \begin{bmatrix} 0 \\ V \\ 0 \end{bmatrix} \quad (2.4.10)$$

In the end, the τ_{xy} diagram can be calculated by introducing $\frac{d\sigma_{xx}}{dx}$ evaluated by (2.4.10) in (2.4.1) equation.

The constitutive relationship used by Benz is MCFT, this formulation can satisfy the equilibrium between the fibre and is able to calculate the resistance and the deformation in a section subjected by M, N, and T. The Hypothesis of plane section remain plane and $\sigma_{yy} = 0$ limit the range of validity of the analysis away from the restrained areas and concentrated loads, the response of elements without shear reinforcement tends to be inaccurate because of the limitations inherent in MCFT. The cyclical behavior of the material has not been implemented, the model also has not been tested in a finite element program which could assemble complex structures.

2.4.3 Remino' Model.

Remino (2004) formulated a fibre Timoshenko force-based beam-column element. The force-based formulation is based on the solution strategy proposed by Spacone et al. (1996). The element (shown in fig. 2.4-5 with without rigid body movements) has two nodes and two degrees of freedom per node:

$$\mathbf{u}(x) = [u(x) \quad \theta_z(x)] \quad (2.4.11)$$

From the nodal forces \mathbf{Q} , the section force vector $\mathbf{D}(x)$ is computed as follows:

$$\mathbf{D}(x) = \mathbf{N}^{st}(x) \cdot \mathbf{Q} \quad (2.4.12)$$

In which $\mathbf{D}(x) = \begin{bmatrix} N \\ M \\ V \end{bmatrix}$, $\mathbf{N}^{st}(x) = \begin{bmatrix} 1 & 0 & 0 \\ 0 & \frac{x}{l} - 1 & \frac{x}{l} \\ 0 & \frac{x}{l} & \frac{1}{l} \end{bmatrix}$, $\mathbf{Q} = \begin{bmatrix} N_j \\ M_i \\ M_j \end{bmatrix}$.

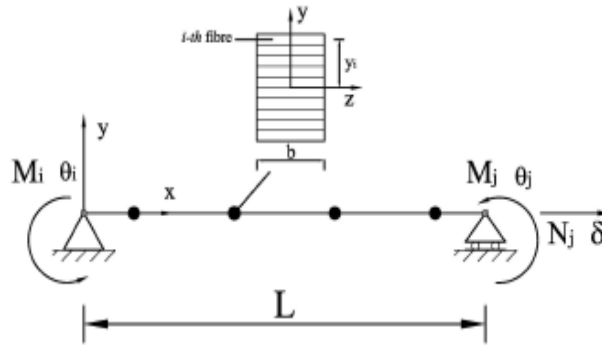
The stiffness matrix is numerically evacuated, using finite difference formula. The m-th-n-th element of the section stiffness matrix is calculated using the following expression:

$$k_{mn} = \frac{D_m \cdot (\mathbf{d} + \delta d_n) - D_m \cdot \mathbf{d}}{\delta d_n} \quad (2.4.13)$$

In which D_m is the m-th element of the section forces vector, \mathbf{d} è section deformation vector, δd_n is a null vector except for the n-th term equal to:

$$\delta d_n = \text{sign}(\Delta d_{n,previous}) \cdot \sqrt{\varepsilon_{tolerance}} \quad (2.4.14)$$

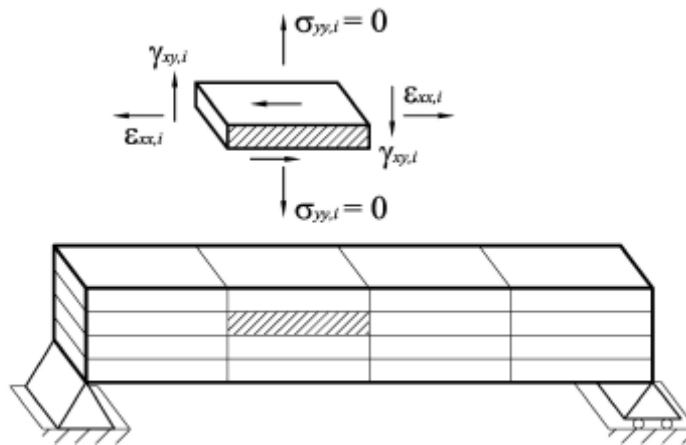
In which $\Delta d_{n,previous}$, is the variation of the n-th section deformation with respect to the last converged step of the analysis: $\varepsilon_{tolerance}$ is the program's numerical tolerance.



Beam element in local reference system – section discretisation at the selected integration points [Remino, 2004]

fig. 2.4-5

The constitutive relationship is derived by Rose-Shing (2001) is similar to MCFT but with some difference in terms of constitutive relation aggregate-interlock law, and crack kinematics. This model is found to be particularly suitable for shear analysis of RC structures, it requires the input quantities illustrated in fig. 2.4-6.



Fibre input data for Rose-Shing model, when used as a constitutive law [Remino, 2004]

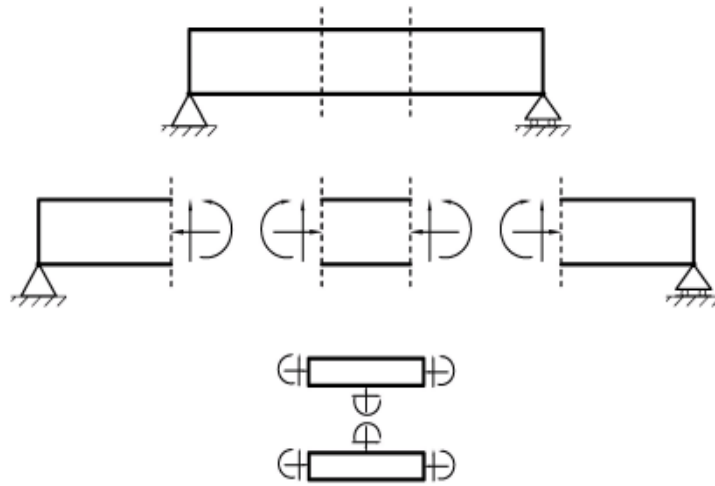
fig. 2.4-6

The main characteristic of this model is the implementation of a "smeared crack" in a program fem for the analysis of complete structures. A direct interaction between the section forces is considered. Unfortunately, numerical difficulties were found in analyzing the cyclical behavior of the fibers, the numerical results compared with the experimental data are not always accurate.

2.4.4 Bairan's Model

Bairan (2005) developed a 3D model for the analysis of reinforced concrete sections subject to bending moment, shear, axial force and torque. The author designed a model that considers the section distortion due to shear and torque through a generalized state of stress strain of the section. This approach allows consider the equilibrium of the section separated from the equilibrium of whole beam, allowing the introduction of models developed separately for sections, in any type of beam formulation.

Given a section, the whole 3D state is obtained through the distorting effects \mathbf{u}^w superimposed to the traditional ones due to the conservation of plane sections \mathbf{u}^{ps} , the physical meaning of this decomposition is schematically shown in fig. 2.4-7.



Decomposition of 3D equilibrium problem in a structural level problem and a local sectional problem
[Bairan, 2005]

fig. 2.4-7

While the structural equilibrium is insured by the resisting forces derived from \mathbf{u}^{ps} , the sectional equilibrium is given by the internal forces resulting from \mathbf{u}^w . Since the displacement field is decomposed as follows:

$$\mathbf{u} = \mathbf{u}^{ps} + \mathbf{u}^w \quad (2.4.15)$$

The same decomposition can be applied in stress and strain field as follow:

$$\boldsymbol{\varepsilon} = \boldsymbol{\varepsilon}^{ps} + \boldsymbol{\varepsilon}^w \quad e \quad \boldsymbol{\sigma} = \boldsymbol{\sigma}^{ps} + \boldsymbol{\sigma}^w \quad (2.4.16)$$

Rewriting in the weak form the 3D differential equilibrium equations of an elementary volume using as weighting function the displacement field \mathbf{u} , the following residual equations of a beam differential element are obtained:

$$\begin{cases} \mathbf{R}^{ps}(x) = \mathbf{G}^{ps}(\boldsymbol{\sigma}') - \mathbf{F}^{ps}(\boldsymbol{\sigma}^{ps}) - \mathbf{F}^{ps}(\boldsymbol{\sigma}^w) = 0 \\ \mathbf{R}^w(x) = \mathbf{G}^w(\boldsymbol{\sigma}') - \mathbf{F}^w(\boldsymbol{\sigma}^{ps}) - \mathbf{F}^w(\boldsymbol{\sigma}^w) = 0 \end{cases} \quad (2.4.17)$$

In which $\mathbf{R}^{ps}(x)$ is the residual in the space of the plane-section displacement field, and $\mathbf{R}^w(x)$ is the residual in the space of the distortion displacement field. This approach consists in founding an appropriate expression of $\boldsymbol{\sigma}_w$ to satisfy the equation $\mathbf{R}^w(x) = 0$, which represents the cross-section constitutive relation, and then in solving the beam equilibrium equation $\mathbf{R}^{ps}(x) = 0$. So the procedure aims to solve a 3D problem through two decoupled components: a 1D beam problem, using standard frame elements to

discretise the plane section field and a 2D sectional problem, using bi-dimensional elements, locally at the beam's integration points, to discretise the distortion field (equations (2.4.17)). In particular, in the case of RC beams, the sections are subdivided in 2D elements simulating the concrete matrix, 1D elements simulating the transversal reinforcements, and point elements simulating the longitudinal reinforcements. Indicated with \mathbf{d}^w the vector of nodal values of these elements, the distortion field results:

$$\mathbf{u}^w = \mathbf{N}^w \cdot \mathbf{d}^w \quad (2.4.18)$$

with \mathbf{N}^w interpolation matrix that contain shape functions. Imposing that the nodal distortions satisfy the equilibrium over the control sections:

$$\mathbf{d}^w = \mathbf{A}^* \cdot \boldsymbol{\xi}^* \quad (2.4.19)$$

In which $\boldsymbol{\xi}^* = [\mathbf{e}_s^* \quad \mathbf{e}_s^{*'}] = [\varepsilon_0 \quad \chi_x \quad \chi_y \quad \chi_z \quad \varepsilon_0' \quad \chi_x' \quad \chi_y' \quad \chi_z']$ is the generalized deformation vector of the section and its derivative, the matrix \mathbf{A}^* is derived by the material stiffness matrix \mathbf{D} , the shape functions \mathbf{N}^w are the derivative of \mathbf{B}^w and \mathbf{B}^{ps*} which are the functions that interpolate the deformations \mathbf{e}_s^* . Referring to (2.4.16) the strains can be expressed as:

$$\boldsymbol{\varepsilon}^{ps} = \mathbf{B}^{ps} \cdot \mathbf{e}_s \quad e \quad \boldsymbol{\varepsilon}^w = \mathbf{B}^w \cdot \mathbf{d}^w = \mathbf{B}^w \cdot \mathbf{A}^* \cdot \boldsymbol{\xi}^* \quad (2.4.20)$$

where $\mathbf{e}_s = [\varepsilon_0 \quad \chi_{xy} \quad \chi_{xz} \quad \chi_x \quad \chi_y \quad \chi_z]$ is the vector of generalised section strains, and the matrix \mathbf{B}^{ps} is the strain interpolation matrix for \mathbf{e}_s .

From (2.4.20), it can be noticed that the distortion field is a linear function of the eight components of the vector $\boldsymbol{\xi}^*$, in which two components are not independent from the others. Hence, a reduction of the required degrees of freedom (from 8 to 6) is obtained by means of the matrix Ξ which condensates the derivatives of axial elongation and torsion curvature taking into account the actual distributed axial load and torsion moment.

$$\boldsymbol{\xi}^* = \Xi \cdot \boldsymbol{\xi} \quad (2.4.21)$$

A crucial step of the model is expressing the $\boldsymbol{\xi}$ vector as a function of the generalized section strains. To reach this goal, the author introduces the generalized shear deformation through the virtual work principle, reaching the following relationship:

$$\boldsymbol{\xi} = \boldsymbol{\Omega} \cdot \mathbf{e}_s \quad (2.4.22)$$

noting that such matrix $\boldsymbol{\Omega}$ has not been explicitly defined for the case of a generic RC

section. Substituting the (2.4.22) and (2.4.21) in (2.4.19) the distortion nodal values result:

$$\mathbf{d}^w = \mathbf{A}^* \cdot \boldsymbol{\Omega} \cdot \mathbf{e}_s \quad (2.4.23)$$

implying that the non-local contribution due to the distortion-warping field can be computed as a function of local variables alone, in particular the generalised section strains. A new definition of $\boldsymbol{\varepsilon}^w$ is obtained by substituting the (2.4.23) in (2.4.20), whilst the stresses of Eq. (2.4.16) can be derived from the following equations:

$$\boldsymbol{\sigma}^{ps} = \mathbf{D} \cdot \boldsymbol{\varepsilon}^{ps} \quad e \quad \boldsymbol{\sigma}^w = \mathbf{D} \cdot \boldsymbol{\varepsilon}^w \quad (2.4.24)$$

In which \mathbf{D} is the material matrix, which can be of any type, in general anisotropic.

Finally, through the virtual work principle, the generalized stresses \mathbf{s}_s are derived and hence the section stiffness matrix is obtained:

$$\begin{aligned} \mathbf{s}_s &= \int_A \mathbf{B}^{psT} \boldsymbol{\sigma} dA + \boldsymbol{\Omega}^T \boldsymbol{\Xi}^T \mathbf{A}^{*T} \int_A \mathbf{B}^{psT} \boldsymbol{\sigma} dA \\ \mathbf{K}_s &= \int_A \mathbf{B}^{psT} \cdot \mathbf{D} \cdot \mathbf{B}^{ps} dA + \int_A \mathbf{B}^{psT} \cdot \mathbf{D} \cdot \mathbf{B}^w dA \cdot \mathbf{A}^* \cdot \boldsymbol{\Omega} \cdot \boldsymbol{\Xi} + \\ &+ \boldsymbol{\Omega}^T \cdot \boldsymbol{\Xi}^T \cdot \mathbf{A}^{*T} \cdot \int_A \mathbf{B}^{wT} \cdot \mathbf{D} \cdot \mathbf{B}^w dA + \boldsymbol{\Omega}^T \cdot \boldsymbol{\Xi}^T \cdot \mathbf{A}^{*T} \cdot \int_A \mathbf{B}^{wT} \cdot \mathbf{D} \cdot \mathbf{B}^w dA \cdot \mathbf{A}^* \cdot \boldsymbol{\Omega} \cdot \boldsymbol{\Xi} \end{aligned} \quad (2.4.25)$$

For the constitutive model was implemented a rotating smeared crack, in which the material behavior is described along the principle directions. For concrete in compression is considered Vecchio Selby (1991) relationship able to model the cyclic loading. For the concrete in tension is considered a linear elastic behavior until the cracking and a descending curve after cracking described by Cervenka (1985), unloading and reloading are assumed linear. For steel has taken a classic elastic-plastic model.

The author used a triaxial stress state to calculate the resistance in the principle directions of breaking through a domain consists of a three-dimensional surface. The stiffness matrix of the material is calculated along the principal directions, then rotated in the x-y direction through an appropriate transformation matrix. Before transformation the matrix result diagonal, whose elements are the secant modulus of the principal directions. The shear modulus is given by

$$G_{ij} = \frac{1}{2} \frac{(\sigma_i - \sigma_j)}{(\varepsilon_i - \varepsilon_j)} \quad (2.4.26)$$

To summarize: the model proposed by Bairan is able to simulate the complete interaction between the six components of internal action and deformation of a general cross section with an arbitrary arrangement of longitudinal reinforcement. This element is certainly an advanced model for reinforced concrete elements, obtained developing a sectional model in which the non-local effects due to section's warping-distortion induced by shear/torsion are derived from local quantities such as the generalized section strains. Hence, equilibrium and compatibility at the sectional level (inter-fibre equilibrium) are satisfied because no a priori hypotheses on the shear flow or strain distribution are needed. On the other hand the development of the model also requires some approximations with regard to the distortion field and its discretization, the variation of distortion along the beam, the behaviour of the material and the discretization of the section. It's not clear how these might affect the quality of approximations, the numerical stability and the field of applicability of the method. Future developments include the implementation of the sectional model proposed in a finite element program for analysis of frames subject to static and dynamic loads. Through this route is expected to give an answer to previous questions.

2.5 Fibre Beam-Column Element Using Damage Models.

The damage models require some concepts of fracture mechanics to simulate the propagation of cracks. These include parameters such as fracture energy, which represents the energy required to create a new rupture of the material expressed unit per length. This parameter is an intrinsic characteristic of the material for concrete and its value is about

$$G_f = 0,3 \frac{kNm}{m}.$$

2.5.1 Modello di Mazars

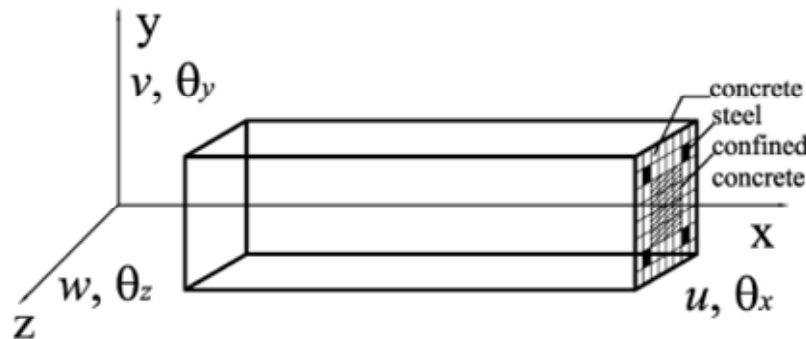
Mazars et al. (2006) developed a 3D element with stiffness approach based on Timoshenko beam theory. The interpolation functions depends on the material properties (Young's modulus and shear modulus for each fiber) only in the first step of loading, while in the following functions are assumed constant. The finite element with two nodes and six degrees of freedom per node, is shown in fig. 2.5-1 while the displacement vector is the following:

$$\mathbf{u}(x) = [u(x) \quad v(x) \quad w(x) \quad \theta_x(x) \quad \theta_y(x) \quad \theta_z(x)] \quad (2.4.27)$$

The section stiffness matrix \mathbf{K}_s , relating the vectors of the generalized stresses $[N \quad V_x \quad V_y \quad M_x \quad M_y \quad M_z]$ and strains (with rigid body movements eliminate) is the calculate as follow:

$$\mathbf{K}_s = \begin{bmatrix} \int_A E dA & 0 & 0 & 0 & \int_A E \cdot z dA & -\int_A E \cdot y dA \\ 0 & k_y \cdot \int_A G dA & 0 & -k_y \cdot \int_A G \cdot z dA & 0 & 0 \\ 0 & 0 & \int_A G dA & k_z \cdot \int_A G \cdot y dA & 0 & 0 \\ 0 & 0 & 0 & k_z \cdot \int_A G \cdot (k_z \cdot y^2 + k_y \cdot z^2) dA & 0 & 0 \\ 0 & 0 & 0 & 0 & \int_A E \cdot z^2 dA & -\int_A E \cdot y \cdot z dA \\ 0 & 0 & 0 & 0 & 0 & \int_A E \cdot y^2 dA \end{bmatrix} \quad (2.4.28)$$

Where A is the section area, E is the young modulus and G is the shear modulus, of each fibre, k_y e k_z are correction factors due to shear, depending on the geometry of the section and the material.

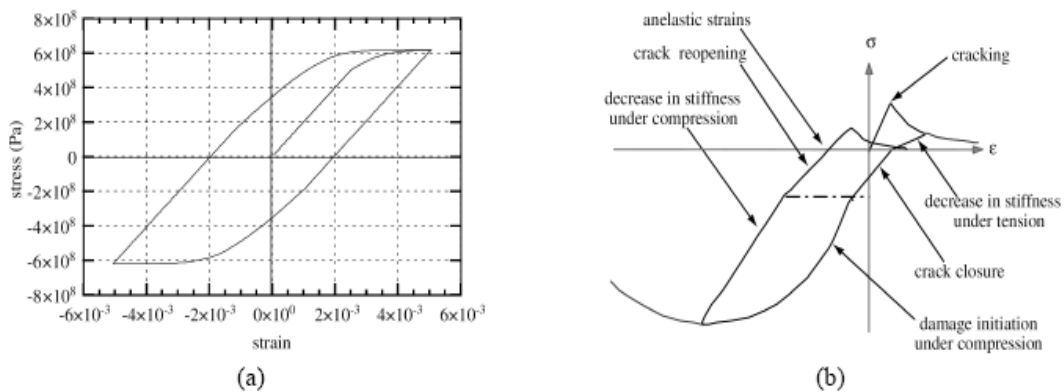


Multifibre beam element to model a RC structural element

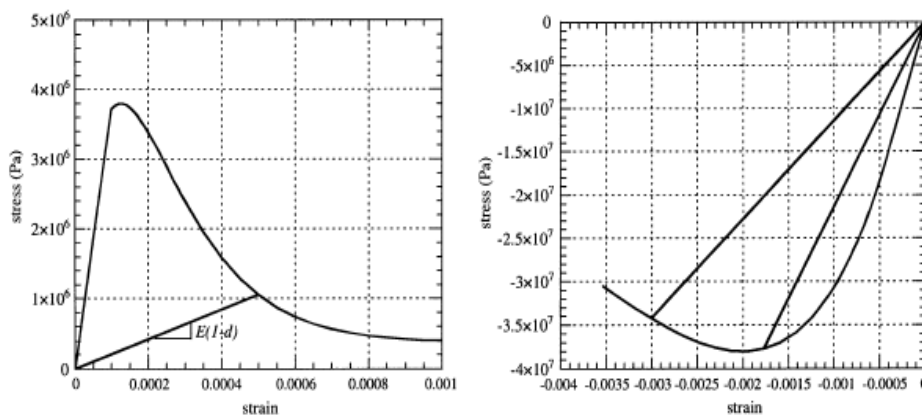
fig. 2.5-1

For steel a classical plasticity model is adopted while for concrete are introduce two different damage models: Mazars (fig. 2.5-2(a)) characterized by a variable damage scale, used for monotonic loadings and La Bordiere (fig. 2.5-2 (b)) which, having two variable scales of damage and including the closing of cracks and permanent effects was adopted to model cyclic loading. In any case, the damage model affects only the normal stresses.

The model is affected by two main limitations, the effect of distortion and damage model of isotropic type are not included. The latter in particular implies that the element is unable to reproduce the typical response of anisotropic sections in reinforced concrete when the cracks are caused by the shear. This means that the model can be used in studying the global behavior of slender elements as shown by the numerical results for general purpose more accurate and robust relationship are required. The use of constitutive relations with local "strain softening"(as this case) mean that the results are mesh-dependent, thus increasing the complexity of the model.



a) Elastoplastic model with kinematics hardening for steel and (b) Uniaxial response of the La Bordiere damage model for concrete [Mazars *et al.*, 2006]



Response of the Mazars damage model for concrete in tension and compression [Mazars *et al.*, 2006]

fig. 2.5-2

CHAPTER 3

Fibre beam-column beam formulation

3.1 Sommario

In questa tesi ci si propone di riuscire a modellare il comportamento di elementi strutturali in cemento armato cercando di cogliere l'interazione che nasce tra sforzo normale, momento flettente e taglio in campo non lineare. Per fare ciò è stato ideato un elemento finito nuovo sulla linea dei modelli "smeared" visti nel capitolo 2. L'elemento finito in questione è un modello a fibre basato sulla flessibilità Spacone Taucer Filippou (1996) sul quale è implementato un legame di tipo biassiale con fessurazione diffusa, per cogliere l'accoppiamento tra le sollecitazioni e descrivere in maniera unitaria e coerente il comportamento strutturale. In questo capitolo è descritta la formulazione analitica dell'elemento finito a fibre, non si fa cenno al legame biassiale che sarà trattato ampiamente nel capitolo successivo e all'implementazione completa descritta in modo dettagliato nel capitolo 5. Verranno comunque accennati alcuni passi dell'algoritmo di Element State Determination in quanto risulta essere una procedura fondamentale per la formulazione completa dell'elemento.

Lo sviluppo analitico sarà svolto nella forma più generale del "mixed method" (metodo misto) visto che questo approccio chiarisce meglio il processo di "state determination" utilizzato nell'algoritmo di analisi non lineare.

Le ipotesi fatte alla base del sono:

- Piccole deformazioni
- Conservazione delle sezioni piane

Le sollecitazioni all'interno dell'elemento sono rappresentate attraverso una funzione d'interpolazione che le lega alle forze nodali dell'elemento stesso, le azioni interne così ottenute sono tali da soddisfare l'equilibrio entro l'intero elemento. Il soddisfacimento dell'equilibrio è proprio la condizione che sta alla base del metodo.

La formulazione proposta presenta notevoli vantaggi, equilibrio e compatibilità sono ovunque soddisfatti lungo l'elemento, l'equilibrio è rispettato con la scelta delle funzioni di interpolazione, la compatibilità è soddisfatta integrando le deformazioni delle sezioni per avere le deformazioni dell'elemento e gli spostamenti di estremità mentre per soddisfare il legame è stata implementata una procedura iterativa.

3.2 Definition of the vectors involved

The finite element is schematically represented in fig. 3.2-1, in which x y are the local coordinates while X Y represents the global reference system: in this description the following notation is adopted: forces are represented by uppercase and displacements and deformations from the corresponding lower case letters in bold are represented vectors and matrices.

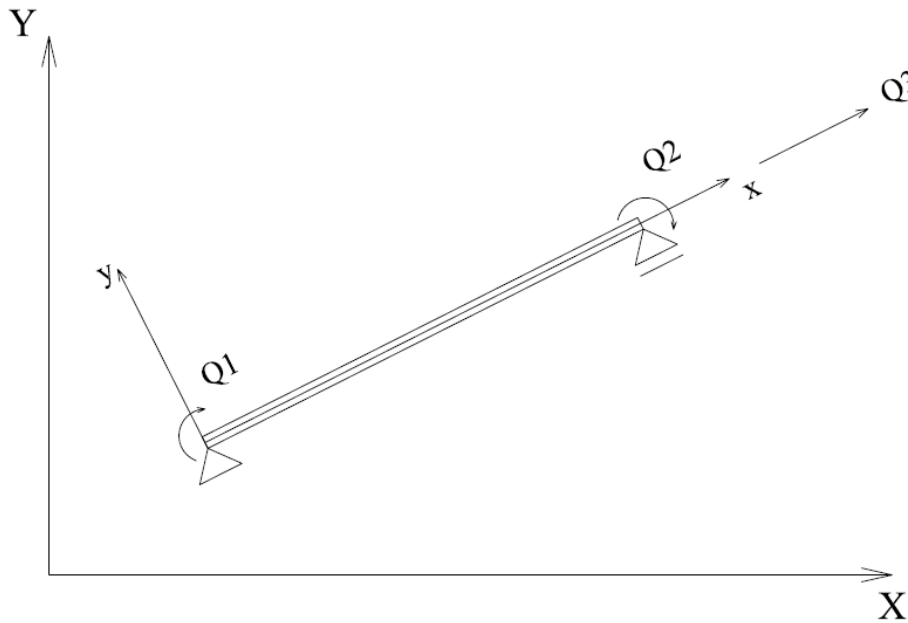


fig. 3.2-1

$$\mathbf{Q} = \begin{Bmatrix} Q_1 \\ Q_2 \\ Q_3 \end{Bmatrix} \text{Element nodal forces} \quad (3.2.1)$$

$$\mathbf{q} = \begin{Bmatrix} q_1 \\ q_2 \\ q_3 \end{Bmatrix} \text{element nodal displacement} \quad (3.2.2)$$

$$\mathbf{D}(x) = \begin{Bmatrix} M(x) \\ T(x) \\ N(x) \end{Bmatrix} \text{section forces} \quad (3.2.3)$$

$$\mathbf{d}(x) = \begin{Bmatrix} \chi(x) \\ \gamma(x) \\ \varepsilon(x) \end{Bmatrix} \text{section deformation} \quad (3.2.4)$$

in order to finalize the study to the shear deformation, the extension to the spatial case was not implemented. This extension can be obtained by adding shear and moment in and orthogonal direction and torque. More sophisticated shape function for the section must be introduced for this extension.

3.3 Formulation of the element starting from mixed method

In general analytical formulation of the element is not considered any constitutive relationship. In agreement with those reported by Spacone et al.(1996) the finite element formulation is based on the mixed method, and it is shown that the particular choice of shape functions dependent on the flexibility, lead to a substantial simplification of the final equation. It is shown that with this particular choice, the mixed method can be reduced to the flexibility method. However the formalism of the mixed method is very useful for understanding the procedure of element determination here described.

In the two fields mixed method Zienkiewicz e Taylor (1989), independent shape functions are used to interpolate the of forces and displacements fields along the element. Called Δ the incrementi of the corresponding quantities, the two fields can be written as follows:

$$\Delta \mathbf{d}^i(x) = \mathbf{a}(x) \cdot \Delta \mathbf{q}^i \quad (3.3.1)$$

$$\Delta \mathbf{D}^i(x) = \mathbf{b}(x) \cdot \Delta \mathbf{Q}^i \quad \text{e} \quad \mathbf{D}^i(x) = \mathbf{b}(x) \cdot \mathbf{Q}^i \quad (3.3.2)$$

Where $\mathbf{a}(x)$ e $\mathbf{b}(x)$ are respectively the interpolation matrices of deformation and forces, the superscript i indicates the i-th iteration. Following the principle of virtual forces we can write the following equation;

$$\int_0^L \delta \mathbf{D}^T(x) \cdot [\delta \mathbf{d}^i(x) - \mathbf{f}^{i-1}(x) \cdot \Delta \mathbf{D}^i(x)] dx = 0 \quad (3.3.3)$$

$\mathbf{f}^{i-1}(x)$ is the flexibility matrix calculated at previous step.

Substituting (3.3.1) and (3.3.2) in (3.3.3) the following equation can be written:

$$\delta \mathbf{Q}^T \cdot \int_0^L \mathbf{b}^T(x) \cdot [\mathbf{a}(x) \cdot \Delta \mathbf{q}^i - \mathbf{f}^{i-1}(x) \cdot \mathbf{b}(x) \cdot \Delta \mathbf{Q}^i] dx = 0 \quad (3.3.4)$$

Since equation (3.3.4) must hold for any $\delta \mathbf{Q}^T$, it follows that:

$$\left[\int_0^L \mathbf{b}^T(x) \cdot \mathbf{a}(x) dx \right] \cdot \Delta \mathbf{q}^i - \left[\int_0^L \mathbf{b}^T(x) \cdot \mathbf{f}^{i-1}(x) \cdot \mathbf{b}(x) dx \right] \cdot \Delta \mathbf{Q}^i = 0 \quad (3.3.5)$$

The expression in square brackets represent the following matrices:

$$\mathbf{F}^{i-1} = \int_0^L \mathbf{b}^T(x) \cdot \mathbf{f}^{i-1}(x) \cdot \mathbf{b}(x) dx \quad (3.3.6)$$

$$\mathbf{T} = \int_0^L \mathbf{b}^T(x) \cdot \mathbf{a}(x) dx \quad (3.3.7)$$

Where \mathbf{F}^{i-1} is the flexibility matrix of the element and \mathbf{T} is a matrix that only depend on the interpolation function matrices. Thus using (3.3.6) and the (3.3.7), the equation(3.3.5) can be written as follow:

$$\mathbf{T} \cdot \Delta \mathbf{q}^i - \mathbf{F}^{i-1} \cdot \Delta \mathbf{Q}^i = 0 \quad (3.3.8)$$

In mixed method the integral form of equilibrium is derived from the virtual displacement principle:

$$\int_0^L \delta \mathbf{d}^T(x) \cdot [\mathbf{D}^{i-1}(x) + \Delta \mathbf{D}^i(x)] dx = \delta \mathbf{q}^T \cdot \mathbf{P}^i \quad (3.3.9)$$

where \mathbf{P} is the vector of applied loads, in equilibrium with the internal forces; substituting the (3.3.1) and the (3.3.2) in the (3.3.9) following equation is obtained:

$$\delta \mathbf{q}^T \cdot \int_0^L \mathbf{a}(x) \cdot [\mathbf{b}(x) \cdot \mathbf{Q}^{i-1} + \mathbf{b}(x) \cdot \Delta \mathbf{Q}^{i-1}] dx = \delta \mathbf{q}^T \cdot \mathbf{P}^i \quad (3.3.10)$$

Since equation (3.3.10) must hold for any $\delta \mathbf{q}$, it follows that:

$$\left[\int_0^L \mathbf{a}^T(x) \cdot \mathbf{b}(x) dx \right] \cdot \mathbf{Q}^{i-1} + \left[\int_0^L \mathbf{a}^T(x) \cdot \mathbf{b}(x) dx \right] \cdot \Delta \mathbf{Q}^{i-1} = \mathbf{P}^i \quad (3.3.11)$$

Written in matrix form:

$$\mathbf{T}^T \cdot \mathbf{Q}^{i-1} + \mathbf{T}^T \cdot \Delta \mathbf{Q}^{i-1} = \mathbf{P}^i \quad (3.3.12)$$

Combining the equations (3.3.8) and (3.3.12) in one system of equations:

$$\begin{bmatrix} -\mathbf{F}^{i-1} & \mathbf{T} \\ \mathbf{T}^T & \mathbf{0} \end{bmatrix} \cdot \begin{Bmatrix} \Delta \mathbf{Q}^i \\ \Delta \mathbf{q}^i \end{Bmatrix} = \begin{Bmatrix} \mathbf{0} \\ \mathbf{P}^i - \mathbf{T}^T \cdot \mathbf{Q}^{i-1} \end{Bmatrix} \quad (3.3.13)$$

The first equation can be solved for $\Delta \mathbf{Q}^i$ and the results substituted in the second equation. In this way the following equation is reached:

$$\mathbf{T}^T \cdot [\mathbf{F}^{i-1}] \cdot \mathbf{T}^T \cdot \Delta \mathbf{q}^i = \mathbf{P}^i - \mathbf{T}^T \cdot \mathbf{Q}^{i-1} \quad (3.3.14)$$

The function $\mathbf{a}(x)$ and $\mathbf{b}(x)$ are completely independent in the general formulation, but can be observed in the equation (3.3.7) how with a particular choice of the shape function $\mathbf{a}(x)$, a

remarkable simplification, in particular a function $\mathbf{a}(x)$ depending on the flexibility can be chosen as follow:

$$\mathbf{a}(x) = f^{i-1} \cdot \mathbf{b}(x) \cdot [\mathbf{F}^{i-1}]^{-1} \quad (3.3.15)$$

An interpolation function thus assigned relates the section deformation with the corresponding element deformation, from (3.3.1) this equation can be written:

$$\Delta \mathbf{d}^i(x) = f^{i-1} \cdot \mathbf{b}(x) \cdot [\mathbf{F}^{i-1}]^{-1} \cdot \Delta \mathbf{q}^i \quad (3.3.16)$$

This particular choice of $\mathbf{a}(x)$ imply that \mathbf{T} is an Identity matrix \mathbf{I} , recalling the (3.3.7):

$$\mathbf{T} = \left[\int_0^L \mathbf{b}^T(x) \cdot f^{i-1} \cdot \mathbf{b}(x) dx \right] \cdot [\mathbf{F}^{i-1}]^{-1} = \mathbf{I} \quad (3.3.17)$$

With this choice of $\mathbf{a}(x)$ the equation (3.3.14) is reduced to:

$$[\mathbf{F}^{i-1}] \cdot \Delta \mathbf{q}^i = \mathbf{P}^i - \mathbf{Q}^{i-1} \quad (3.3.18)$$

This choice of $\mathbf{a}(x)$ reduce the mixed method to the flexibility method. The equation (3.3.18) is the linearized relation between applied loads $\mathbf{P}^i - \mathbf{Q}^{i-1}$ and the corresponding deformation increments $\Delta \mathbf{q}^i$.

Although the classical flexibility method provide the same system of equations (3.3.18), the derivation described above has the following advantages:

- The mixed method provide directly an expression, flexibility dependent for the deformation shape functions $\mathbf{a}(x)$
- It show the consistent implementation of the state determination process.
- Is more general because it allow the choice of different shape functions $\mathbf{a}(x)$.

Since $\mathbf{a}(x)$ and $\mathbf{b}(x)$ are independent and not change during the iterative process, the proposed method coincides with the classical flexibility method, the procedure also reduces to the stiffness method if the constitutive relationship is linear elastic. In other words, the independence between the two fields is not inherent in the definition of shape the functions, but comes from the material nonlinearity.

3.4 Element state determination

The flexibility method was chosen in this work, because is shown in several studies that leads to significant advantages in nonlinear analysis of structures. The main problem of this method is the determination of the resisting forces starting from the deformations of the element. This problem

arises when the finite element formulation is based on the virtual forces principle. The procedure used in the solution of this problem is called element state determination. The problem has been faced and solved through a procedure presented by Spacone et al. (1996).

Although the element is based on flexibility, it is implemented in a program that uses the direct stiffness method, so every step that yield all the general displacement of the structural degrees of freedom. Since the element is based on flexibility there aren't shape functions that correlate deformation strain field along the element with the nodal displacements. The process of finding the resisting forces that correspond to the given element deformation is known as state determination.

3.4.1 Description of the procedure

The state determination process consist of three different phases:

- Section state determination: Starting from section deformation, this procedure determine the section forces. While in general, this phase is simple and direct, in this work is represented by a complex procedure described in next chapter.
- Element state determination: Starting from the nodal displacement, in this phase the nodal resisting forces are calculated. Element state determination has section state determination inside.
- Structure state determination: In this phase the forces of each element are assembled, giving the structure resisting forces. This forces must be compared with the applied loads, this comparison give the unbalanced forces that must be applied to the structure in an iterative procedure until convergence is reached.

In the algorithm described below three levels of iteration are introduced, two outermost processes denoted by k and i indices that involve structural degrees of freedom and an innermost process denoted by index j that corresponds to the element state determination.

The section state determination is not reported in this chapeter.

In fig. 3.4-1 is represented the structure and element evolution during a load step $\Delta \mathbf{P}_E^k$.

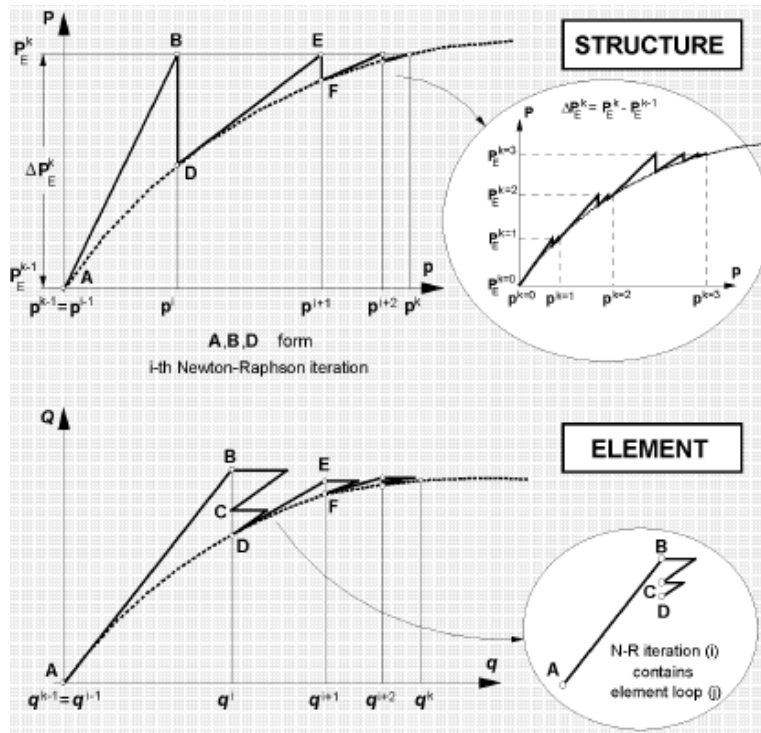


fig. 3.4-1

3.4.2 Element state determination algorithm.

In the following pages the subsequent steps of the procedure will be described in detail, not considering for the type of element and the section state determination in order to focus the attention on the element state determination.

- k = denote the applied load step
- i = is the index for the Newton-Raphson iteration scheme at structural level
- j = is the index for the element state determination process.

(1) *First of all the global system of equation is solved and the displacement of the structure are updated.*

$$\mathbf{K}_s^{i-1} \cdot \Delta \mathbf{p}^i = \Delta \mathbf{P}_E^i \quad (3.4.1)$$

$$\mathbf{p}^i = \mathbf{p}^{i-1} + \Delta \mathbf{p}^i \quad (3.4.2)$$

(2) *Deformation increment for the elements are calculated starting from nodal displacement of the structure, subsequently the element deformation are updated.*

$$\Delta \mathbf{q}^i = \mathbf{L}_{ele} \cdot \Delta \mathbf{p}^i \quad (3.4.3)$$

$$\mathbf{q}^i = \mathbf{q}^{i-1} + \Delta \mathbf{q}^i \quad (3.4.4)$$

The matrix \mathbf{L}_{ele} include two transformation, tin the first the element displacement in global reference system are transformed to the displacement in local reference system. In the second

transformation the element displacement are transformed to the element deformation by a static condensation that consist into an elimination of the rigid body movments.

(3) *Start element state determination procedure, some iteration are carried out for each element f the structure.*

The procedure start by the calculation of the nodal forces increment in the element

$$\Delta \mathbf{Q}^j = \mathbf{k}^{j-1} \cdot \Delta \mathbf{q}^j \quad (3.4.5)$$

When $j=1$ $\mathbf{k}^{j-1} = \mathbf{k}^0$, $\mathbf{Q}^{j-1} = \mathbf{Q}^0$ e $\Delta \mathbf{q}^{j-1} = \Delta \mathbf{q}^i$ where $i-1$ correspond to the state of the element calculated at the last Newton-Raphson iteration.

Nodal forces are updated:

$$\mathbf{Q}^j = \mathbf{Q}^{j-1} + \Delta \mathbf{Q}^j \quad (3.4.6)$$

(4) *Determine the section forces increment for all control section.*

In order to calculate the section forces the equation (3.3.2) is used; this equation relate section and nodal forces, in the following chapters this matrix will be better explained.

$$\Delta \mathbf{D}^j(x) = \mathbf{b}(x) \cdot \Delta \mathbf{Q}^j \quad (3.4.7)$$

$$\mathbf{D}^j(x) = \mathbf{D}^{j-1}(x) + \Delta \mathbf{D}^j(x) \quad (3.4.8)$$

(5) *Determine section deformation increment for each control section:*

Residual deformation $\mathbf{r}^{j-1}(x)$ must be added to the previous iteration. For $j=1$, $\mathbf{r}^0(x) = 0$

$$\Delta \mathbf{d}^j(x) = \mathbf{f}^{j-1}(x) \cdot \Delta \mathbf{D}^j(x) + \mathbf{r}^{j-1}(x) \quad (3.4.9)$$

$$\mathbf{d}^j(x) = \mathbf{d}^{j-1}(x) + \Delta \mathbf{d}^j(x) \quad (3.4.10)$$

(6) *Flexibility and stiffness tangent matrix of the section $\mathbf{f}^j(x) = [\mathbf{k}^j(x)]^{-1}$ and the resisting forces $\mathbf{D}_R^j(x)$ has been subsequently calculated starting from the deformation $\mathbf{d}^j(x)$.*

(7) *Once known the resisting forces, unbalanced section forces $\mathbf{D}_U^j(x)$ can be calculated by the following difference:*

$$\mathbf{D}_U^j(x) = \mathbf{D}^j(x) - \mathbf{D}_R^j(x) \quad (3.4.11)$$

(8) *Using the new flexibility matrix and the unbalanced forces, residual deformation can be calculated as follow:*

$$\mathbf{r}^j(x) = \mathbf{f}^j(x) \cdot \mathbf{D}_U^j(x) \quad (3.4.12)$$

(9) *A new flexibility and stiffness matrix for the element can be calculated by integration:*

$$\mathbf{F}^j = \int_0^L \mathbf{b}^T(x) \cdot \mathbf{f}^j(x) \cdot \mathbf{b}(x) dx \quad (3.4.13)$$

$$\mathbf{K}^j = [\mathbf{F}^j]^{-1} \quad (3.4.14)$$

(10) *Check for the element convergence*

If the unbalanced forces for each section are smaller than a fixed tolerance, the element has converged and after setting $\mathbf{Q}^i = \mathbf{Q}^j$ e $\mathbf{K}^i = \mathbf{K}^j$, the procedure continues. If some section has not converged the residual element deformation \mathbf{s}^j are calculated by integration of the residual section deformation $\mathbf{r}^j(x)$.

$$\mathbf{s}^j = \int_0^L \mathbf{b}^T(x) \cdot \mathbf{r}^j(x) dx \quad (3.4.15)$$

J is incremented as $j=j+1$ and the algorithm returns to the step (3) with $\Delta \mathbf{q}^{j+1} = -\mathbf{s}^j$ until convergence is reached.

(11) *Determine resisting forces and new stiffness matrix of the structure.*

When all elements have converged the i -th Newton-Raphson step is complete and the element force vectors are assembled.

$$\mathbf{P}_R^i = \sum_{ele=1}^n \mathbf{L}_{ele}^T \cdot (\mathbf{Q}^i)_{ele} \quad (3.4.16)$$

A new structure tangent stiffness matrix is then assembled as follows:

$$\mathbf{K}_s^i = \sum_{ele=1}^n \mathbf{L}_{ele}^T \cdot (\mathbf{K}^i)_{ele} \cdot \mathbf{L}_{ele} \quad (3.4.17)$$

Where n is the number of elements of the whole structure.

The resisting forces are then compared with the applied loads and if the difference between these forces ($\Delta \mathbf{P}_u^i$) is greater than a fixed tolerance, the unbalanced forces imposed to the structure, the index i is incremented in $i=i+1$ and the next Newton-Raphson iteration begins with $\Delta \mathbf{P}_u^i = \Delta \mathbf{P}_E^{i+1}$.

In this chapter there aren't any references to the fibers model just to focus on the formulation of the element, in particular the flexibility method deduced from the mixed method to the description of the element state determination. In following chapters is described the procedure applied to a fiber element that includes flexure and shear component, is also explained a section state determination that allows the coupling of flexure and shear in a nonlinear field.

CHAPTER 4

Constitutive Relationship: Section state determination

4.1 *Sommario*

In questo capitolo ci si propone di illustrare la teoria che sta alla base del legame costitutivo per l'elemento finito descritto nel capitolo precedente. Come già accennato il legame utilizzato è di tipo biassiale, le relazioni sono tratte dalla MCFT (modified compression field theory) Vecchio Collins (1986) e sui successivi sviluppi quali la DSFM (disturbed stress field model) Vecchio (2000). Le teorie citate sono state sviluppate per modellare lo stato tensionale e deformativo di elementi in c.a. soggetti a stati piani di tensione. Nel modello il c.l.s. fessurato è considerato come un materiale ortotropo in cui equilibrio compatibilità e legame sono formulati in termini di tensioni e deformazioni medie; a parte sono poi introdotte considerazioni sullo stato locale della fessura nella quale sono poste delle limitazioni per quel che riguarda il livello tensionale. Tutte le relazioni per il calcestruzzo fessurato derivano prove sperimentali su 30 provini sollecitati a diverse sollecitazioni (dal puro taglio al puro sforzo di membrana) svolte presso la Toronto University.

In sostanza il modello presentato in questo capitolo rientra nella categoria di quelli a fessurazione diffusa (smeared) con angolo di fessura variabile.

Nell'originaria MCFT per quanto fosse previsto un controllo sulla fessura, la relazione tra il calcestruzzo teso e le tensioni locali non erano dirette. Tuttavia lo scorrimento dovuto alle tensioni tangenziali sulla frattura (shear slip) era trascurato e quindi non messo in conto nella deformazione complessiva dell'elemento.

Proprio in questa direzione viene in aiuto la DSFM che, basata sulla MCFT, tenta di fornire una migliore rappresentazione del comportamento del calcestruzzo valutando esplicitamente lo scorrimento sulle fessure.

Nei paragrafi che seguiranno saranno illustrate le due teorie evidenziandone le differenze e le analogie.

4.2 Modified compression field theory

4.2.1 Introduction

The membrane element shown in fig. 4.2-1 represent a portion of reinforced concrete structure with uniform thickness and uniform reinforcement in two direction x and y. Loads acting on the element edge and they consist in uniform axial stresses f_x , f_y and shear stresses v_{xy} . The deformed shape is defined by two normal strains ϵ_x , ϵ_y and γ_{xy} , the deformation keep parallel the edges. The problem consist in finding the relationship between tension and deformation according to the following hypothesis:

- For each strain state there exists only one corresponding stress state; situations in which the influence of loading history is significant will not be treated (cyclic loading).
- Stresses and strains can be considered in terms of average values when taken over areas or distances large enough to include several cracks.
- Perfect bond between concrete and reinforcements
- Uniform distribution of longitudinal and transverse reinforcing bars

Tensile stresses and tensile strains will be treated as positive quantities while compressive stresses and strains will be taken as negative.

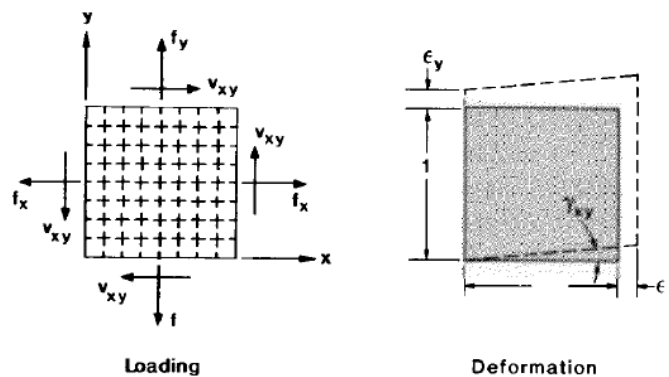


fig. 4.2-1

4.2.2 Compatibility condition

From the third hypothesis deformation in concrete must be equal for steel (no prestrains are considered), thus this equation can be written:

$$\varepsilon_{sx} = \varepsilon_{cx} = \varepsilon_x \quad (4.2.1)$$

$$\varepsilon_{sy} = \varepsilon_{cy} = \varepsilon_y \quad (4.2.2)$$

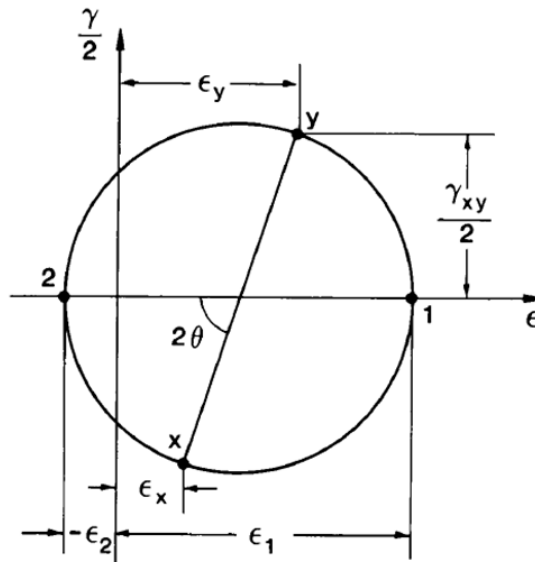
Knowing the deformation components in x and y direction ε_x , ε_y and γ_{xy} , the deformation component in every direction can be calculated using the Mohr circles (fig. 4.2-2) using these equations:

$$\gamma_{xy} = \frac{2 \cdot (\varepsilon_x - \varepsilon_2)}{\tan \theta} \quad (4.2.3)$$

$$\varepsilon_x + \varepsilon_y = \varepsilon_1 + \varepsilon_2 \quad (4.2.4)$$

and

$$\tan^2 \theta = \frac{\varepsilon_x - \varepsilon_2}{\varepsilon_y - \varepsilon_2} = \frac{\varepsilon_1 - \varepsilon_y}{\varepsilon_1 - \varepsilon_x} = \frac{\varepsilon_1 - \varepsilon_y}{\varepsilon_y - \varepsilon_2} = \frac{\varepsilon_x - \varepsilon_2}{\varepsilon_1 - \varepsilon_x} \quad (4.2.5)$$



(b) Mohr's Circle for Average Strains

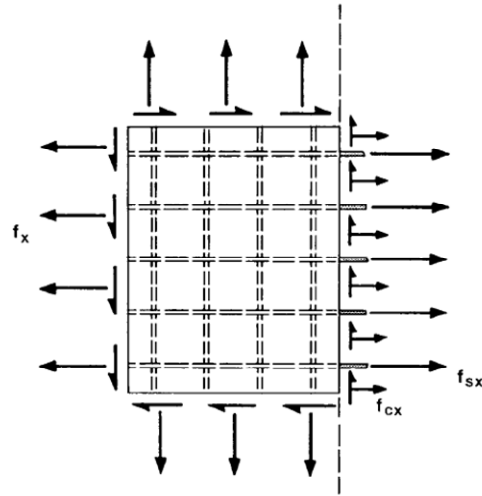
Compatibility conditions for cracked element

fig. 4.2-2

where ε_1 e ε_2 are the principal deformation.

4.2.3 Equilibrium Condition

The forces applied to the element must be balanced by internal forces due to concrete and steel bars. This condition is written for not restrained body and is represented by fig. 4.2-3.



Free-body diagram of part of element

fig. 4.2-3

Analytically, this condition can be written for x direction with this equilibrium equation:

$$\int_A f_x dA = \int_{A_c} f_{cx} dA_c + \int_{A_s} f_{sx} dA_s \quad (4.2.6)$$

Neglecting the concrete area reduction due to the presence of steel bars, the equation (4.2.6) can be written as follow:

$$f_x = f_{cx} + \rho_{sx} \cdot f_{sx} \quad (4.2.7)$$

Similarly in y direction:

$$f_y = f_{cy} + \rho_{sy} \cdot f_{sy} \quad (4.2.8)$$

$$v_{xy} = v_{cx} + \rho_{sx} \cdot v_{sx} \quad e \quad v_{xy} = v_{cy} + \rho_{sy} \cdot v_{sy} \quad (4.2.9)$$

assuming:

$$v_{cxy} = v_{cx} = v_{sy} \quad (4.2.10)$$

The tension field in concrete is completely defined by f_{cx} , f_{cy} e v_{cxy} .

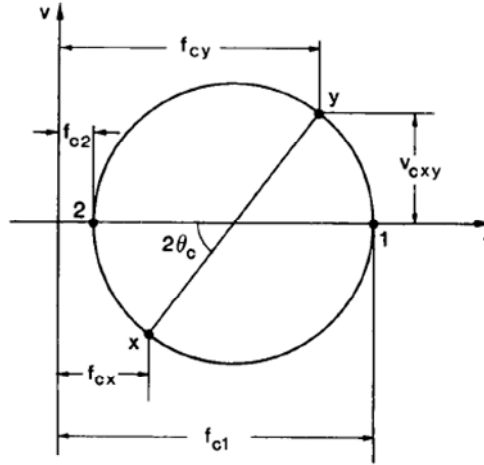
The Mohr circle (fig. 4.2-4) for concrete give the following equations:

$$f_{cx} = f_{c1} - \frac{v_{cxy}}{\tan \theta_c} \quad (4.2.11)$$

$$f_{cy} = f_{c1} - v_{cxy} \cdot \tan \theta_c \quad (4.2.12)$$

and

$$f_{c2} = f_{c1} - v_{cxy} \left(\tan \theta_c + \frac{1}{\tan \theta_c} \right) \quad (4.2.13)$$



(c) Mohr's Circle for Average Concrete Stresses

Stresses in cracked concrete

fig. 4.2-4

4.2.4 Constitutive relationship

Constitutive relationship for concrete and steel are introduced to link average stresses to the average strains. These average stress-strain relations may differ significantly from the usual local stress-strain relations determined from standard material tests. Furthermore, the average stress-strain relationships for the reinforcement and for the concrete will not be completely independent of each other, although this will be assumed to maintain the simplicity of the model. For steel a simple elastic perfectly plastic model is assumed without taking into account the average shear stresses in the steel bars. With these assumption the constitutive relationship for steel is the following:

$$f_{sx} = E_s \cdot \varepsilon_{sx} \leq f_{yx} \quad (4.2.14)$$

$$f_{sy} = E_s \cdot \varepsilon_{sy} \leq f_{yy} \quad (4.2.15)$$

$$v_{sx} = v_{sy} = 0 \quad (4.2.16)$$

For the concrete, the main assumption is that principal directions of stresses and strains coincide $\theta_c = \theta$. The principal compressive stress in the concrete f_{c2} was found to be a

function not only of the principal compressive strain ε_{c2} but also of the co-existing principal tensile strain ε_{c1} . The relationship deduced from standard tests carried out in Toronto University is the following:

$$f_{c2} = f_{c\max} \cdot \left[2 \cdot \left(\frac{\varepsilon_2'}{\varepsilon_c} \right) - \left(\frac{\varepsilon_2'}{\varepsilon_c} \right)^2 \right] \quad (4.2.17)$$

In which:

$$\frac{f_{c2\max}}{f_c'} = \frac{1}{0.8 - 0.34 \cdot \frac{\varepsilon_1'}{\varepsilon_c}} \leq 1.0 \quad (4.2.18)$$

It's important to observe that ε_c' is a negative quantities (normally -0.002), than increasing ε_1' , $\frac{f_{c2\max}}{f_c'}$ is reduced.

Regarding f_{c1} is assumed that the stress-strain relation is linear elastic, prior cracking:

$$f_{c1} = E_c \cdot \varepsilon_1 \quad (4.2.19)$$

The concrete modulus can assume this value $E_c = 2 \cdot \frac{f_c'}{\varepsilon_c}$

In post cracking phase, MCFT suggest the following equation:

$$f_{c1} = \frac{f_{cr}}{1 + \sqrt{200 \cdot \varepsilon_1}} \quad (4.2.20)$$

4.2.5 Transmitting loads across the cracks

The formulation described above doesn't give information about the local variation of stresses over the cracks, because is written in average terms.

At a crack, the tensile stresses in the reinforcement will be higher than average, while between cracks they will be lower than average. On the other the concrete tensile stresses, hand, will be zero at a crack and higher than average midway between cracks. These local variations are important because the ultimate capacity of the element may be governed by the reinforcement's ability to transmit tension across the cracks.

To make this evaluation the element in fig. 4.2-5 must be considered; on the plane 1, the average value describes the element behaviour, while in the plane 2, crack values must be considered.

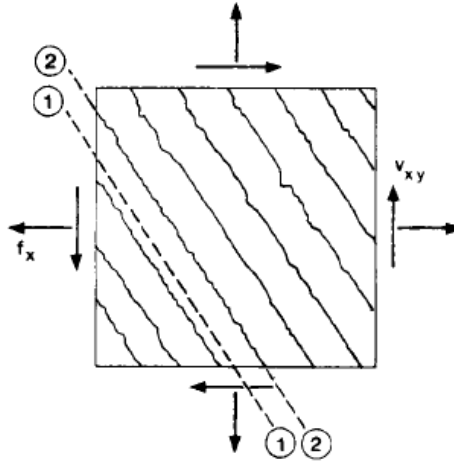


fig. 4.2-5

The crack is inclined orthogonally to the compression principal direction; while along the direction 1 the average shear stresses are 0 (as a principal direction) , a local shear stress over the crack (plane 2) can be found, These shear stresses v_{ci} , may be accompanied by small local compressive stresses f_{ci} across the crack.. The applied external stresses f_x, f_y, v_{xy} are fixed, so the two sets of stresses shown in fig. 4.2-6 must be statically equivalent. Assuming a unit area for both plane 1 and plane 2, the requirement that the two sets of stresses produce the same force in the x-direction is represented by (4.2.21), while the same condition in y direction is given by (4.2.22).

$$\rho_{sx} \cdot (f_{sxcr} - f_{sx}) = f_{c1} + f_{ci} + \frac{v_{c1}}{\tan \theta} \quad (4.2.21)$$

$$\rho_{sy} \cdot (f_{sy cr} - f_{sy}) = f_{c1} + f_{ci} + \frac{v_{c1}}{\tan \theta} \quad (4.2.22)$$

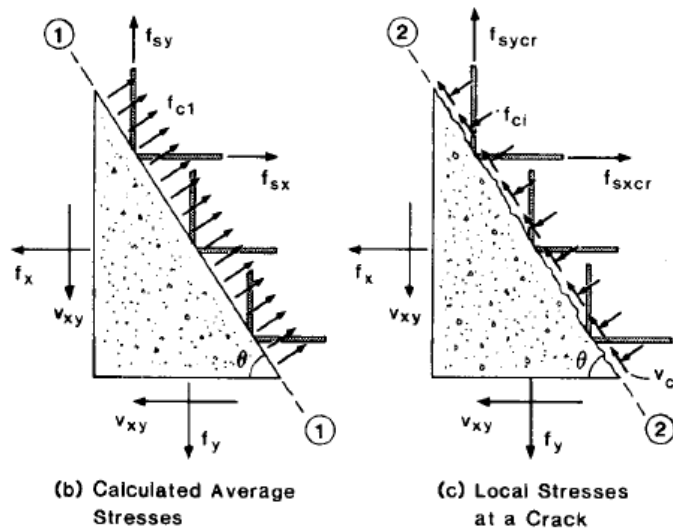


fig. 4.2-6

The equilibrium equations (4.2.21) e (4.2.22) can be satisfied without compressive f_{ci} and shear stresses v_{ci} increasing the steel stresses with this relation:

$$\rho_{sy} \cdot (f_{sy-cr} - f_{sy}) = \rho_{sx} \cdot (f_{sx-cr} - f_{sx}) \quad (4.2.23)$$

However, the tension in reinforcement on the crack can't exceed the yielding point, so if averages reinforcements tensions are high it may be impossible to satisfy the (4.2.23). In this case, the equilibrium requires the shear stress on the fracture that must necessarily arise. It's important to analyze the physical nature of these shear stresses: generally in concrete, cracking will occur along the interface between the cement paste and the aggregate particles. The resulting rough cracks can transfer shear by aggregate interlock. The relationship between shear over the crack surfaces v_{ci} , the crack width w and compression stresses over the fracture f_{ci} have been studied by Walraven (1981) who deduced the following experimental relationship:

$$v_{ci} = 0.18 \cdot v_{ci-max} + 1.64 \cdot f_{ci} - 0.82 \cdot \frac{f_{ci}^2}{v_{ci-max}} \quad (4.2.24)$$

In which:

$$v_{ci-max} = \frac{\sqrt{-f_c'}}{0.31 + 24 \cdot \frac{w}{(a+16)}} \quad (4.2.25)$$

where a is the aggregate dimension measured in mm, tension are expressed in Mpa.

The crack width can be found by the principal strain and the crack spacing with this relation:

$$w = \varepsilon_{c1} \cdot s_{\theta} \quad (4.2.26)$$

Where the crack spacing is:

$$s_{\theta} = \frac{1}{\frac{\sin \theta}{s_{mx}} + \frac{\cos \theta}{s_{my}}} \quad (4.2.27)$$

In which s_{mx} e s_{my} are the indicators of the crack control characteristics of the x and y reinforcement.

In this way a combination of v_{ci} ed f_{ci} that satisfy the equilibrium equations (4.2.21) and (4.2.22) by the (4.2.25) can be founded. If the solution can't be found because of the yielding steel in the crack, the principle tensile stress f_{c1} must be reduced until an equilibrate configuration is reached.

4.3 Disturbed stress field model.

In order to overcome some problem present in MCFT, a new theory was formulated on the same theoretical basis. The improvements made in DSFM formulation are substantially a new approach for the orientation of stress and strain fields in concrete, removing the hypothesis of the coincidence of the two fields and the inclusion of shear slip in the global deformation of the element. Shear slip is the deformation due to the shear tension on the fracture. The new theory can also consider prestrains and can model with more accuracy problems in which MCFT revealed some deficiencies as:

- Panels containing heavy amounts of reinforcement in both directions, panels subjected to high biaxial compressions in addition to shear, or in panels where the reinforcement and loading conditions are such that there is no rotation of the principal stress or strain conditions, MCFT underestimate the shear strength.
- Shear strength and stiffness are generally overestimated for uniaxially reinforced panels or for panels containing very light reinforcement in the transverse direction.
- Reduced accuracy also has been observed in shear-critical beams containing very little or no transverse reinforcement

Consider the principal directions of stress and strain coincident leads to errors, because while in pre-cracking state both fields are inclined by 45° in relation to the horizontal direction, after the opening of the first cracks, the deformation field increase its inclination more than the stress field does. Then both directions grow with a regular interval. After yielding of the transverse reinforcement, the reorientation of the stress field accelerated in accordance with the pattern of the change in the principal strain direction.

4.3.1 General overview

Consider the shear wall shown in fig. 4.3-1, will be used for illustrative purposes. load is carried through the structure by internal stress fields in the concrete and by strut or tie forces in the reinforcement.

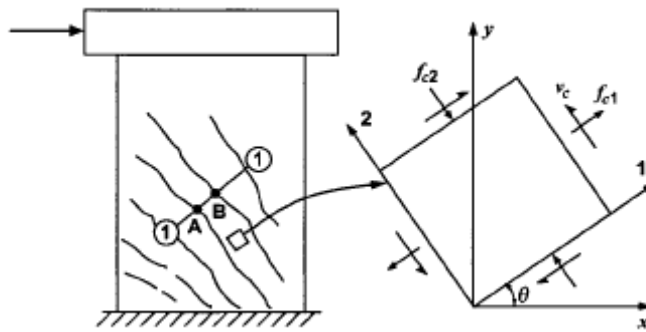


fig. 4.3-1

Narrowing the focus to a smaller region of the wall, consider an area spanning several cracks but one where the sectional forces can be considered relatively constant, taking a section 1-1 with Points A and B located at cracks. (Note that the orientation of the section line is taken normal to the crack direction.) The tension profiles along the section 1-1 are drawn in fig. 4.3-2. In Particular the principal tensile tension in concrete f_{c1} will approach zero at the crack locations but will be greater than zero between the cracks due to tension stiffening and other mechanism. Compensating this reduction at crack location the compression stress f_{c2} in concrete and the tensile stresses in reinforcement f_s increase their value. The average shear stresses v_{ci} are zero, while at the crack location these are necessary for the equilibrium.

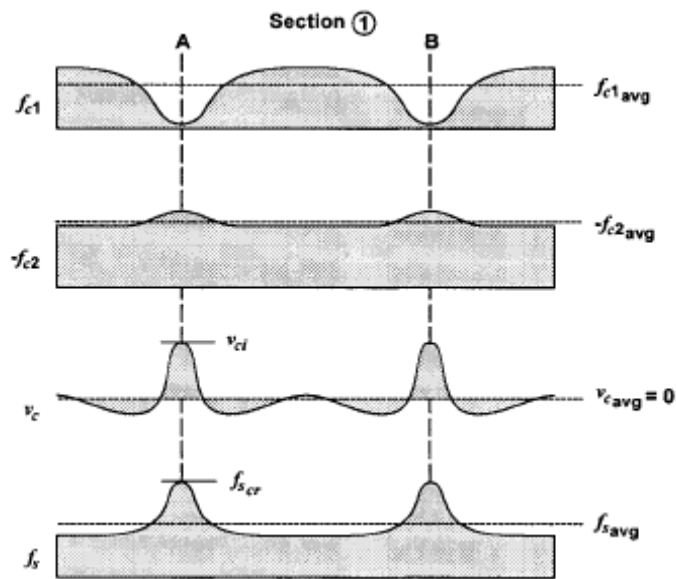


fig. 4.3-2

This theory attempt to model the average and local behavior (over the crack), combined together by the development of equilibrium, compatibility, and constitutive relations.

4.3.2 Equilibrium equation

Consider the element shown in fig. 4.3-3 subjected to the uniform tension $\sigma = [\sigma_x \ \sigma_y \ \tau_{xy}]$, the element is reinforced along two direction, generally oriented referring to the references axes. Reinforcement are considered smeared. Equilibrium will be analyzed in average terms over the area and locally in crack location.

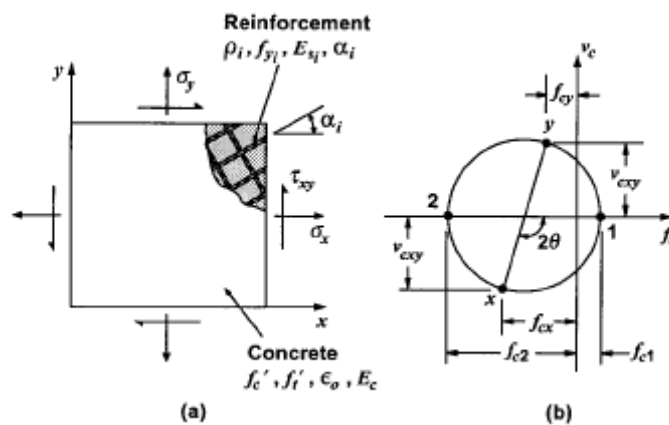


fig. 4.3-3

Concrete is treated as an orthotropic material with rotating cracks, the principal tensions f_{c1} e f_{c2} are parallel and perpendicular to the crack direction θ (shown in fig. 4.3-4) respectively.

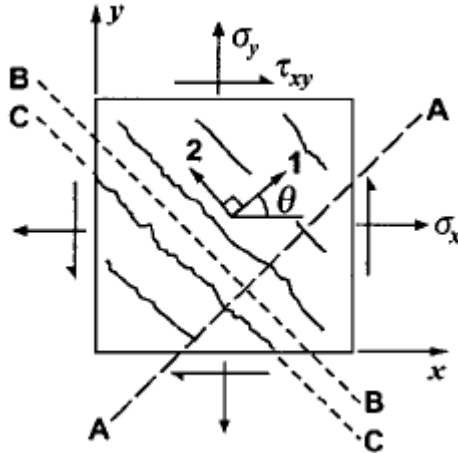


fig. 4.3-4

The equilibrium equation is the following:

$$\boldsymbol{\sigma} = \mathbf{D}_c \cdot \boldsymbol{\varepsilon}_c + \sum_{i=1}^n [\mathbf{D}_s]_i \cdot [\boldsymbol{\varepsilon}_s]_i \quad (4.3.1)$$

In which \mathbf{D}_c e \mathbf{D}_s are the material matrices, whose elements are a function of the principal directions in the concrete and inclination of the reinforcement, the index i is for the i-th reinforcement. In case of the reinforcement are parallel to the edges the following equations can be written:

$$\begin{aligned} \sigma_x &= f_{cx} + \rho_x \cdot f_{sx} \\ \sigma_y &= f_{cy} + \rho_y \cdot f_{sy} \\ \tau_{xy} &= v_{cxy} \end{aligned} \quad (4.3.2)$$

f_{cx} , f_{cy} e v_{cxy} can simply be determined through the use of Mohr circles (fig. 4.3-3 (b)).

On crack location, the following equilibrium equation must be satisfied:

$$\sum_{i=1}^n \rho_i \cdot (f_{scri} - f_{si}) \cdot \cos^2 \theta_{ni} = f_{ci} \quad (4.3.3)$$

In which ρ_i is the percentage of reinforcement over the area, f_{si} is the average tension in steel and f_{scri} is the local tension in steel corresponding to the strain ε_{scri} . The angle θ_{ni} is defined as this difference $\theta_{ni} = \theta - \alpha$.

The increase of tension in the reinforcement at the crack, leads to the development of shear stress along the surface of the fracture, these stresses can be estimated as:

$$v_{ci} = \sum_{i=1}^n \rho_i \cdot (f_{scri} - f_{si}) \cdot \cos \theta_{ni} \cdot \sin \theta_{ni} \quad (4.3.4)$$

4.3.3 Compatibility relations

Consider the compatibility conditions in a reinforced concrete element that is experiencing deformations composed of both continuum straining and discontinuous slip along crack surfaces. Such an element is depicted in fig. 4.3-5. The continuum straining is the result of mechanical compliance to stress and to the smearing of crack widths over a finite area. The slip component is the result of rigid body movement along a crack interface. The total strain will be written with the vector $\boldsymbol{\varepsilon} = [\varepsilon_x \quad \varepsilon_y \quad \gamma_{xy}]$, the inclination of principal direction of the apparent deformation (total strain) θ_ε can be found by:

$$\theta_\varepsilon = \frac{1}{2} \cdot \tan^{-1} \left[\frac{\gamma_{xy}}{\varepsilon_x - \varepsilon_y} \right] \quad (4.3.5)$$

Decoupling the two effects, calling $\boldsymbol{\varepsilon}_c = [\varepsilon_{cx} \quad \varepsilon_{cy} \quad \gamma_{cxy}]$ the continuum strain of the whole concrete element and $\boldsymbol{\varepsilon}^s$ the component of shear slip over the crack, the principal strains for $\boldsymbol{\varepsilon}_c$ are:

$$\varepsilon_{c1}, \varepsilon_{c2} = \frac{(\varepsilon_{cx} + \varepsilon_{cy})}{2} \pm \frac{1}{2} \cdot \sqrt{(\varepsilon_{cx} - \varepsilon_{cy})^2 + \gamma_{cxy}^2} \quad (4.3.6)$$

These strains are represented in fig. 4.3-5 (a), and their inclination is:

$$\theta_\sigma = \frac{1}{2} \cdot \arctan \left(\frac{\gamma_{cxy}}{\varepsilon_{cx} - \varepsilon_{cy}} \right) \quad (4.3.7)$$

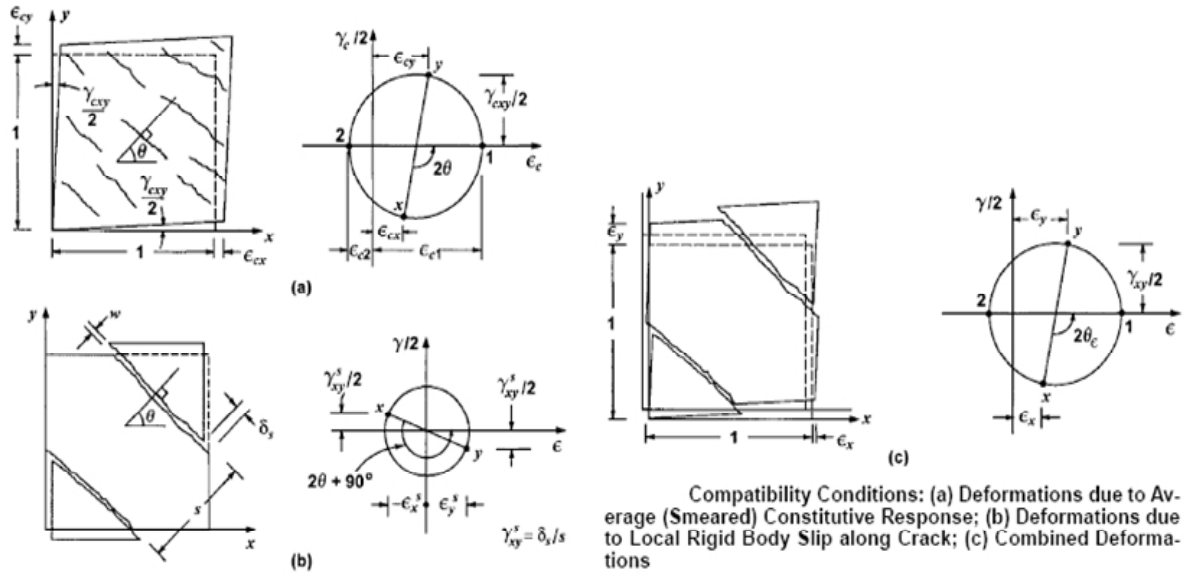


fig. 4.3-5

Consider the slip over the crack δ_s depicted in fig. 4.3-5 (b), an average slip can be defined as:

$$\gamma_s = \frac{\delta_s}{s} \quad (4.3.8)$$

γ_s is function of the crack opening w and the reinforcement spacing s .

Using Mohr's circle, the slip can be expressed, by the decomposition in the following component: $\boldsymbol{\varepsilon}^s = [\varepsilon_x^s \quad \varepsilon_y^s \quad \gamma_{xy}^s]$ in which:

$$\begin{aligned} \varepsilon_x^s &= -\frac{\gamma_s}{2} \cdot \sin(2\theta) \\ \varepsilon_y^s &= \frac{\gamma_s}{2} \cdot \sin(2\theta) \\ \varepsilon_x^s &= \gamma_s \cdot \cos(2\theta) \end{aligned} \quad (4.3.9)$$

In addition to these analyzed effects, the element may also be subject to:

- Thermal and mechanical expansion collected in the elastic strain offset ε_c^o
- Plastic offsets due to cyclic loading conditions ε_c^p

Thus the full strain vector is represented as follow:

$$\boldsymbol{\varepsilon} = \boldsymbol{\varepsilon}_c + \boldsymbol{\varepsilon}^s + \boldsymbol{\varepsilon}_c^o + \boldsymbol{\varepsilon}_c^p \quad (4.3.10)$$

The ‘‘lag’’ in the rotation of the principal stresses in the continuum, relative to the rotation of the apparent principal strains, will be defined as:

$$\Delta\theta = \theta_\varepsilon - \theta_\sigma \quad (4.3.11)$$

To correlate the apparent (or total) deformation with the actual orientation of the stress and strain field in the continuum part, the following equation is used:

$$\gamma_s = \gamma_{xy} \cdot \cos(2\theta_\sigma) + (\varepsilon_y - \varepsilon_x) \cdot \sin(2\theta_\sigma) \quad (4.3.12)$$

Since the bars are considered perfectly bonded with concrete the average tension in the steel are calculated from total strain:

$$\varepsilon_{si} = \frac{\varepsilon_x + \varepsilon_y}{2} + \frac{\varepsilon_x - \varepsilon_y}{2} \cdot \cos(2\alpha_i) + \frac{\gamma_{xy}}{2} \cdot \sin(2\alpha_i) \quad (4.3.13)$$

α_i is the inclination angle of the reinforcement, the local stresses and strains on the crack in reinforcement must be increased to compensate the stress reduction in concrete. It is assumed $\Delta\varepsilon_{1cr}$ the local strain increased in the principal stress direction such as to satisfy the equilibrium condition represented by (4.3.3). The local strain in the reinforcement will be:

$$\varepsilon_{scri} = \varepsilon_{si} + \Delta\varepsilon_{1cr} \cdot \cos^2 \theta_{ni} \quad (4.3.14)$$

4.3.4 Constitutive Relations

The compressive behavior in concrete is influenced by an high softening due to cracking in the transverse direction. The principal stress in compression is therefore influenced by both the principal compression and tension strains, and this influence is captured by the reduction factor β_d :

$$\beta_d = \frac{1}{1 + C_s \cdot C_d}$$

$$C_d = 0.35 \cdot \left(-\frac{\varepsilon_{c1}}{\varepsilon_{c2}} - 0.28 \right)^{0.8} \quad (4.3.15)$$

$$C_s = 0.55$$

C_d and C_s are taken from experimental evidence, β_d factor is used to define the stress value in the pick of the curve, as follow:

$$\begin{aligned} f_p &= -\beta_d \cdot f_c' \\ \varepsilon_p &= -\varepsilon_d \cdot \varepsilon_0 \end{aligned} \quad (4.3.16)$$

A proper response curve in compression is:

$$f_{c2} = f_p \cdot \frac{n \cdot \left(\frac{\varepsilon_{c2}}{\varepsilon_p} \right)}{(n-1) + \left(\frac{\varepsilon_{c2}}{\varepsilon_p} \right)^{n-k}} \quad (4.3.17)$$

$$n = 0.80 - \frac{f_p}{17} ; \quad k = 1 \quad \text{se} \quad \varepsilon_p < \varepsilon_{c2} < 0 ; \quad k = \left(0.67 - \frac{f_p}{62} \right) \quad \text{se} \quad \varepsilon_{c2} < \varepsilon_p$$

While, regarding tensile behaviour in concrete, before cracking a linear elastic relation can be used:

$$f_{c1} = E_c \cdot \varepsilon_{c1} \quad \text{con} \quad 0 < \varepsilon_{c1} < \varepsilon_{cr} \quad (4.3.18)$$

Where E_c is the elastic tangent modulus for concrete and ε_{cr} is the cracking strain.

In post cracking field, the tension stress in concrete can be estimante by two mechanism, one associated with tension softening f_{c1}^a is calculated by the following equations:

$$f_{c1}^a = f_t' \left[1 - \frac{(\varepsilon_{c1} - \varepsilon_{cr})}{(\varepsilon_{ts} - \varepsilon_{cr})} \right] \quad (4.3.19)$$

Where: $\varepsilon_{ts} = 2 \cdot \frac{G_f}{f_t' \cdot L_r}$ e $G_f = 7.5 N/m$, $L_r = 750 mm$, $f_t' = 0.65 \cdot (f_c')^{0.33}$.

As in the MCFT, the concrete tension stiffening stresses are calculated as follows:

$$f_{c1}^b = \frac{f_t'}{1 + \sqrt{c_t \cdot \varepsilon_{c1}}} \quad (4.3.20)$$

In which the terms have the following value: $c_t = 2.2 \cdot m$ ed $\frac{1}{m} = \sum_{i=1}^n \frac{4 \cdot \rho_i}{d_{bi}} \cdot |\cos(\theta_{ni})|$,

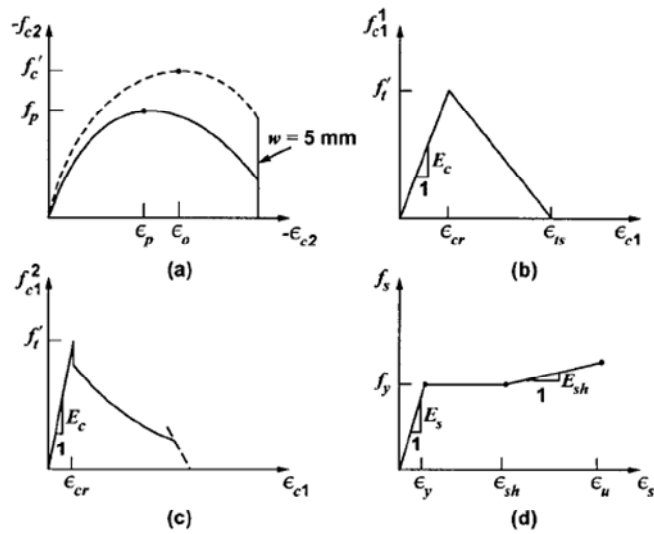
d_{bi} is the rebar diameter. So the tension in cracked concrete will be given by:

$$f_{c1} = \max \{ f_{c1}^a ; f_{c1}^b \} \quad (4.3.21)$$

Regarding to the steel classical trilinear diagram described by the following equations is used:

$$\begin{aligned}
 f_s &= E_s \cdot \varepsilon_s & 0 < \varepsilon_s < \varepsilon_y; \\
 f_s &= f_y & \varepsilon_y < \varepsilon_s < \varepsilon_{sh}; \\
 f_s &= f_y + E_{sh} \cdot (\varepsilon_s - \varepsilon_{sh}) & \varepsilon_{sh} < \varepsilon_s < \varepsilon_u; \\
 f_s &= 0 & \varepsilon_s > \varepsilon_u;
 \end{aligned}
 \tag{4.3.22}$$

The constitutive relations described above are depicted in fig. 4.3-6.



Constitutive Relations: (a) Compressive Softening Model; (b) Tension Softening Model; (c) Tension Stiffening Model; (d) Reinforcing Steel Response

fig. 4.3-6

4.3.5 Shear slip model

Several studies are carried out in order to quantify δ_s along the crack surface as a function of shear stress v_{ci} . These formulations are generally influenced by the cracks opening w , the aggregates size a , and the cylindrical f_c' and cubic f_{cc} compressive stresses. The relation adopted is given by Walraven (1981):

$$\delta_s^a = \frac{V_{ci}}{1.8 \cdot w^{-0.8} + (0.234 \cdot w^{-0.707} - 0.20) \cdot f_{cc}}
 \tag{4.3.23}$$

This approach is not always effective, in particular, does not model well the case where there are no shear reinforcement, in particular in this case the equilibrium equations give a zero shear stresses on the crack surface.

An additional approach is related to the change in direction between the principal stress and strain. The rotation of the stress field remains delayed of a certain range compared to strain field. This range is stable after the first crack and remains constant, until the longitudinal reinforcement starts yielding. Experimental evidence shows that this initial interval is around 5 °-10 ° in function of the reinforcement. Regarding to the initial direction of crack θ_{ic} the rotation of the principal apparent deformation $\Delta\theta_\varepsilon$ can be calculate as follow:

$$\Delta\theta_\varepsilon = \theta_\varepsilon - \theta_{ic} \quad (4.3.24)$$

Knowing θ^l (around 5°-10°) e $\Delta\theta_\varepsilon$ the variation in direction of the stress field can be calculate:

$$\begin{aligned} \Delta\theta_\sigma &= \Delta\theta_\varepsilon - \theta^l & |\Delta\theta| > \theta_l \\ \Delta\theta_\sigma &= \Delta\theta_\varepsilon & |\Delta\theta| \leq \theta_l \end{aligned} \quad (4.3.25)$$

In which θ^l is 5° for biaxial reinforced elements, 7.5°, for uniaxial reinforced element, 10° for elements reinforced in other way. The inclination of the stress field is calculated as follow:

$$\theta_\sigma = \theta_{ic} + \Delta\theta_\sigma \quad (4.3.26)$$

Thus, using equation (4.3.12) γ_s^b can be calculated. Combining the two approach in a hybrid formulation, the lacks of each mechanism can be eliminated. The deformation γ_s due to the shear slip can be determinate as:

$$\gamma_s = \max\{\gamma_s^a; \gamma_s^b\} \quad (4.3.27)$$

In the early stages of loading or in case of no shear reinforced elements, the problem is governed by the second criterion, while in more advanced step of loading is the Walraven formulation to be predominant.

In conclusion, DSFM is an extension of MCFT, by which the following restrictions can be overcome:

- The inclinations of the principal stresses and principal strains are no longer necessarily equal.

- Behavior and failure conditions influenced by crack shear slip are better represented.
- The check on the crack shear stress is no longer necessary.
- The softening of the compression response is reduced, this behavior is more consistent with that reported by others.

CHAPTER 5

Implementation of the model

5.1 *Sommario*

L'oggetto di questa tesi è lo studio del comportamento non lineare di strutture tozze, l'approccio a questa problematica è stato affrontato in via del tutto generale sviluppando un elemento finito a fibre, seguendo l'approccio "member by member" visto nel primo capitolo. La scelta dell'elemento a fibre è nata proprio dalla volontà di affrontare l'argomento in modo generale; sono infatti note le potenzialità di questo genere di modellazione ed i possibili sviluppi ed ampliamenti che vi si possono operare. Gli svantaggi sono pur tuttavia presenti, uno tra tutti è l'appesantimento computazionale che un elemento di questo tipo apporta in un programma ad elementi finiti.

Per lo scopo si è realizzato interamente un codice di calcolo originale agli elementi finiti in grado di modellare qualsiasi struttura con membrature monodimensionali, dai generici telai alle semplici travi.

La base teorica per la formulazione dell'elemento è spiegata nel capitolo 3 mentre il legame costitutivo del cemento armato consiste nella teoria DSFM illustrata nel capitolo 4, di seguito verranno esplicitati tutti i vettori le matrici ed i passi dell'algoritmo implementati nel programma compilato in linguaggio Matlab[®]. La descrizione è organizzata suddividendo le diverse state determination dal livello di struttura a quello di elemento fino a quello di sezione. Sono infine riportati i diagrammi di flusso del codice per i tre livelli.

5.2 Definition input vectors and matrices

In this chapter we will analyze only the core of the program, ignoring the initial data entry and output results. The input quantities required by the algorithm are as follows:

- *Node coordinates (vnodi):*

Matrix that collects the nodal coordinates of the elements:

$$\mathbf{vnodi} = \begin{matrix} & \begin{matrix} x & y \end{matrix} \\ \begin{matrix} node\ 1 \\ \vdots \\ node\ n \end{matrix} & \begin{bmatrix} .. & .. \\ \vdots & \vdots \\ .. & .. \end{bmatrix} \end{matrix} \quad (5.2.1)$$

- *Connection matrix (LCO):*

Number of rows in this matrix coincide with the number of beams, row 1 indicates the beam 1, row n indicates the beam n. The elements of the matrix are the numbers of beam ends nodes.

$$\mathbf{LCO} = \begin{matrix} & \begin{matrix} node\ i & node\ j \end{matrix} \\ \begin{matrix} beam\ 1 \\ \vdots \\ beam\ n \end{matrix} & \begin{bmatrix} .. & .. \\ \vdots & \vdots \\ .. & .. \end{bmatrix} \end{matrix} \quad (5.2.2)$$

- *Boundary matrix (BL):*

Matrix that collect node and direction restrained (direction are indicate as x=1 y=2 φ=3)

$$\mathbf{BL} = \begin{matrix} & \begin{matrix} node & direction \end{matrix} \\ & \begin{bmatrix} .. & .. \\ \vdots & \vdots \\ .. & .. \end{bmatrix} \end{matrix} \quad (5.2.3)$$

- *Applied load vector P:*

$$\mathbf{P} = \text{node 1} \left\{ \begin{array}{c} P_x \\ P_y \\ M \\ \vdots \end{array} \right. \quad (5.2.4)$$

- *Section compatibility matrix (I):*

Is a matrix that relate the section deformation $\begin{bmatrix} \chi \\ \varepsilon \\ \gamma \end{bmatrix}$ with the fibres deformation $\begin{bmatrix} \varepsilon_{fib} \\ \gamma_{fib} \end{bmatrix}$.

Is a tridimensional matrix, its dimension is [2 number of fibres x 3 x number of beams]

$$\mathbf{I} = \begin{bmatrix} y_1 & 0 & 1 \\ 0 & 1 & 0 \\ y_{fib} & 0 & 1 \\ 0 & 1 & 0 \\ \vdots & \vdots & \vdots \end{bmatrix} \quad (5.2.5)$$

- *Fibre area matrix (A):*

Are diagonal matrix, whose dimension is [2 number of fibres x 2 number of fibres x number of beams], on the diagonal are given respectively to the index i and i +1 the area of the i-th fiber.

$$\mathbf{A} = \begin{bmatrix} A_1 & 0 & 0 & 0 \\ 0 & A_1 & 0 & 0 \\ 0 & 0 & \ddots & 0 \\ 0 & 0 & 0 & \ddots \end{bmatrix} \quad (5.2.6)$$

- *Reinforcement matrix (ro):*

This matrix collect all the reinforcement characteristics for each fibre, its dimension is [number of beams x 8]

$$\mathbf{ro} = \begin{bmatrix} \rho_x & As_x & n^\circ \text{ferri } x & \rho_y & \phi_y & n^\circ \text{ferri } y & sx & sy \\ \vdots & \vdots \end{bmatrix} \quad (5.2.7)$$

Where s_x e s_y are the reinforcement spacing, ρ_x e ρ_y are the percentage of steel in x and y direction.

- *Matrix that collect the characteristics of materials (carmat):*

$$\mathbf{carmat} = \begin{bmatrix} f_y & f_c \\ f_t & f_{ct} \\ \varepsilon_u & \varepsilon_{c0} \\ E_s & \varepsilon_{cu} \\ \nu_s & \nu_c \end{bmatrix} \quad (5.2.8)$$

Input require also the number of nodes, the number of beams, the number of directions restrained and the number of fibers. There are other matrix that will be explained below.

5.3 Algorithm steps:

(1) Creation of initial modulus matrix:

Two matrices whose size is equal to the areas marix \mathbf{A} , are built by collecting the modulus of elasticity. A matrix for a steel \mathbf{E}_s and one for concrete \mathbf{E}_c , these matrix are the following:

$$\mathbf{E}_s = \begin{bmatrix} E_{s1} & 0 & 0 & 0 \\ 0 & \frac{G_{s1}}{\chi_1} & 0 & 0 \\ 0 & 0 & \ddots & 0 \\ 0 & 0 & 0 & \ddots \end{bmatrix} \quad e \quad \mathbf{E}_c = \begin{bmatrix} E_{c1} & 0 & 0 & 0 \\ 0 & \frac{G_{c1}}{\chi_1} & 0 & 0 \\ 0 & 0 & \ddots & 0 \\ 0 & 0 & 0 & \ddots \end{bmatrix} \quad (5.3.1)$$

(2) Creation of the initial stiffness matrix

First of all the section stiffness matrix can be calculate as follow:

$$\mathbf{k} = \mathbf{I}^T \cdot (\mathbf{E}_s \cdot \rho_x \mathbf{A} + \mathbf{E}_c \cdot \mathbf{A}) \cdot \mathbf{I} \quad (5.3.2)$$

Knowing the section stiffness matrix , by inversion, section flexibility matrix can be calculate: $\mathbf{f} = \mathbf{k}^{-1}$. By integration the flexibility matrix of the element \mathbf{F} can be calculate as follow:

$$\mathbf{F} = \int_0^L \mathbf{b}^T(x) \cdot \mathbf{f}(x) \cdot \mathbf{b}(x) dx \quad (5.3.3)$$

$\mathbf{b}(x)$, is the forces interpolation matrix, this matrix interpolate the nodal forces, giving the section forces in control sections.

$$\mathbf{b}(x) = \begin{bmatrix} \frac{x}{l}-1 & \frac{x}{l} & 0 \\ \frac{1}{l} & \frac{1}{l} & 0 \\ 0 & 0 & 1 \end{bmatrix} \quad (5.3.4)$$

The relation between nodal forces and section forces is written below, the nodal forces are represented in fig. 5.3-2 (a).

$$\begin{bmatrix} M(x) \\ T(x) \\ N(x) \end{bmatrix} = \begin{bmatrix} \frac{x}{l}-1 & \frac{x}{l} & 0 \\ \frac{1}{l} & \frac{1}{l} & 0 \\ 0 & 0 & 1 \end{bmatrix} \cdot \begin{bmatrix} Q_1 \\ Q_2 \\ Q_3 \end{bmatrix} \quad (5.3.5)$$

Then, two operators are defined, one is the rotation matrix :

$$\mathbf{T}_a = \begin{bmatrix} \cos \theta & \sin \theta & 0 & 0 & 0 & 0 \\ -\sin \theta & \cos \theta & 0 & 0 & 0 & 0 \\ 0 & 0 & 1 & 0 & 0 & 0 \\ 0 & 0 & 0 & \cos \theta & \sin \theta & 0 \\ 0 & 0 & 0 & -\sin \theta & \cos \theta & 0 \\ 0 & 0 & 0 & 0 & 0 & 1 \end{bmatrix} \quad (5.3.6)$$

Where θ is the angle of the beam in global reference system fig. 5.3-1

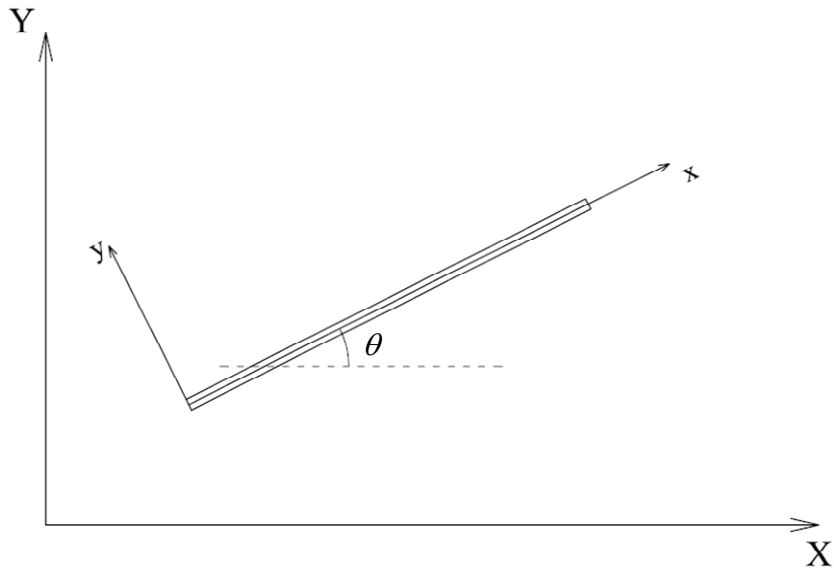


fig. 5.3-1

The other operator is a condensation matrix:

$$\mathbf{R} = \begin{bmatrix} 0 & \frac{1}{l_a} & 1 & 0 & -\frac{1}{l_a} & 0 \\ 0 & \frac{1}{l_a} & 0 & 0 & \frac{1}{l_a} & 1 \\ -1 & 0 & 0 & 1 & 0 & 0 \end{bmatrix} \quad (5.3.7)$$

This matrix is used to relate the system in fig. 5.3-2 a to the system in fig. 5.3-2 b:

$$\begin{bmatrix} N_1 \\ T_1 \\ M_1 \\ N_2 \\ T_2 \\ M_2 \end{bmatrix} = \begin{bmatrix} 0 & 0 & -1 \\ \frac{1}{l_a} & \frac{1}{l_a} & 0 \\ 1 & 0 & 0 \\ 0 & 0 & 1 \\ -\frac{1}{l_a} & -\frac{1}{l_a} & 0 \\ 0 & 1 & 0 \end{bmatrix} \cdot \begin{bmatrix} Q_1 \\ Q_2 \\ Q_3 \end{bmatrix} \quad (5.3.8)$$

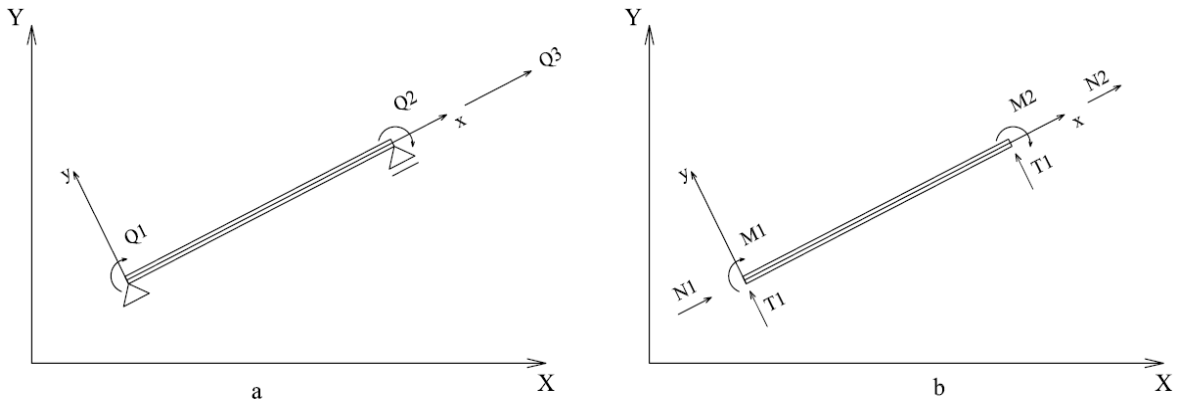


fig. 5.3-2

Once Known all the quantities defined above, is possible to calculate the element stiffness matrix:

$$\mathbf{k}_a = \mathbf{T}\mathbf{a}^T \cdot \mathbf{R}^T \cdot \mathbf{F}^{-1} \cdot \mathbf{R} \cdot \mathbf{T}\mathbf{a} \quad (5.3.9)$$

In the element formulation (Taucer et al.1996) presented in the third chapter, this transformation matrix is indicated with the letter \mathbf{L}_{ele} .

The procedure is carried out for each beam, at the end, the stiffness matrix in GRS (global reference system) is known for every element, than the structure stiffness matrix is assembled by the connection matrix \mathbf{LCO} .

The algorithm is organized on three levels, Structure state determination, element state determination and section state determination. These levels are each within the other, in particular structure state determination contain element state determination that contain section state determination.

5.3.1 Structure state determination

Each loading step is characterized by Newton-Raphson iterations indicated with superscript i . At each iteration the global system of equation is solved, and the structural displacements \mathbf{p} are updated:

$$\mathbf{K}_{str}^{i-1} \cdot \Delta\mathbf{p}^i = \Delta\mathbf{P}_E^i \quad (5.3.10)$$

$$\mathbf{p}^i = \mathbf{p}^{i-1} + \Delta\mathbf{p}^i \quad (5.3.11)$$

where \mathbf{K}_{str} is the structure stiffness matrix and \mathbf{P}_E are the external loads. Using matrix \mathbf{L}_{ele} , the element deformation increments are derived from the structural displacement increments and then the element deformations are updated:

$$\Delta\mathbf{q}^i = \mathbf{L}_{ele} \cdot \Delta\mathbf{p}^i \quad (5.3.12)$$

$$\mathbf{q}^i = \mathbf{q}^{i-1} + \Delta \mathbf{q}^i \quad (5.3.13)$$

At this point an element state determination is activated for each element with the purpose to determine the element resisting forces \mathbf{Q}^i and the element stiffness matrix \mathbf{K}^i associated to the element deformations \mathbf{q}^i . When the element state determination is concluded, the resisting nodal forces of the single elements are expressed in the global reference system through the matrix \mathbf{L}_{ele} . The structural resisting forces are then obtained by summation of the resisting forces of all elements:

$$\mathbf{P}_R^i = \sum_{ele=1}^{nele} \mathbf{L}_{ele}^T \cdot (\mathbf{Q}^i)_{ele} \quad (5.3.14)$$

By assembling the current element stiffness matrices it is formed the new structure stiffness matrix:

$$\mathbf{K}_{str}^i = \sum_{ele=1}^{nele} \mathbf{L}_{ele}^T \cdot (\mathbf{K}^i)_{ele} \cdot \mathbf{L}_{ele} \quad (5.3.15)$$

The unbalanced nodal forces correspond to the difference between the applied and resisting forces:

$$\Delta \mathbf{P}_u^i = \Delta \mathbf{P}_E^i - \mathbf{P}_R^i \quad (5.3.16)$$

If these unbalanced forces are not below a certain tolerance, the index i is incremented to $i+1$ and a new Newton-Raphson iteration is started by applying the unbalanced forces to the structure; otherwise the subsequent load increment is applied and the analysis is continued.

5.3.2 Element state determination

The element state determination, based on the one proposed by Taucer et al. (1996), is characterized by an iterative procedure where each iteration is identified by the index j . The first step is the determination of the increments of the element nodal forces from those of the element deformations and the updating of the element nodal forces:

$$\Delta \mathbf{Q}^j = \mathbf{K}^{j-1} \cdot \Delta \mathbf{q}^j \quad (5.3.17)$$

$$\mathbf{Q}^j = \mathbf{Q}^{j-1} + \Delta \mathbf{Q}^j \quad (5.3.18)$$

When $j=1$, $\mathbf{K}^0 = \mathbf{K}^{i-1}$, $\Delta \mathbf{q}^1 = \Delta \mathbf{q}^i$ and $\mathbf{Q}^0 = \mathbf{Q}^{i-1}$, where the quantities denoted by the index $i-1$ are evaluated considering the state of the element at the last Newton-Raphson iteration.

The section forces are then updated considering the section force increments obtained from the element deformation increments:

$$\Delta \mathbf{D}^j(x) = \mathbf{b}(x) \cdot \Delta \mathbf{Q}^j \quad (5.3.19)$$

$$\mathbf{D}^j(x) = \mathbf{D}^{j-1}(x) + \Delta \mathbf{D}^j(x) \quad (5.3.20)$$

Using the section flexibility matrix it is possible to determine the section deformation increments from the section force increments and to update the section deformations:

$$\Delta \mathbf{d}^j(x) = \mathbf{f}^{j-1}(x) \cdot \Delta \mathbf{D}^j(x) + \mathbf{r}^{j-1}(x) \quad (5.3.21)$$

$$\mathbf{d}^j(x) = \mathbf{d}^{j-1}(x) + \Delta \mathbf{d}^j(x) \quad (5.3.22)$$

where $\mathbf{r}^{j-1}(x)$ are the residual section deformations due to the section unbalanced forces for the previous iterations. When $j=1$, $\mathbf{r}^0=\mathbf{0}$. At this point a section state determination is activated for each control section with the purpose to determine the section resisting forces $\mathbf{D}_R^j(x)$ and the section flexibility matrix $\mathbf{f}^j(x)$ associated to the section deformations $\mathbf{d}^j(x)$. By calculating the difference between the applied and the resisting forces it is possible to derive the section unbalanced forces for the current iteration:

$$\mathbf{D}_u^j(x) = \mathbf{D}^j(x) - \mathbf{D}_R^j(x) \quad (5.3.23)$$

The new element flexibility matrix is obtained by integration of the section flexibility matrices:

$$\mathbf{F}^j = \int_0^L \mathbf{b}^T(x) \cdot \mathbf{f}^j(x) \cdot \mathbf{b}(x) dx \quad (5.3.24)$$

This matrix is then inverted to obtain the element stiffness matrix \mathbf{K}^j . The residual section deformations for the current iteration are calculated from the section unbalanced forces:

$$\mathbf{r}^j(x) = \mathbf{f}^j(x) \cdot \mathbf{D}_u^j(x) \quad (5.3.25)$$

The residual nodal displacement are determined by integration of the residual section deformations:

$$\mathbf{s}^j = \int_0^L \mathbf{b}^T(x) \cdot \mathbf{r}^j(x) dx \quad (5.3.26)$$

As usual for the distributed plasticity models, the integrals of the Eqs.(5.3.24) and (5.3.26) are solved numerically by monitoring the response in given sections along the element, called control sections. The element convergence is reached when the unbalanced forces at all the control sections are sufficiently small. This check may be performed through energy

criteria (Taucer et al. 1996). If the element reaches the convergence it is assumed $\mathbf{Q}^i = \mathbf{Q}^j$ and $\mathbf{K}^i = \mathbf{K}^j$ and the procedure continues with the element state determination of another element. After completing the element state determination of all elements the procedure continues with the research of the overall equilibrium of the structure with the Newton-Raphson iterations. If the element does not converge another iteration is performed by considering the following element deformation increments:

$$\Delta \mathbf{q}^{j+1} = -\mathbf{s}^j \quad (5.3.27)$$

5.3.3 Section state determination

The section state determination is aimed to calculate, for each control section, the resisting forces $\mathbf{D}_R(x)$ and the flexibility matrix $\mathbf{f}(x)$ corresponding to the deformations $\mathbf{d}(x)$. From the section deformation vector it is possible to obtain the condensed deformation vector $\bar{\mathbf{e}}(x, y) = \{\varepsilon_x \gamma_{xy}\}^T$ of the fibre at a distance y from the axis z :

$$\bar{\mathbf{e}}(x, y) = \mathbf{I}(y) \cdot \mathbf{d}(x) \quad (5.3.28)$$

The matrix \mathbf{I} is defined on the basis of the assumptions that plane sections remain plane and shear strain is constant along the height of the section:

$$\mathbf{I}(y) = \begin{bmatrix} -y & 0 & 1 \\ 0 & 1 & 0 \end{bmatrix} \quad (5.3.29)$$

The determination of the strains in concrete is performed through an iterative procedure, which is activated at the fibre level. The strains in concrete, in fact, depend on the strains associated to shear slip. Moreover, also the value of the transversal strain ε_y cannot be derived directly. Initially tentative values are assumed for the strains in concrete and the total transversal strains. The strains in steel are then defined as follows:

$$\begin{aligned} \varepsilon_{sy} &= \varepsilon_y \\ \varepsilon_{sx} &= \varepsilon_x \end{aligned} \quad (5.3.30)$$

Once the strains in concrete and steel are known, the corresponding stresses are calculated according to the material constitutive relationships. These stresses represent the average stresses calculated between cracks. For concrete the principal strain direction are calculated:

$$\varepsilon_{c1}, \varepsilon_{c2} = \frac{(\varepsilon_{cx} + \varepsilon_{cy})}{2} \pm \frac{1}{2} \cdot \sqrt{(\varepsilon_{cx} - \varepsilon_{cy})^2 + \gamma_{cxy}^2} \quad \theta_{\sigma} = \frac{1}{2} \cdot \arctan\left(\frac{\gamma_{cxy}}{\varepsilon_{cx} - \varepsilon_{cy}}\right)$$

$$\theta_{\varepsilon} = \frac{1}{2} \cdot \arctan\left(\frac{\gamma_{xy}}{\varepsilon_x - \varepsilon_y}\right) \quad (5.3.31)$$

The response of the cracked concrete is characterized by a significant softening that comes from the cracking, the principal compressive stress is a function not only of both principal compressive and tensile strain.

This influence is caught by β_d factor

$$\beta_d = \frac{1}{1 + C_s \cdot C_d}$$

$$C_d = 0.35 \cdot \left(-\frac{\varepsilon_{c1}}{\varepsilon_{c2}} - 0.28 \right)^{0.8}$$

$$C_s = 0.55 \quad (5.3.32)$$

β_d is used to find peak stress

$$f_p = -\beta_d \cdot f'_c$$

$$\varepsilon_p = -\varepsilon_d \cdot \varepsilon_0 \quad (5.3.33)$$

Calculation of principal compressive stress in concrete f_{c2} :

$$f_{c2} = f_p \cdot \frac{n \cdot \left(\frac{\varepsilon_{c2}}{\varepsilon_p} \right)}{(n-1) + \left(\frac{\varepsilon_{c2}}{\varepsilon_p} \right)^{n \cdot k}} \quad (5.3.34)$$

$$n = 0.80 - \frac{f_p}{17} ; \quad k = 1 \quad \text{se } \varepsilon_p < \varepsilon_{c2} < 0 ; \quad k = \left(0.67 - \frac{f_p}{62} \right) \quad \text{se } \varepsilon_{c2} < \varepsilon_p$$

Calculation of principal tensile stress in concrete f_{c1} :

$$f_{c1} = \frac{f'_t}{1 + \sqrt{c_t \cdot \varepsilon_{c1}}}$$

$$\text{dove } c_t = 2.2 \cdot m \quad \text{ed} \quad m = \frac{\phi_x}{n_x \cdot 4 \cdot \rho_x} \cdot \cos(\theta_{\sigma}) + \frac{\phi_y}{n_y \cdot 4 \cdot \rho_y} \cdot \cos\left(\theta_{\sigma} - \frac{\pi}{2}\right) \quad (5.3.35)$$

Calculation of average stresses in steel

$$\begin{aligned}
 f_s &= E_s \cdot \varepsilon_s & 0 < \varepsilon_s < \varepsilon_y; \\
 f_s &= f_y & \varepsilon_y < \varepsilon_s < \varepsilon_{sh}; \\
 f_s &= f_y + E_{sh} \cdot (\varepsilon_s - \varepsilon_{sh}) & \varepsilon_{sh} < \varepsilon_s < \varepsilon_u; \\
 f_s &= 0 & \varepsilon_s > \varepsilon_u;
 \end{aligned} \tag{5.3.36}$$

An important check is performed with regard to the transmission of the stresses across the cracks. Local increases of stresses and strains are required in the reinforcement to transfer average concrete tensile stresses across a crack. These increases allow to compensate for the local reduction in the concrete average tensile stresses. The local strains in reinforcements are calculated as follows:

$$\varepsilon_{sy-cr} = \varepsilon_{sy} + \Delta\varepsilon_{1-cr} \cdot \cos^2\left(\theta_\sigma - \frac{\pi}{2}\right) \tag{5.3.37}$$

$$\varepsilon_{sx-cr} = \varepsilon_{sx} + \Delta\varepsilon_{1-cr} \cdot \cos^2(\theta_\sigma) \tag{5.3.38}$$

The local incremental strain $\Delta\varepsilon_{1-cr}$ in the principal stress direction is calculated in order to satisfy the equilibrium condition expressed by:

$$\sum_{i=1}^n \rho_i \cdot (f_{s-cri} - f_{s-i}) \cdot \cos^2 \theta_{ni} = f_{c1} \tag{5.3.39}$$

which is here adapted to the case of reinforcements parallel to x and y axes:

$$\rho_x \cdot (f_{sx-cr} - f_{sx}) \cdot \cos^2(\theta_\sigma) + \rho_y \cdot (f_{sy-cr} - f_{sy}) \cdot \cos^2\left(\theta_\sigma - \frac{\pi}{2}\right) = f_{c1} \tag{5.3.40}$$

where f_{sx-cr} and f_{sy-cr} are derived from the constitutive relationships as functions of ε_{sx-cr} e ε_{sy-cr} . The solution of Eq. (5.3.40) is obtained numerically by considering increasing values of $\Delta\varepsilon_{1-cr}$ from an initial value equal to zero. Once the equilibrium equation is satisfied, the shear stress in the concrete fracture is calculated according to:

$$v_{ci} = \sum_{i=1}^n \rho_i \cdot (f_{s-cri} - f_{s-i}) \cdot \cos \theta_{ni} \cdot \sin \theta_{ni} \tag{5.3.41}$$

rearranged in the following form:

$$v_{ci} = \rho_x \cdot (f_{sx-cr} - f_{sx}) \cdot \cos(\theta_\sigma) \cdot \sin(\theta_\sigma) + \rho_y \cdot (f_{sy-cr} - f_{sy}) \cdot \cos\left(\theta_\sigma - \frac{\pi}{2}\right) \cdot \sin\left(\theta_\sigma - \frac{\pi}{2}\right) \tag{5.3.42}$$

From the shear stress v_{ci} it is possible to derive the shear slip γ_s along the crack surface the slip δ_s is determined according to two approaches (vecchio2000). In the first approach it is

calculated as a function of shear stress v_{ci} , crack width w and cubic compressive strength f_{cc} :

$$\delta_s^a = \frac{v_{ci}}{1.8 \cdot w^{-0.8} + (0.234 \cdot w^{-0.707} - 0.20) \cdot f_{cc}} \quad (5.3.43)$$

where w is a function of the crack spacing s . The crack width is calculated as follows:

$$w = \varepsilon_{c1} \cdot s \quad (5.3.44)$$

$$s = \frac{1}{\frac{\sin \theta_\sigma}{s_x} + \frac{\cos \theta_\sigma}{s_y}} \quad (5.3.45)$$

A further approach is related to the difference which arises between the rotation of the principal stresses and the apparent strains. This difference stabilize after the first crack and remains constant, until the reinforcement starts yielding. Experimental evidence (Vecchio 2000) shows that this initial difference θ^l is around 5° - 10° depending on the type of reinforcement. By denoting with θ_{ic} the inclination of principal stresses in concrete at first cracking, it is possible to derive the angle $\Delta\theta_\varepsilon$ between the apparent principal strains at the current load stage and the principal stresses at first cracking:

$$\Delta\theta_\varepsilon = \theta_\varepsilon - \theta_{ic} \quad (5.3.46)$$

The variation of the principal stress directions can be calculated as follow:

$$\Delta\theta_\sigma = \Delta\theta_\varepsilon - \theta^l \quad |\Delta\theta_\varepsilon| > \theta_l \quad (5.3.47)$$

$$\Delta\theta_\sigma = \Delta\theta_\varepsilon \quad |\Delta\theta_\varepsilon| \leq \theta_l \quad (5.3.48)$$

where $\theta^l = 5^\circ$ for elements with biaxial reinforcement, $\theta^l = 7.5^\circ$ for elements with uniaxial reinforcement and $\theta^l = 10^\circ$ for elements with other types of reinforcement. The inclination of the principal stresses in concrete is:

$$\theta_\sigma = \theta_{ic} + \Delta\theta_\sigma \quad (5.3.49)$$

The shear strain due to shear slip can then be calculated as follows:

$$\gamma_s^b = \gamma_{xy} \cdot \cos(2 \cdot \theta_\sigma) + (\varepsilon_y - \varepsilon_x) \cdot \sin(2 \cdot \theta_\sigma) \quad (5.3.50)$$

Combining the two approaches in a hybrid formulation, the shear strain due to shear slip along the crack surface can be evaluated as the maximum of the two corresponding values:

$$\gamma_s = \max \left\{ \gamma_s^a = \frac{\delta_s^a}{s}; \gamma_s^b \right\} \quad (5.3.51)$$

where s is the crack spacing.

The deformation components associated to shear slip are calculated as follows:

$$\begin{aligned} \varepsilon_x^s &= -\frac{\gamma_s}{2} \cdot \sin(2\theta) \\ \varepsilon_y^s &= \frac{\gamma_s}{2} \cdot \sin(2\theta) \\ \gamma_{xy}^s &= \gamma_s \cdot \cos(2\theta) \end{aligned} \quad (5.3.52)$$

where γ_s is the shear strain due to slip along the crack surface.

New values of strains in concrete are then calculated:

$$(\boldsymbol{\varepsilon}_c)' = \boldsymbol{\varepsilon} - \boldsymbol{\varepsilon}^s \quad (5.3.53)$$

where $\boldsymbol{\varepsilon}_c$ is the vector of the strains in concrete and $\boldsymbol{\varepsilon}^s$ is the vector of the strains due to slip. With the new values of concrete strains a new iteration is performed. At this stage it is performed also the correction of the value of the total transversal strain ε_y in order to satisfy the transversal equilibrium condition:

$$\sigma_y = f_{cy} + \rho_y \cdot f_{sy} \quad (5.3.54)$$

with $\sigma_y = 0$.

While the original MCFT is formulated on the basis of the secant stiffness matrix, the model presented here, according to the one proposed by Taucer et al. 1996, is based on the tangent stiffness matrix. The tangent modules relative to the two principal directions are calculated from the material constitutive laws as functions of the principal strains. The

tangent modules are collected in material stiffness matrices related to the principal directions:

$$\mathbf{E}_c^* = \begin{bmatrix} E_{c1} & 0 & 0 \\ 0 & E_{c2} & 0 \\ 0 & 0 & G_c \end{bmatrix} \quad (5.3.55)$$

$$\mathbf{E}_{sx}^* = \begin{bmatrix} \rho_x E_{sx} & 0 & 0 \\ 0 & 0 & 0 \\ 0 & 0 & 0 \end{bmatrix} \quad (5.3.56)$$

For the reinforcement steel parallel to the y direction it is adopted a matrix \mathbf{E}_{sy}^* which can be obtained by replacing in Eq. (5.3.56) $\rho_x E_{sx}$ with $\rho_y E_{sy}$. These matrices are then transformed to the x and y directions:

$$\mathbf{E}_c = \mathbf{T}^T \cdot \mathbf{E}_c^* \cdot \mathbf{T} \quad (5.3.57)$$

$$\mathbf{E}_{sx} = \mathbf{T}^T \cdot \mathbf{E}_{sx}^* \cdot \mathbf{T} \quad (5.3.58)$$

This transformation is applied also to matrix \mathbf{E}_{sy}^* . The transformation matrix is given by:

$$\mathbf{T} = \begin{bmatrix} \cos^2 \psi & \sin^2 \psi & \cos \psi \sin \psi \\ \sin^2 \psi & \cos^2 \psi & -\cos \psi \sin \psi \\ -2 \cos \psi \sin \psi & 2 \cos \psi \sin \psi & (\cos^2 \psi - \sin^2 \psi) \end{bmatrix} \quad (5.3.59)$$

where $\psi = \theta_\sigma$ for the concrete, $\psi = 0$ for the reinforcements in x direction and $\psi = 90^\circ$ for the reinforcements in y direction. The total material stiffness \mathbf{E} is evaluated by summation:

$$\mathbf{E} = \mathbf{E}_c + \mathbf{E}_{sx} + \mathbf{E}_{sy} \quad (5.3.60)$$

Finally the matrix \mathbf{E} is condensed in order to obtain the matrix $\bar{\mathbf{E}}$, referred to the two deformation components ε_x and γ_{xy} .

The stresses in concrete relative to the two principal directions are calculated from the material constitutive laws as functions of the principal strains. The values of the stresses in concrete relative to x and y axes are derived through these transformations:

$$\begin{aligned} f_{cx} &= f_{c1} - \frac{(f_{c1} - f_{c2})}{(1 + \tan(\theta_\sigma)^2)} \\ f_{cy} &= f_{c1} - \frac{(f_{c1} - f_{c2}) \cdot \tan(\theta_\sigma)^2}{(1 + \tan(\theta_\sigma)^2)} \\ v_{cxy} &= \frac{(f_{c1} - f_{c2}) \cdot \tan(\theta_\sigma)}{(1 + \tan(\theta_\sigma)^2)} \end{aligned} \quad (5.3.61)$$

By knowing also the stresses in the reinforcements parallel to the x and y directions it is possible to determine the total stresses with the equilibrium conditions:

$$\begin{aligned}\sigma_x &= f_{cx} + \rho_x \cdot f_{sx} \\ \sigma_y &= f_{cy} + \rho_y \cdot f_{sy} \\ \tau_{xy} &= v_{cxy}\end{aligned}\tag{5.3.62}$$

The stresses σ_x and τ_{xy} , used to derive the section resisting forces, are then collected in the condensed stress vector $\bar{\sigma}$.

The matrix $\bar{\mathbf{E}}$ and the vector $\bar{\sigma}$ are relative to a single fibre, so they are functions of the position of the fibre and of the control section, and can be written as $\bar{\mathbf{E}}(x, y)$ and $\bar{\sigma}(x, y)$.

The section stiffness matrix and the resisting forces of the control section can be calculated by integration:

$$\mathbf{k}(x) = \int_A \mathbf{I}^T(y) \cdot \bar{\mathbf{E}}(x, y) \cdot \mathbf{I}(y) dA \tag{5.3.63}$$

$$\mathbf{D}_R(x) = \int_A \mathbf{I}^T(y) \cdot \bar{\sigma}(x, y) dA \tag{5.3.64}$$

As usual for the fibre models, these integrals are solved numerically by subdividing the control sections into a number of fibres. The modules and the stresses are computed at the midpoint of each fibre. Due to the formulation of the constitutive model of the fibres, the steel areas are considered smeared over the concrete fibres and each fibre may contains both concrete and steel at the same location.

5.4 Solution strategies

Regarding the solution strategies adopted in the program, it must be noted first that the code works in forces control. This characteristic substantially prevents to catch a softening behavior and has convergence problems in case where the stiffness matrix tends to zero. to overcome this last problem a variable loading step technique has been adopted.

- *Variable loading step*

This technique consists in changing λ (load multiplier), in function of the Newton-Raphson's iterations convergence. If the convergence is not reached after a certain number of iteration, the algorithm automatically set $\lambda = \frac{\lambda}{2}$ and repeat the calculation from the

previous load step. Has been given a limitation of $\frac{\lambda}{16}$ beyond which the non-convergence is accepted and the calculation proceeds with a warning alert. Similarly, if the convergence is reached with a tolerance greater than $1e-10$ the algorithm set $\lambda = 2\lambda$ with the aim to optimize the computational time.

- *Convergence criteria*

The convergence criterion adopted, in terms of structural level is based on an energy criteria. In particular, as shown in Taucer et al. 1996 it was assumed that the general convergence of Newton Raphson iteration is achieved when the ratio between the current work increment and the initial work increment is less than a certain tolerance.

$$\frac{\left\{ \left[(\Delta \mathbf{P}_E^k)^i \right]^T \cdot (\delta \Delta \mathbf{p}^k)^i \right\}}{\left\{ \left[(\Delta \mathbf{P}_E^k)^1 \right]^T \cdot (\delta \Delta \mathbf{p}^k)^1 \right\}} = \frac{\left\{ \left[(\Delta \mathbf{P}_U^k)^i \right]^T \cdot (\delta \Delta \mathbf{p}^k)^i \right\}}{\left\{ \left[(\Delta \mathbf{P}_E^k)^1 \right]^T \cdot (\delta \Delta \mathbf{p}^k)^1 \right\}} \leq Stol \quad (5.4.1)$$

Even with regard to the element state determination convergence, an energy criterion was chosen. the increase of energy at the current iteration j is calculated and compared to the energy associated with the element iteration $j = 1$. This criteria is described by the following equation:

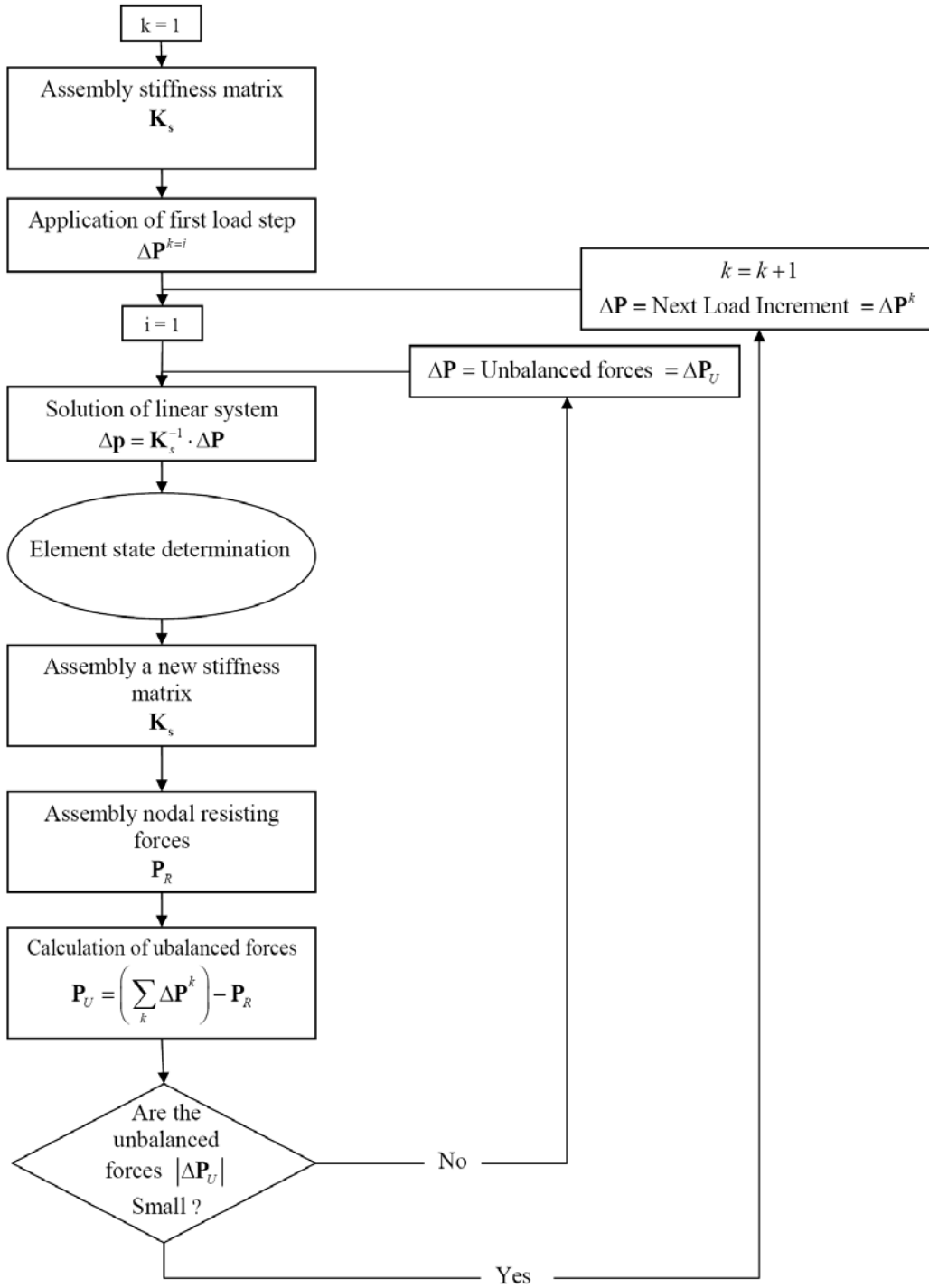
$$\frac{\left\{ \left[\left((\delta \Delta \mathbf{Q}^k)^i \right)^j \right]^T \cdot \left((\delta \Delta \mathbf{q}^k)^i \right)^j \right\}}{\left\{ \left[\left((\delta \Delta \mathbf{Q}^k)^i \right)^1 \right]^T \cdot \left((\delta \Delta \mathbf{q}^k)^i \right)^1 \right\}} = \frac{\left\{ \left[\left((\mathbf{s}^k)^i \right)^{j-1} \right]^T \cdot \left((\mathbf{k}_a^k)^i \right)^{j-1} \cdot \left((\mathbf{s}^k)^i \right)^{j-1} \right\}}{\left\{ \left[\left((\delta \Delta \mathbf{q}^k)^i \right)^1 \right]^T \cdot \left(\mathbf{k}_a^k \right)^{i-1} \cdot \left(\delta \Delta \mathbf{q}^k \right)^i \right\}} \leq Etol \quad (5.4.2)$$

where the numerator carries the quantities calculated in step j and the denominator the initial quantities.

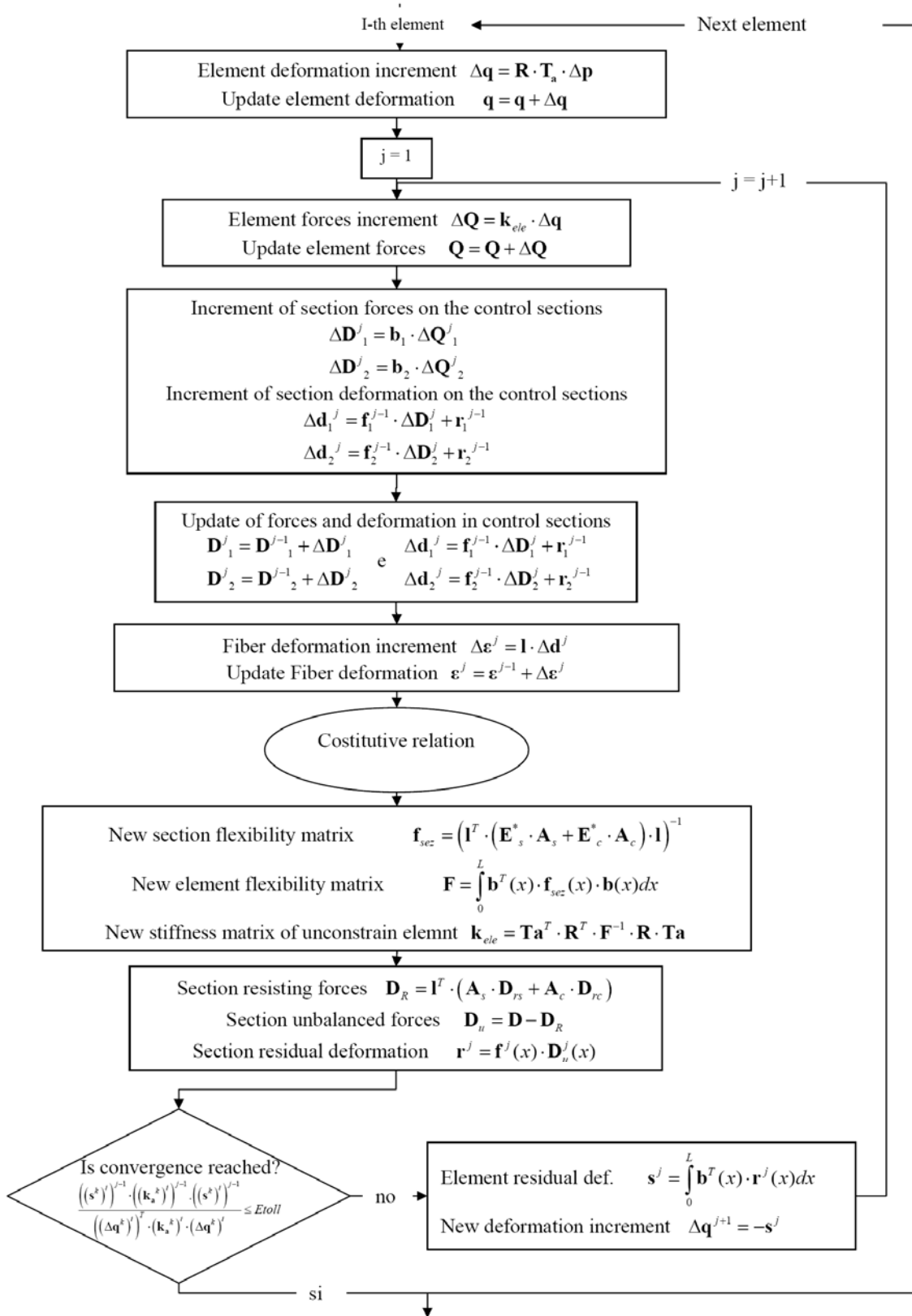
The default tolerance for both are set to the same value $Stol = Etol = 10^{-6}$. This criteria has the great advantage of controlling the unbalancing forces and residual deformations simultaneously.

5.5 Flow Chart

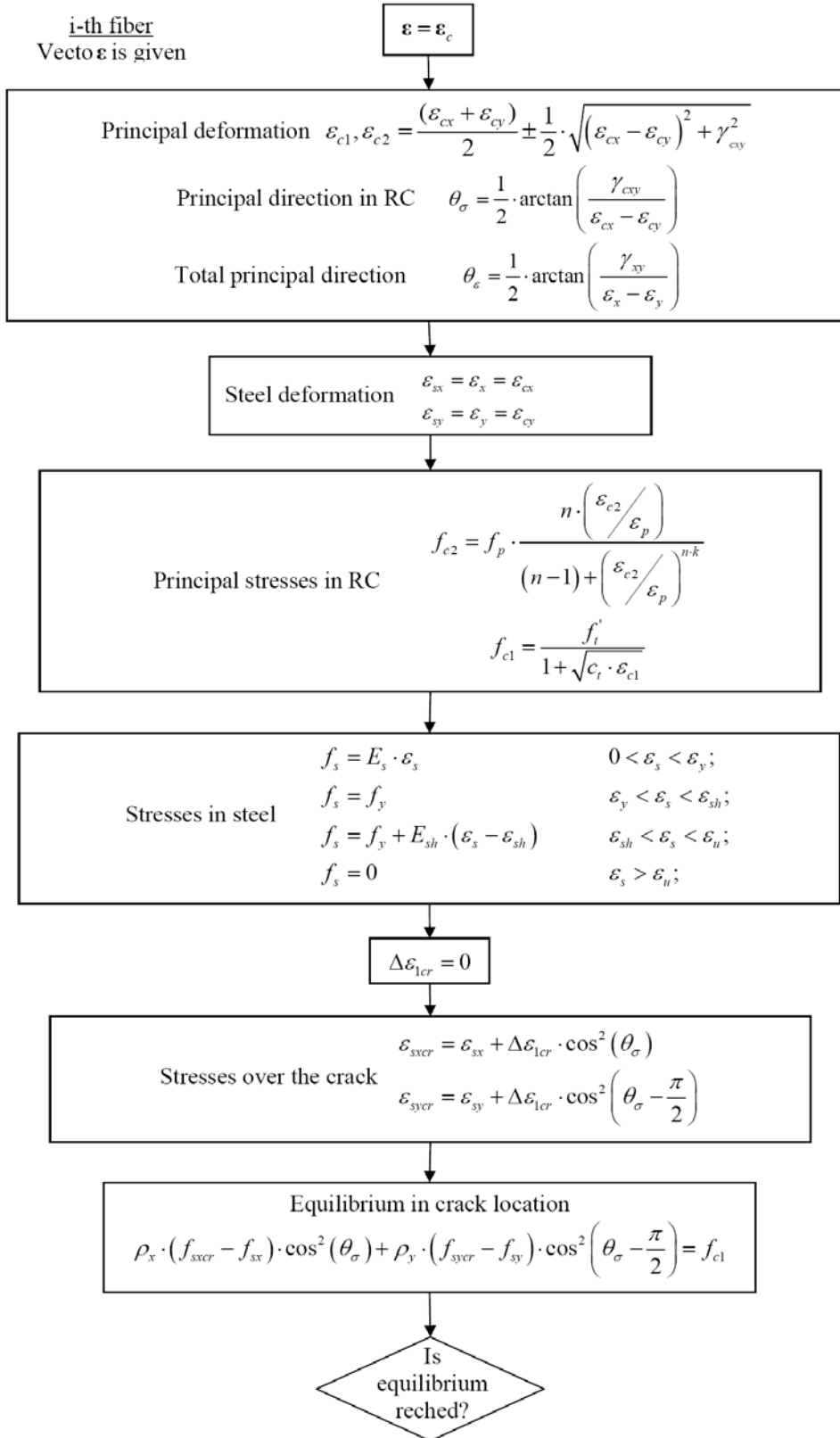
5.5.1 Structure state determination

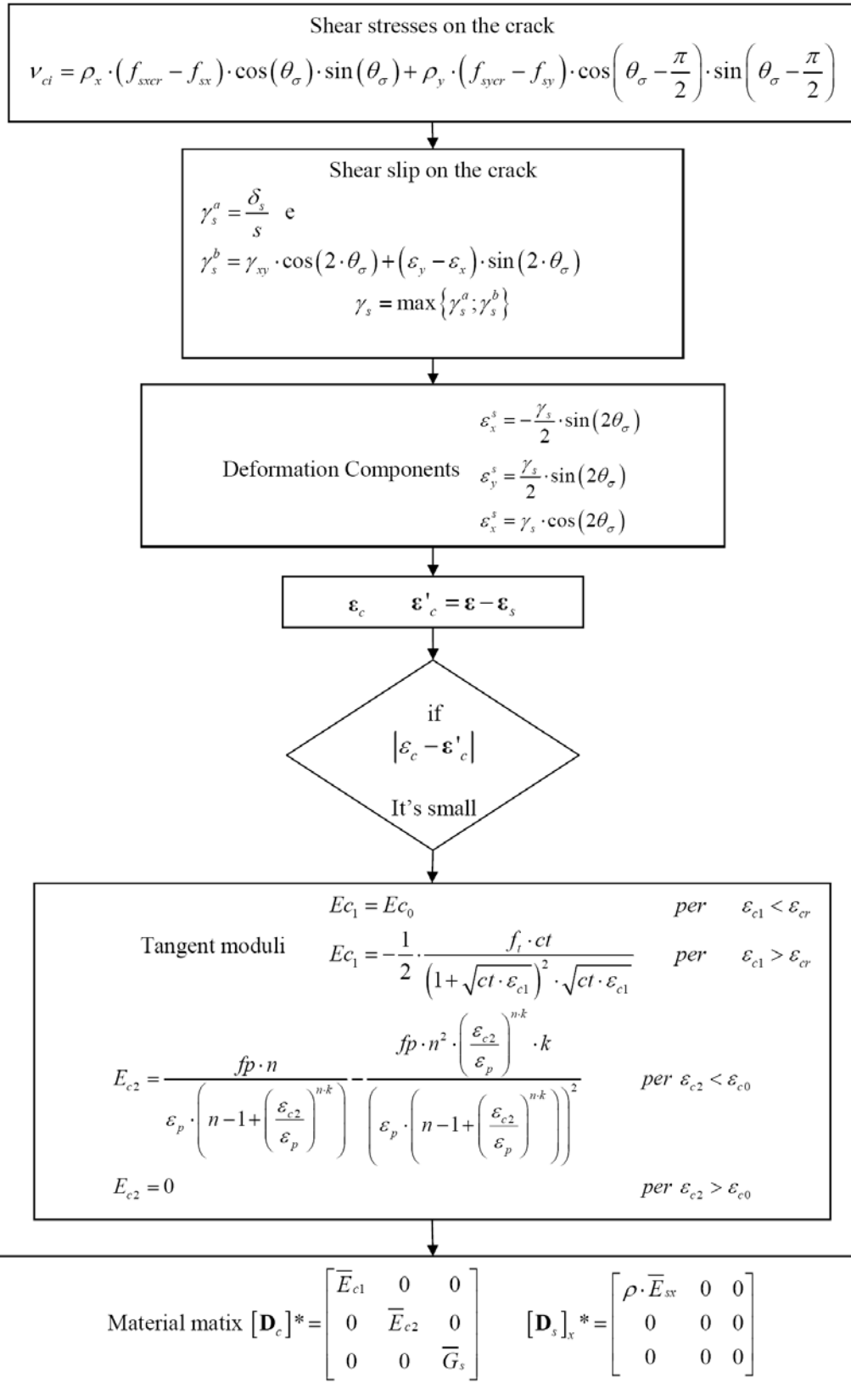


5.5.2 Element state determination



5.5.3 Section state determination





Rotation matrix, where $\psi = \theta_c$ for concrete, $\psi = 0$ for steel

$$\mathbf{T} = \begin{bmatrix} \cos^2 \psi & \sin^2 \psi & \cos \psi \sin \psi \\ \sin^2 \psi & \cos^2 \psi & -\cos \psi \sin \psi \\ -2 \cos \psi \sin \psi & 2 \cos \psi \sin \psi & (\cos^2 \psi - \sin^2 \psi) \end{bmatrix}$$

$$\mathbf{E}_c = \mathbf{T}^T \cdot \mathbf{D}_c \cdot \mathbf{T} \quad \mathbf{E}_{sx} = \mathbf{T}^T \cdot \mathbf{D}_{sx} \cdot \mathbf{T}$$

By summation the material matrix can be calculated $\mathbf{E} = \mathbf{E}_c + \mathbf{E}_{sx} + \mathbf{E}_{sy}$

Stresses are then calculated and collected in stress vector

$$\boldsymbol{\sigma} = \begin{bmatrix} f_{cx} = f_{c1} - \frac{(f_{c1} - f_{c2})}{(1 + \tan(\theta_\sigma)^2)} \\ f_{cy} = f_{c1} - \frac{(f_{c1} - f_{c2}) \cdot \tan(\theta_\sigma)^2}{(1 + \tan(\theta_\sigma)^2)} \\ v_{cxy} = \frac{(f_{c1} - f_{c2}) \cdot \tan(\theta_\sigma)}{(1 + \tan(\theta_\sigma)^2)} \end{bmatrix}$$

Vector stresses $\boldsymbol{\sigma}$ and material matrix \mathbf{E} are then condensed by the transverse equilibrium of the section in $\bar{\boldsymbol{\sigma}}$ ed \mathbf{E} that do not contain the degree of freedom in y direction

CHAPTER 6

Numerical analysis and validation

6.1 *Sommario*

Diverse analisi sono state svolte al fine di validare l'elemento finito proposto e di studiare l'effettiva influenza che l'interazione taglio flessione ha sul comportamento globale della strutture caratterizzate da una geometria prevalentemente tozza.

Per la validazione del modello con risultati sperimentali si è fatto riferimento all'ampia campagna di prove sperimentali condotte dalla Portland Cement Association (Oesterele et al. 1976). Le prove sono state condotte su diverse tipologie di pareti, da semplicemente rettangolari, con pilastri e flangiate con diverse dimensioni ed armature. Nel report a cui si è fatto riferimento sono evidenziati per ogni prova sperimentale i contributi che taglio e flessione portano allo spostamento finale della parete. Questa tipologia di dati ha dato un'ulteriore stimolo al tentativo di modellare i vari contributi. Le pareti testate rappresentano dei modelli in scala di pareti reali, dove il fattore di scala è pari a 1/3. La parete esaminata col codice di calcolo è indicata nel report come specimen B4.

E' stato inoltre svolto un confronto di tipo numerico, in termini di comportamento globale, tra il modello proposto nella tesi ed il codice di calcolo Vector II sviluppato presso l'Università di Toronto. Il codice in questione è un programma ad elementi finiti bidimensionali il quale utilizza la stessa teoria del modello oggetto della tesi come legame costitutivo.

Sono state inoltre svolte numerose analisi parametriche su due tipologie di strutture tozze ricorrenti, una pila da ponte ed una parete di taglio. Lo scopo delle analisi parametriche è quello di mostrare come l'interazione taglio-flessione influenzi il comportamento di strutture sostanzialmente tozze e di capire, secondo il modello oggetto di studio, qual è la snellezza limite oltre la quale l'effetto delle non linearità taglianti risulti di secondaria importanza.

6.2 Comparisons between numerical and experimental results

The model was validated by performing comparisons with available experimental results. The comparisons presented in this paper regard some experiments conducted by the Portland Cement Association. These tests were conducted on different types of RC shear walls characterized by different shapes of the cross-section: rectangular, barbell and flanged represented in fig. 6.2-1. For each section different dimensions and reinforcements were considered in the tests. The wall examined in this study is indicated in the cited report Oesterele et al. (1976) as Specimen B4. For this specimen the different contributions due to shear and bending to the lateral displacement of the wall were available from experimental results. This distinction in the displacement data gave the opportunity to find out if the model can catch the different components of displacement. The tested walls are scale models of real walls, where the scale factor is 1/3.

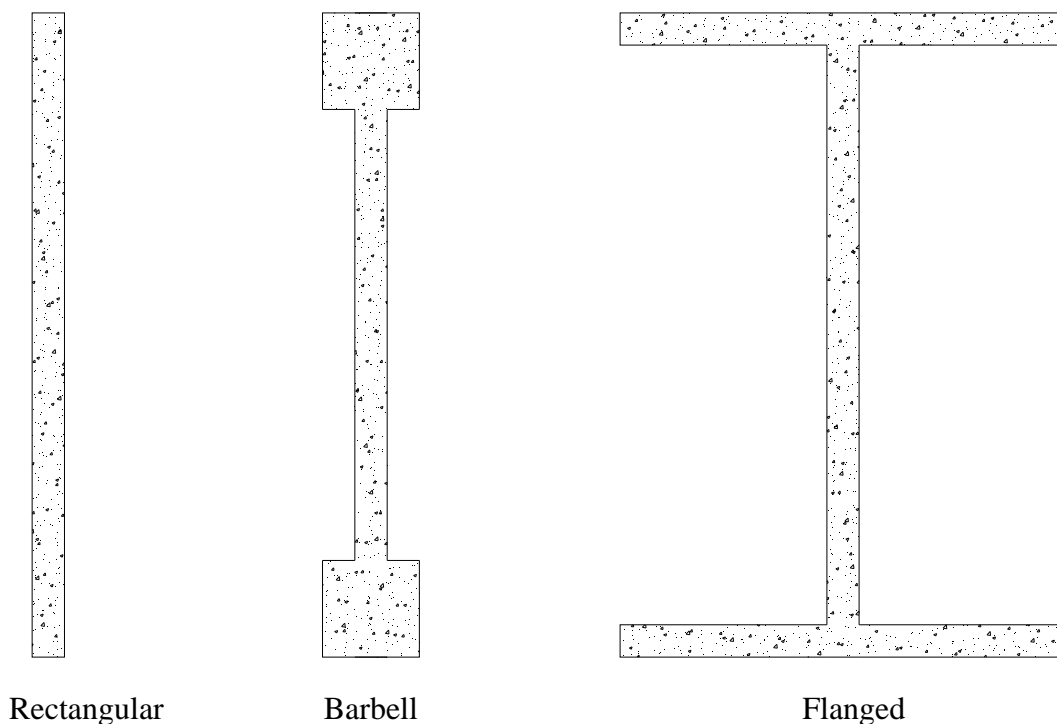


fig. 6.2-1

6.2.1 Geometry of specimen B4 and modelling criteria

The cross-section has the dimensions shown in fig. 6.2-2, the specimen was designed with all lengths expressed in inches but here are reported in millimetre. Along his height, the

specimen was monitored at each floor as described in fig. 6.2-3. The vertical reinforcement ratio of this specimen was set equal to 1.11% in each column. The mechanical properties of materials are shown in Tables 1 and 2.

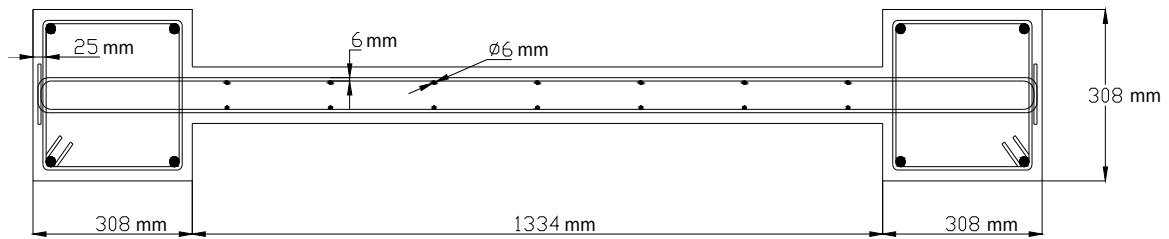


fig. 6.2-2

The wall was modelled with seven finite elements, in which the control sections were taken at the ends. Each section monitored in the experimental tests was associated to a control section of the model. The modelling of the wall with finite elements is shown in fig. 6.2-4a while the cross-section discretization with fibres is shown in fig. 6.2-4b.

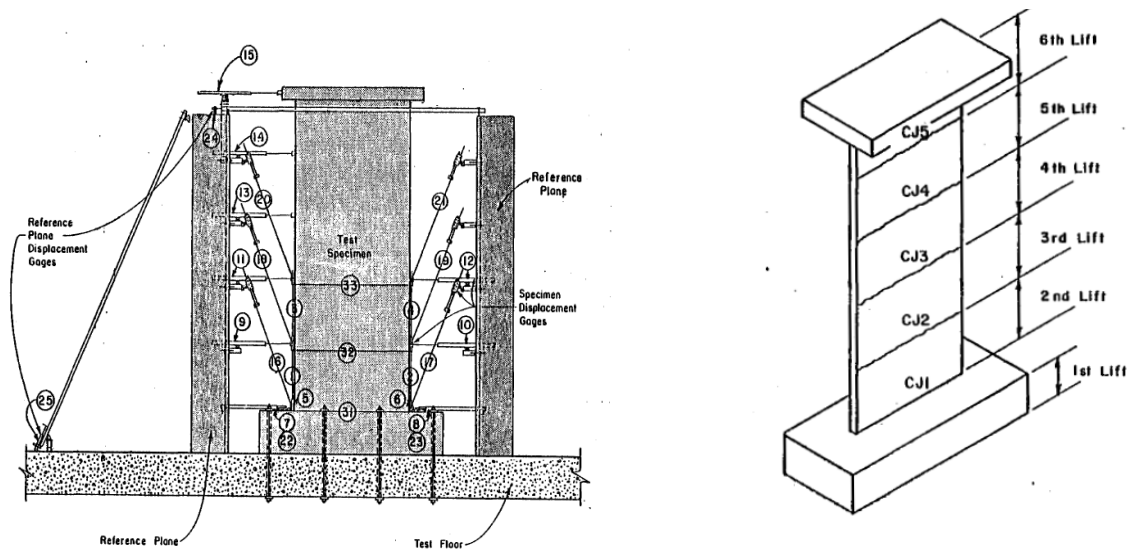


fig. 6.2-3

The steel was considered spread in each concrete fibre according with the model assumption. All the analyses were carried out considering a normal stress proportional to the self weight of the wall.

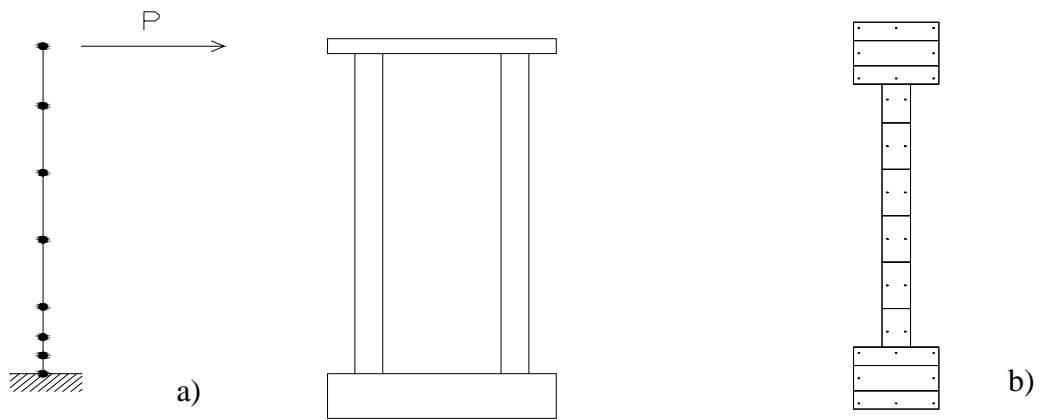


fig. 6.2-4

Table 1. Mechanical properties of steel of tested specimen.

	f_y	f_u	E_s	ϵ_u
Steel	73.20 (Ksi)	98.80 (Ksi)	32900 (Ksi)	12.6%
	511 (MPa)	690 (MPa)	229807 (MPa)	

Table 2. Mechanical properties of concrete of tested specimen.

	Day	f'_c	E_c
Concrete	68	6.53 (Ksi)	4100 (Ksi)
		46 (MPa)	28639 (MPa)

6.2.2 Results of the comparison

The diagrams obtained with the model, characterized by thicker lines, were superimposed to the diagrams related to the experimental results, characterized by thinner lines.

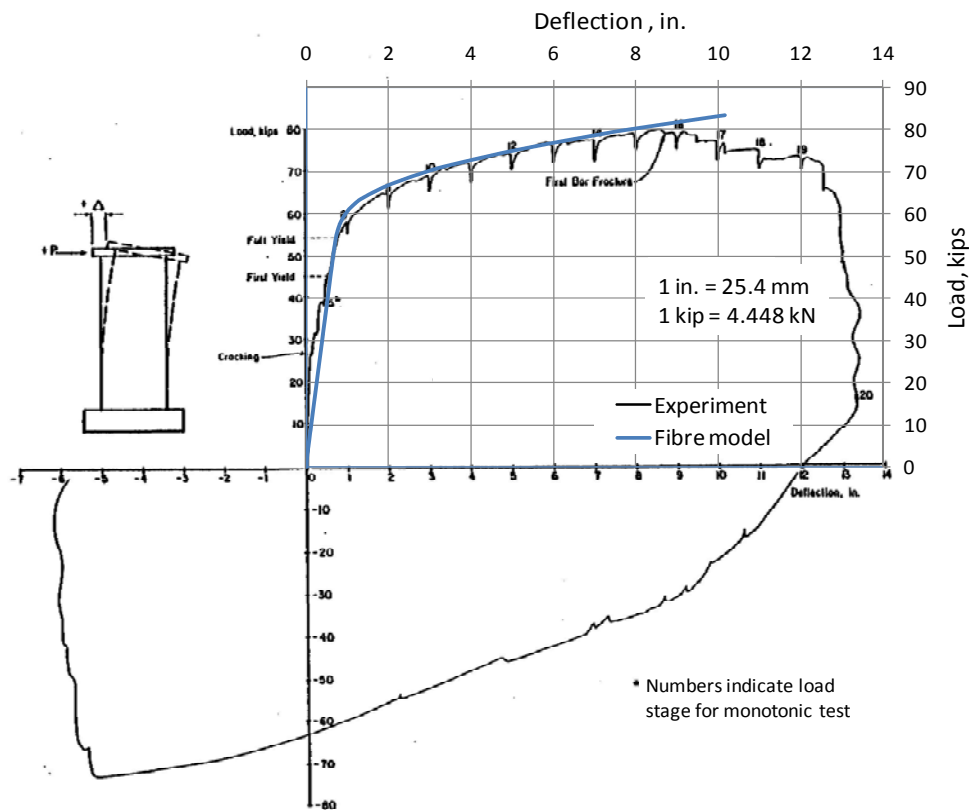


fig. 6.2-5

The first comparison was performed with reference to the pushover curve in fig. 6.2-5. This comparison shows that the graph obtained from the analysis matches well the experimental results.

It was not possible to represent the softening branch since this analysis was performed under load control. Another comparison was carried out in terms of moment-rotation diagrams at different levels. In particular, the diagrams were obtained at the following locations: at the base and at distances equal to 3ft (915 mm) and 6ft (1830 mm) from the base. The rotation at the base was measured at the first monitored section, located 250 mm

from the base. Even for the moment-rotation diagrams, the curves obtained numerically can approximate the experimental response as shown in fig. 6.2-6. Similarly, in fig. 6.2-7, the shear-distortion diagrams derived from the analyses are compared with those presented in the report. It is possible to notice also in this case that the numerical results approximate well the experimental response.

The diagrams in fig. 6.2-8 show the different contributions due to flexure and shear to the deflected shape in the nonlinear range.

To distinguish these contributions, the analysis was performed first with the model that takes into account the flexure-shear interaction. Then the analysis was repeated by neglecting, in the model, the shear deformation. This analysis provided the contribution of flexure while the shear deflection was derived as difference between the results of the two analysis.

As it is possible to notice in fig. 6.2-8, the total horizontal displacements along the height obtained numerically are close to those from experimental tests. For each type of contribution, flexure or shear, different diagrams, associated to different loading steps, are illustrated. The results relative to the last loading step are not shown since they are relative to the softening branch in the force-displacement diagram. From fig. 6.2-8 it is evident that the model was able to simulate accurately the different contributions due to flexure and shear in the nonlinear response of the wall. Moreover, the model was able to capture also the interaction between flexure and shear. The nonlinear response, in fact, is variable along the height while the shear is constant. This result may be interpreted as the effect of the variation of the bending moment on the shear response, and it is examined also in the next paragraph.

Numerical analysis and validation

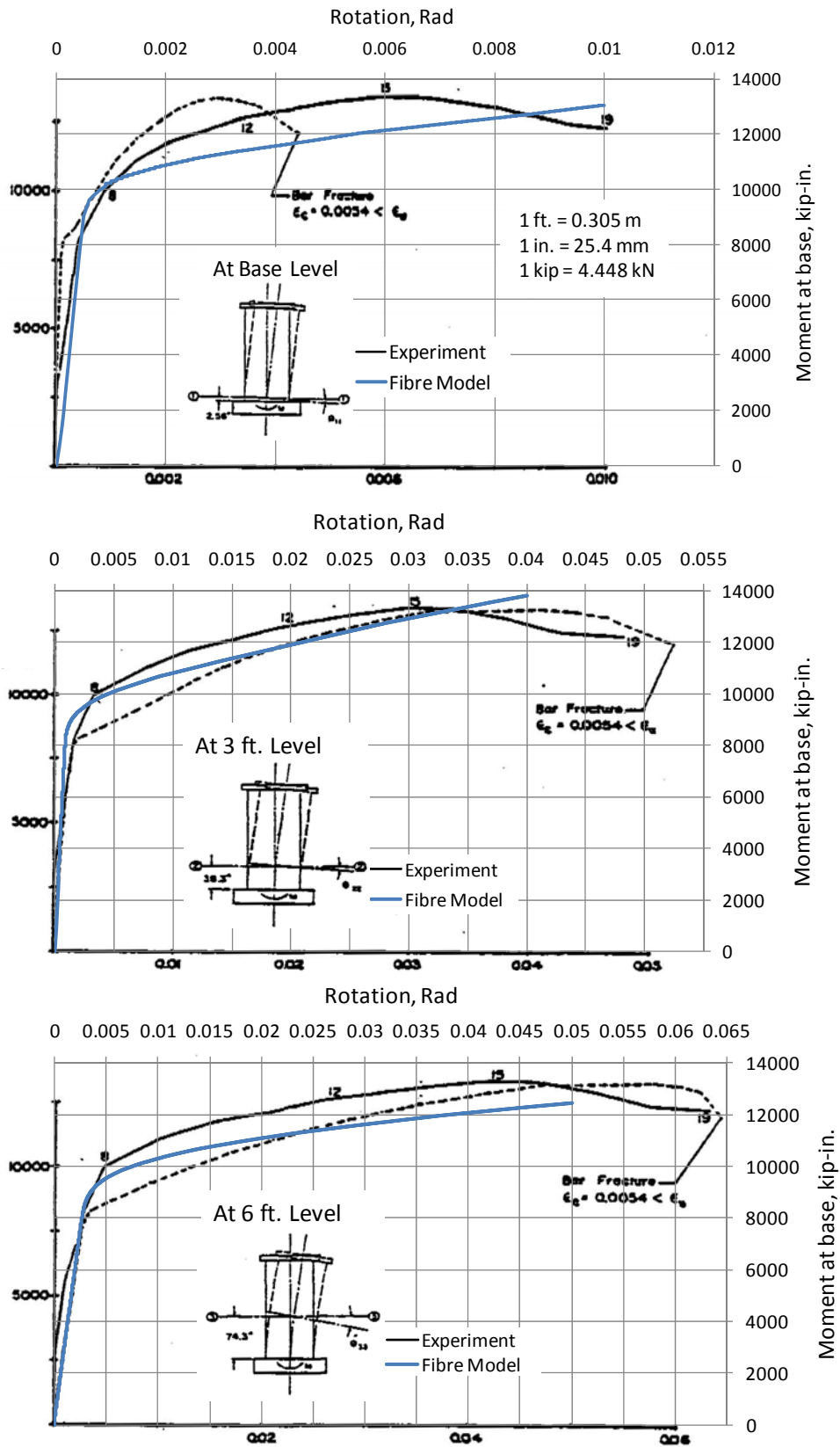


fig. 6.2-6

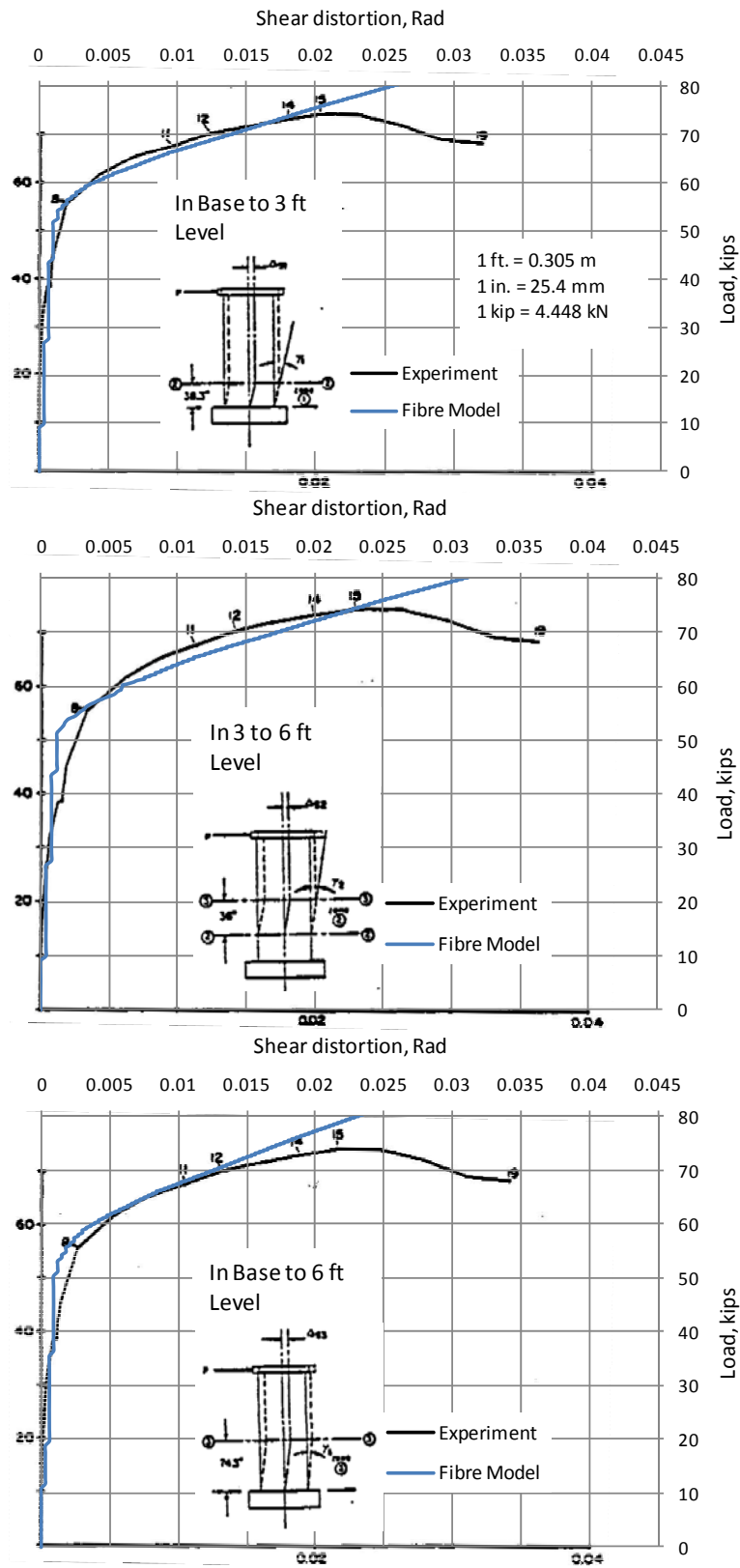


fig. 6.2-7

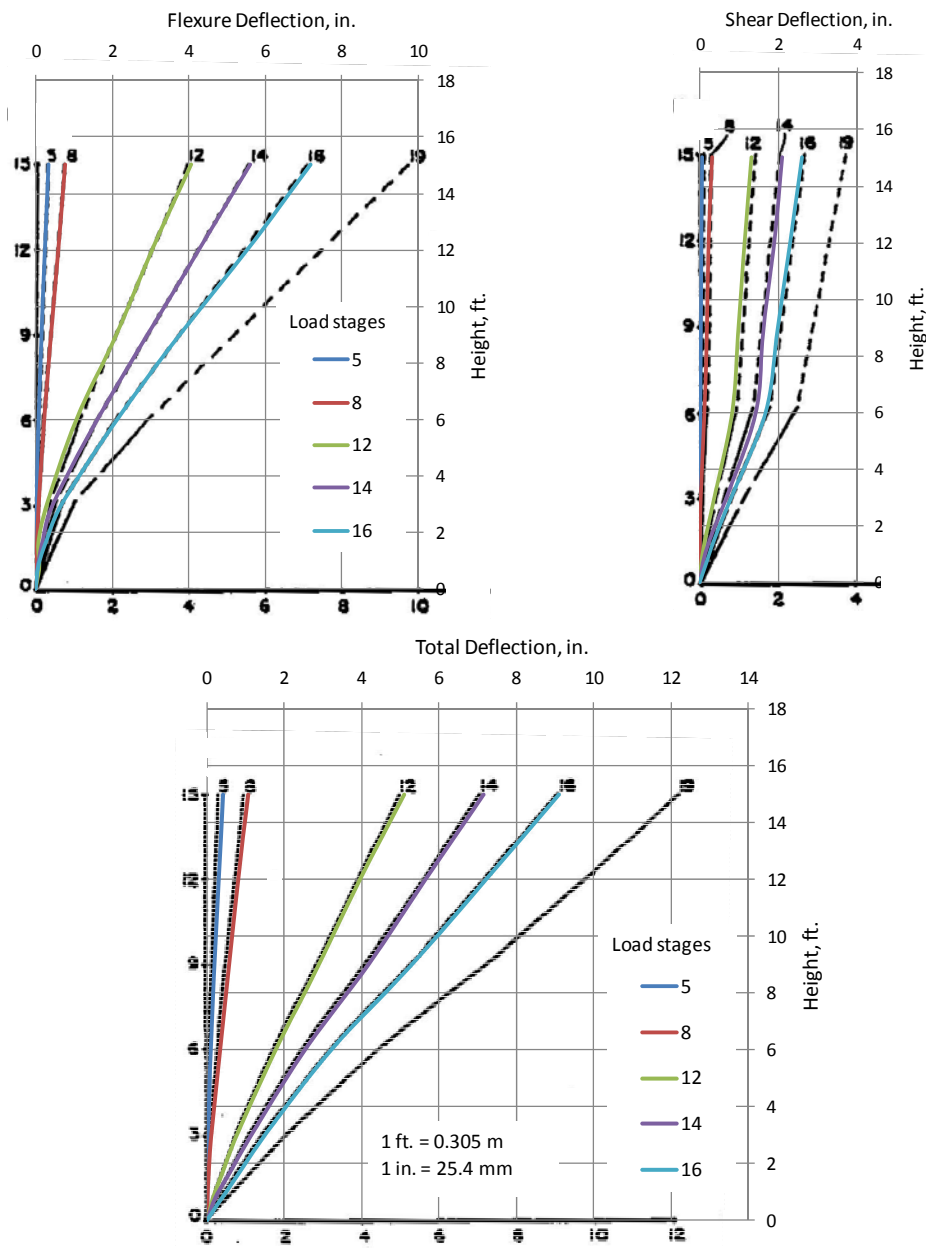


fig. 6.2-8

6.3 Numerical comparison with VecTor2

The proposed model was tested also through various comparisons with other models, implemented in available computer programs. This paragraph illustrates an example of a comparison with the computer code VecTor2, based on bi-dimensional finite elements and on MCFT constitutive law. The example regards a squat RC wall whose geometric characteristics are shown in fig. 6.3-1. The adopted material properties are: concrete cylinder compressive strength equal to 25 MPa and steel yielding stress equal to 450 MPa.

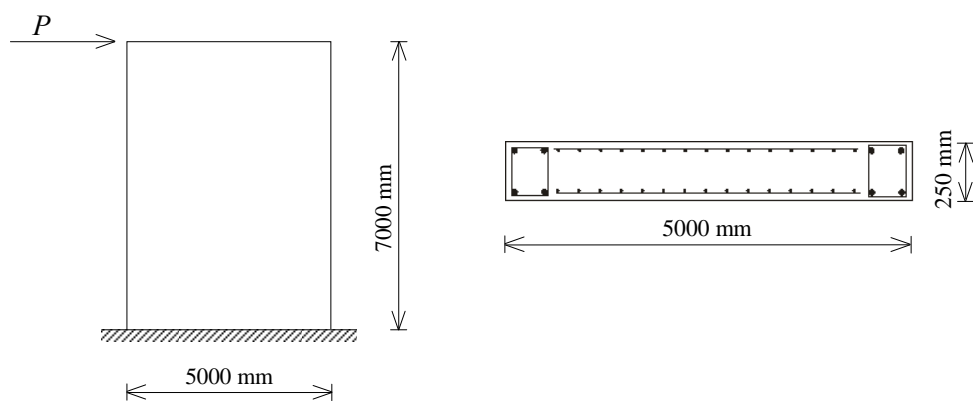


fig. 6.3-1

Web reinforcements are bars with a diameter equal to 8 mm at a spacing equal to 20 cm, pillars reinforcement are 4 bars with a diameter equal to 16 mm. The proposed model was applied considering for this structure 7 finite elements with 2 control sections per element and 23 fibres per section fig. 6.3-2

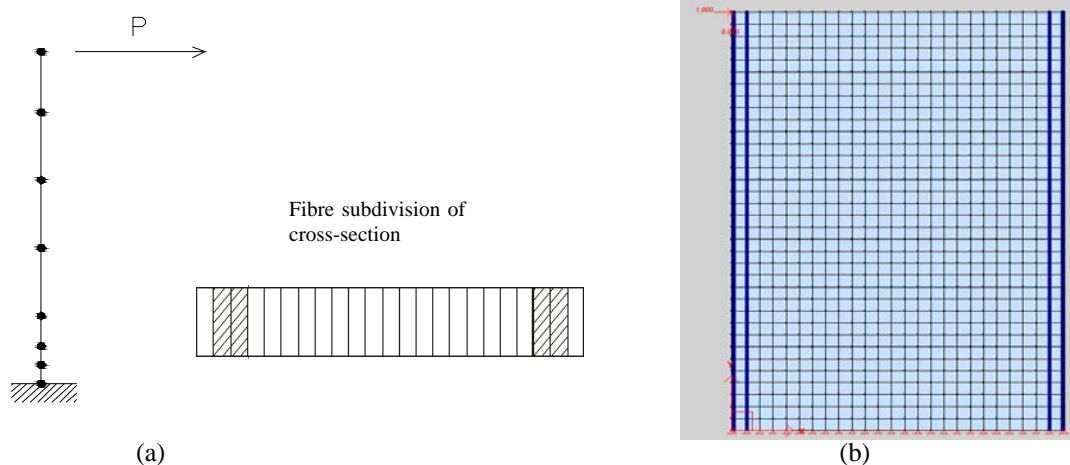


fig. 6.3-2

As it can be observed from fig. 6.3-3, the two computer programs provided similar results in terms of base shear-top displacement curve. The two models, while using the same constitutive relationship, are based on completely different nonlinear finite elements, so it is interesting to highlight a similarity in the results.

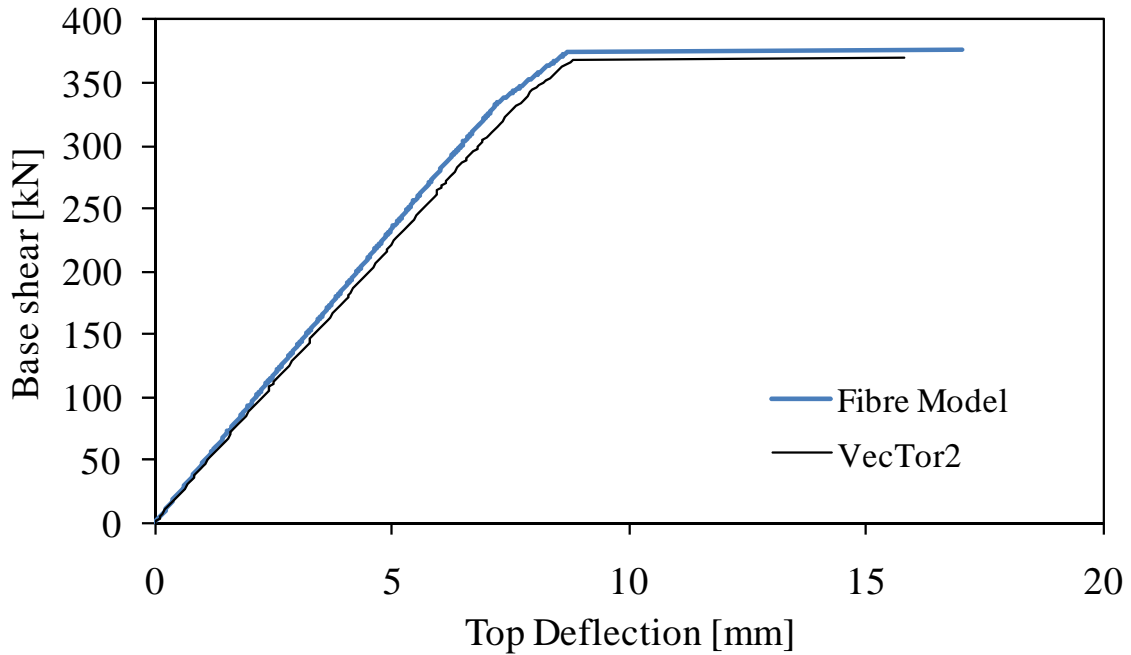


fig. 6.3-3

6.4 Investigation on the influence of flexure-shear interaction

The proposed model was then applied for investigating the nonlinear flexure-shear coupling. The investigation regarded two classical example of squat structure, a bridge pier with circular cross-section loaded by a force at its free end and a shear wall.

6.4.1 Parametric analysis on bridge pier

The analyses were repeated changing the height of the pier L and maintaining the same section diameter, in order to keep the ratio L/D as the control parameter of the analysis. Description of examined piers and modelling assumptions are shown in fig. 6.4-1 and Table 3.

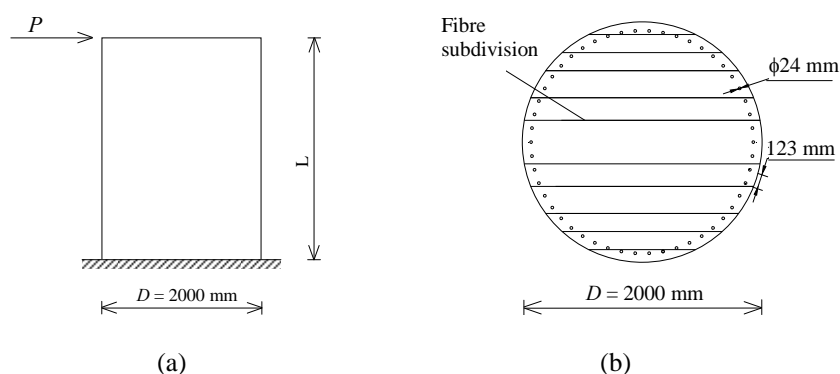


fig. 6.4-1

Table 3. Geometrical dimensions and modelling assumptions of RC piers under study

Diameter (m)	2	2	2	2	2	2	2	2	2	2
Height (m)	2	4	6	8	10	12	14	16	18	20
L/D	1	2	3	4	5	6	7	8	9	10
Number of elements	2	4	5	6	7	8	8	9	10	11
Element length (m)	1.00	1.00	1.20	1.33	1.42	1.50	1.75	1.77	1.80	1.81

With regard to mechanical properties of materials, a concrete with cylinder compressive strength equal to 45 MPa and a steel with yielding stress equal to 430 MPa were considered. For each L/D ratio, two types of analysis were made: one considering nonlinear flexural behaviour and linear shear response, uncoupled by the flexural one; the other considering coupled nonlinear flexural and shear behaviour.

By calling with d_{MV} the top displacement associated to the base shear at yielding and calculated considering nonlinear flexure-shear interaction, and with d_M the same type of displacement obtained by keeping linear the shear behaviour, the results of the parametric analysis are illustrated in fig. 6.4-2. In the Figure the ratio d_{MV}/d_M is plotted as a function of the ratio L/D . This graph shows that nonlinear flexure-shear interaction affected the response in a significant way for values of L/D lower than 4.

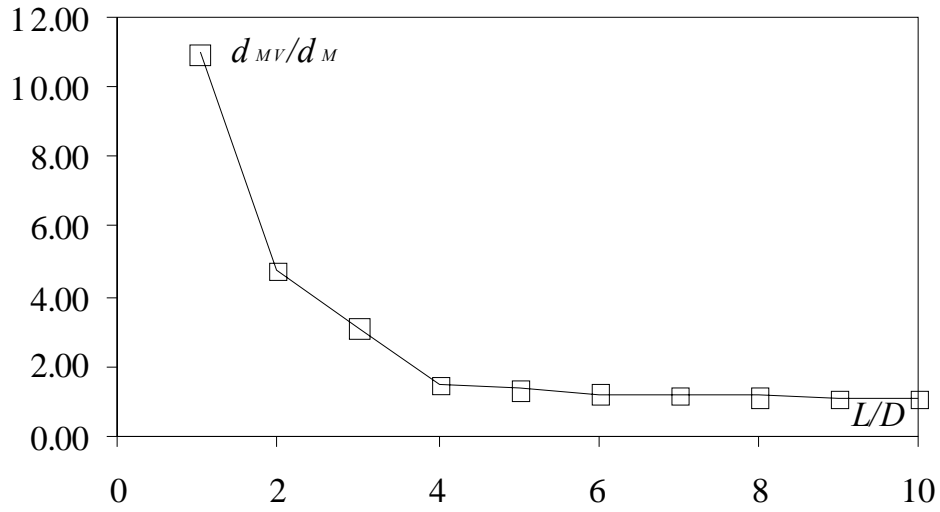


fig. 6.4-2

In fig. 6.4-3 V_M is the value of base shear calculated considering linear shear behaviour while V_{MV} is the value of base shear obtained considering nonlinear shear behaviour. Figure 19 illustrates the ratio V_M/V_{MV} calculated at fixed values of top displacement in the non-linear range and plotted as a function of the ratio L/D . This diagram shows again the importance of nonlinear shear response. The inclusion of shear deformation, in fact, increases the flexibility of the structure with the consequence that for obtaining given displacement values, lower values of lateral load are required. In the range of L/D between 2 and 4 the obtained values of the ratio V_M/V_{MV} are around 1.15.

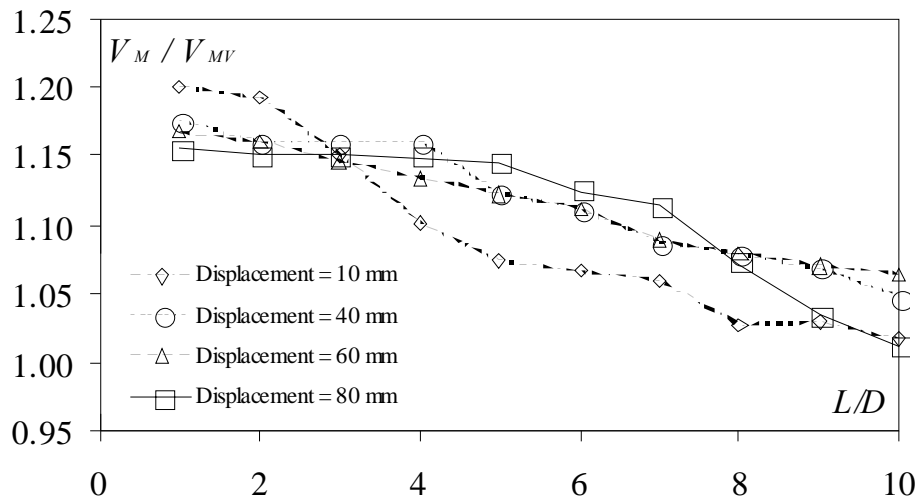


fig. 6.4-3

fig. 6.4-4 illustrates the diagrams of base shear versus shear deformation evaluated at different locations along the height of the pier. This graph shows that the shear response changes along the height when nonlinear flexure-shear interaction is included in the analysis. On the other hand the diagram of base shear versus shear deformation remains linear and constant along the height when linear shear response is considered. Since shear forces are constant along the height while diagrams of shear versus shear deformation does change, it is clear also in these investigations, as noticed in the experimental results, that the variation of bending moment along the height affects the shear deformations. This result highlights the influence of flexure-shear interaction in the nonlinear response.

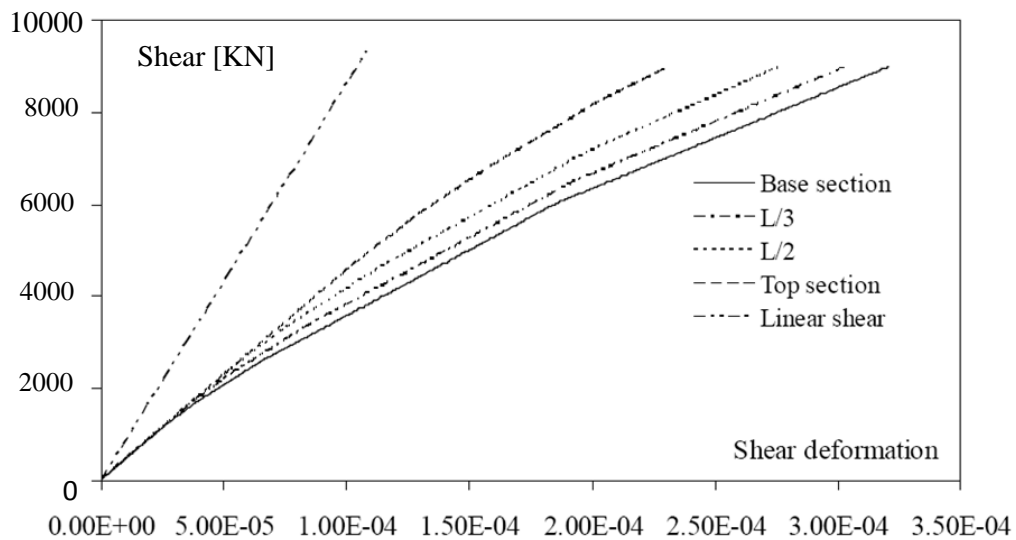


fig. 6.4-4

6.4.2 Parametric analysis on a shear wall

This analysis was carried out, similar to the previous on a shear wall. Numerical results are obtained keeping the section (reported in fig. 6.4-5) and varying the height. The main analysis and results are reported below:

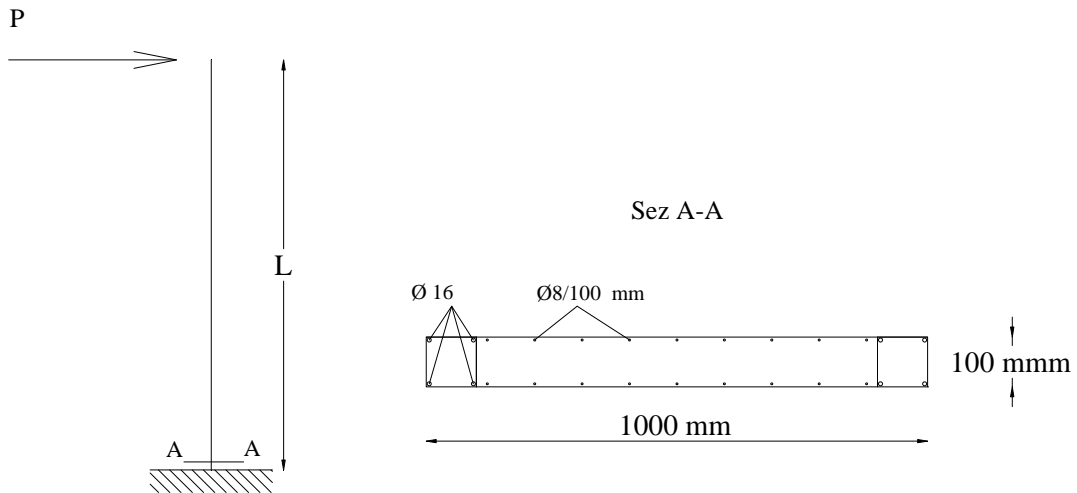


fig. 6.4-5

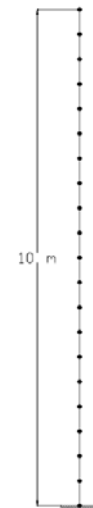
6.4.3 Analysis with the ratio $\frac{L}{d} = 10$ (slender shear wall).

The wall was schematized with 20 elements (21 nodes). The geometrical discretization and mechanical characteristics of the wall are reported in of the analysis are shown in

Steel	fsy [Mpa]	ft [Mpa]	ey	et	Es [Mpa]	vs
	430	540	0,002	0,1	210000	0,3

Concrete	fc [Mpa]	fct [Mpa]	ec0	ecu	Es [Mpa]	vs
	-30	3	-0,002	-0,0035	210000	0,25

fig. 6.4-6



From the analysis the following diagrams are obtained. In red curve is represented the flexural model keeping shear in linear elastic range, in blue curve a full coupling between flexure and shear is considered. The results are reported in terms of pushover curve, moment curvature and shear-shear distortion.

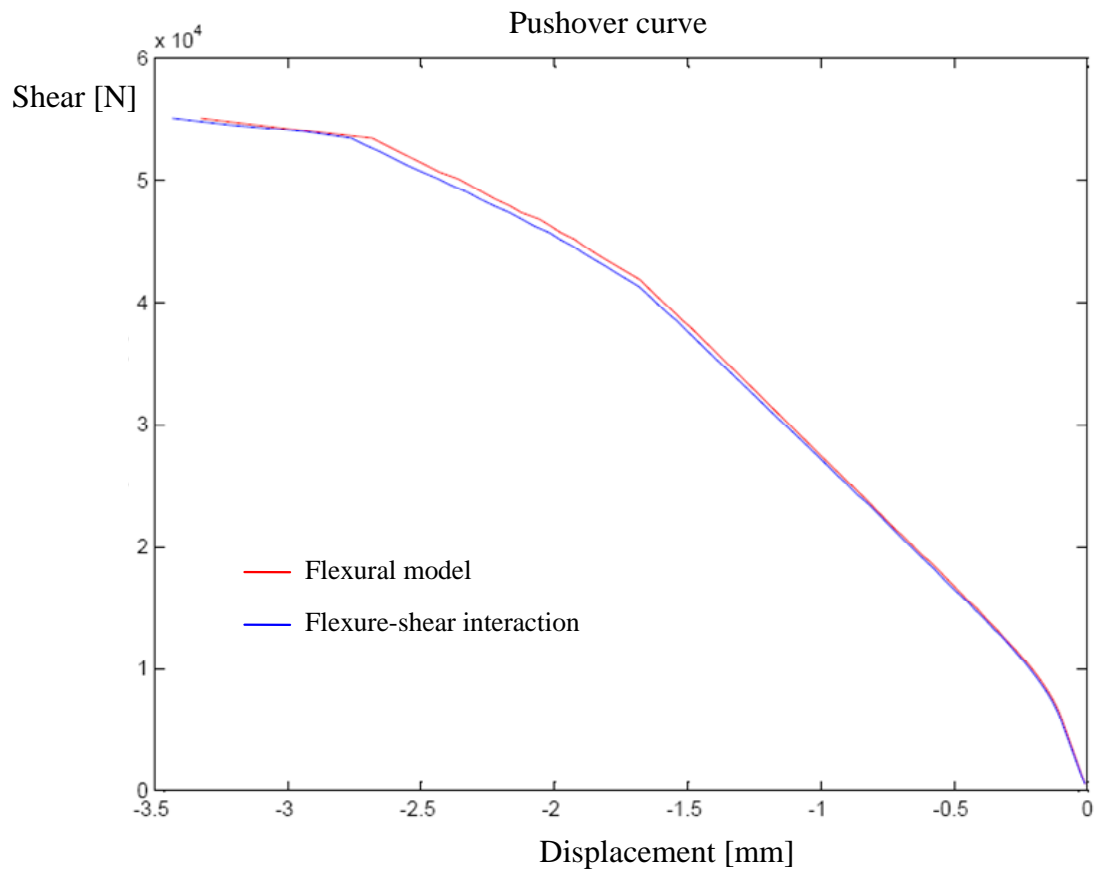


fig. 6.4-7

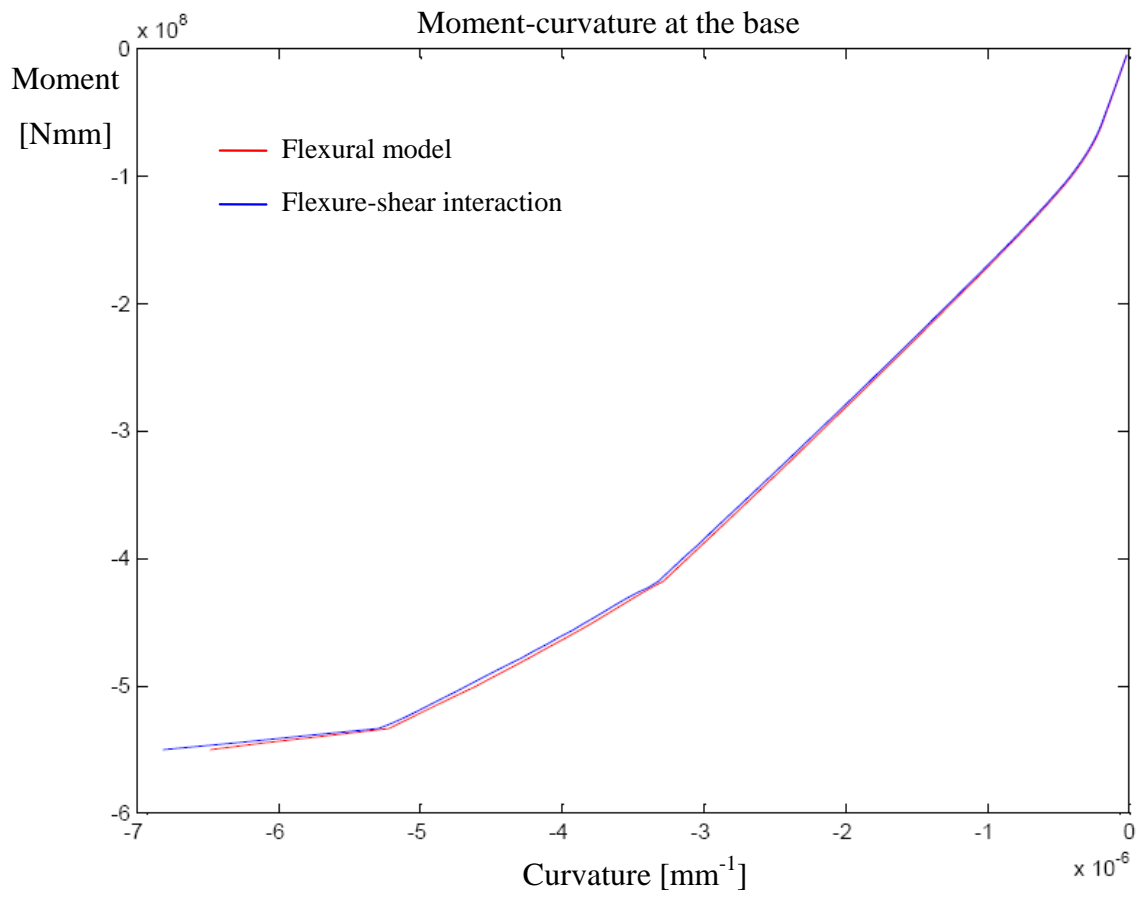


fig. 6.4-8

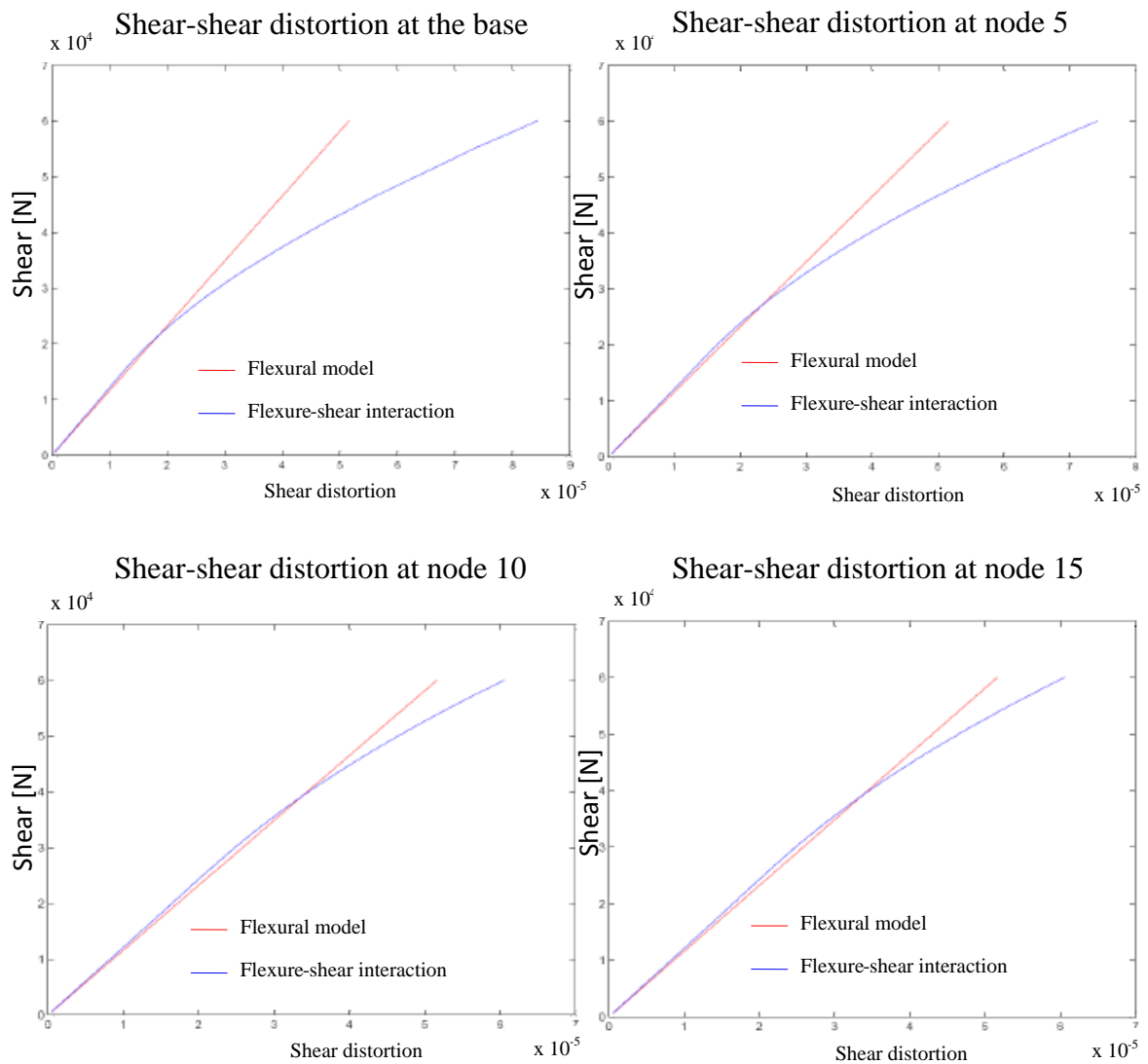
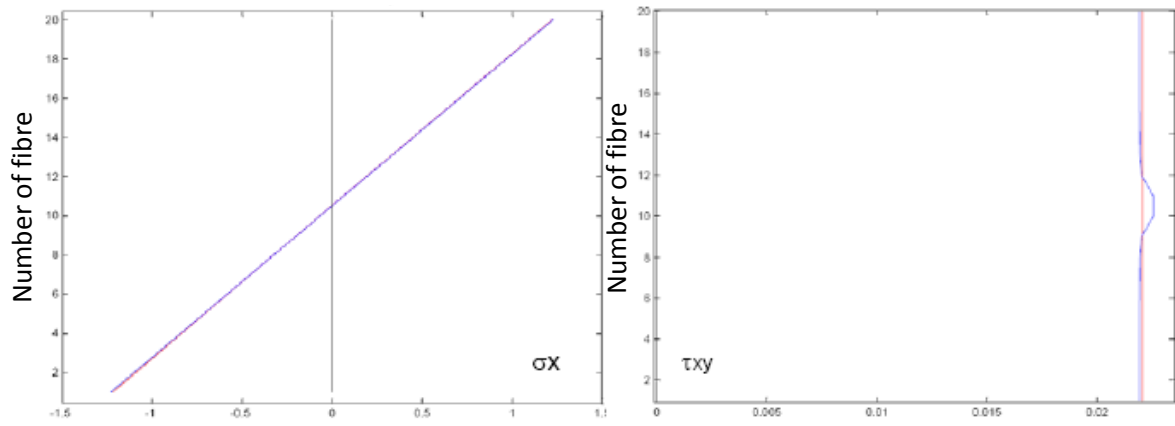


fig. 6.4-9

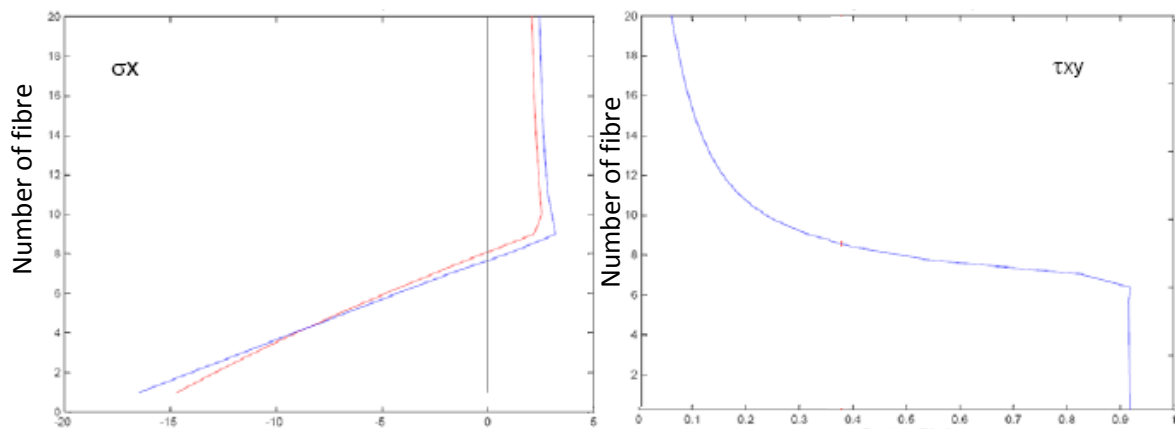
Also in this example we can observe the capacity of the model to catch the flexure-shear interaction, in particular is observed how the bending moment affects the $T - \gamma$ diagram.

In fact the diagram shear-shear distortion varies along the height of the beam, even though the shear is obviously constant on the wall.

Stresses evaluated in earlier load steps



Stresses evaluated in latter load steps



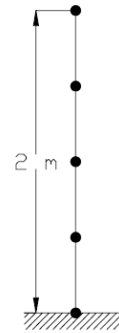
6.4-10

6.4.4 Analysis with the ratio $\frac{L}{d} = 2$.

In this second example, the wall was schematized with 4 nodes and 5 elements. Geometrical and mechanical characteristics of the analysis are shown in 6.4-11

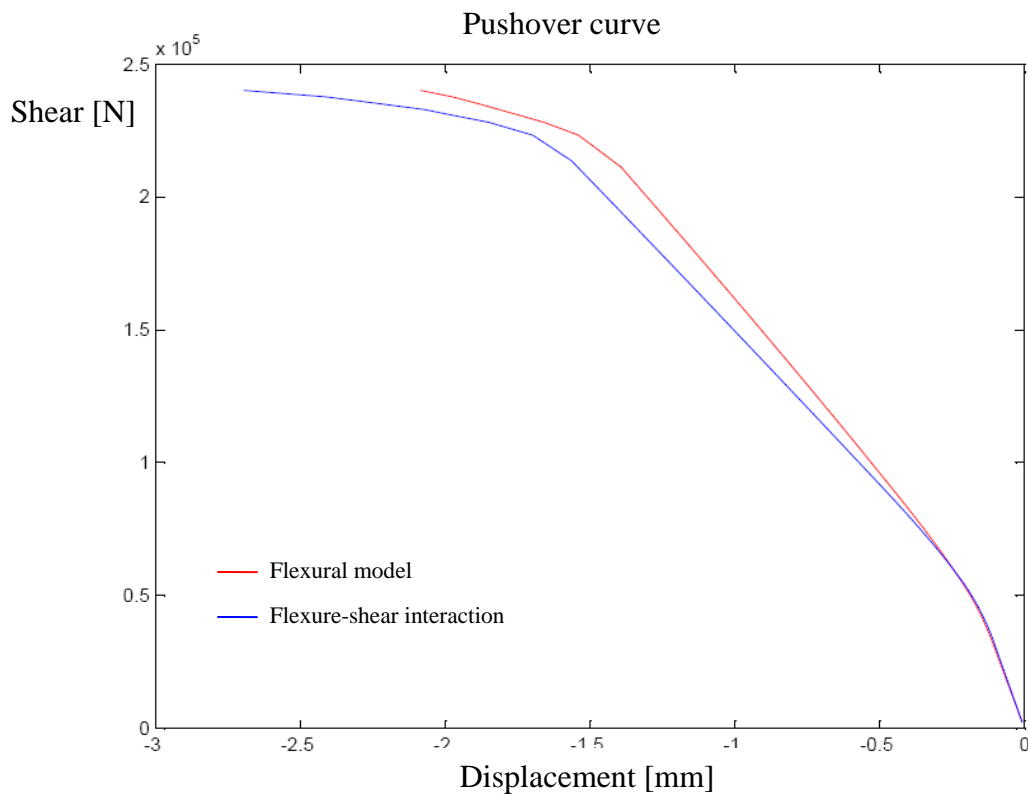
Steel	fsy [Mpa]	ft [Mpa]	εy	εt	Es [Mpa]	νs
	430	540	0,002	0,1	210000	0,3

Concrete	fc [Mpa]	fct [Mpa]	εc0	εcu	Es [Mpa]	νs
	-30	3	-0,002	-0,0035	210000	0,25

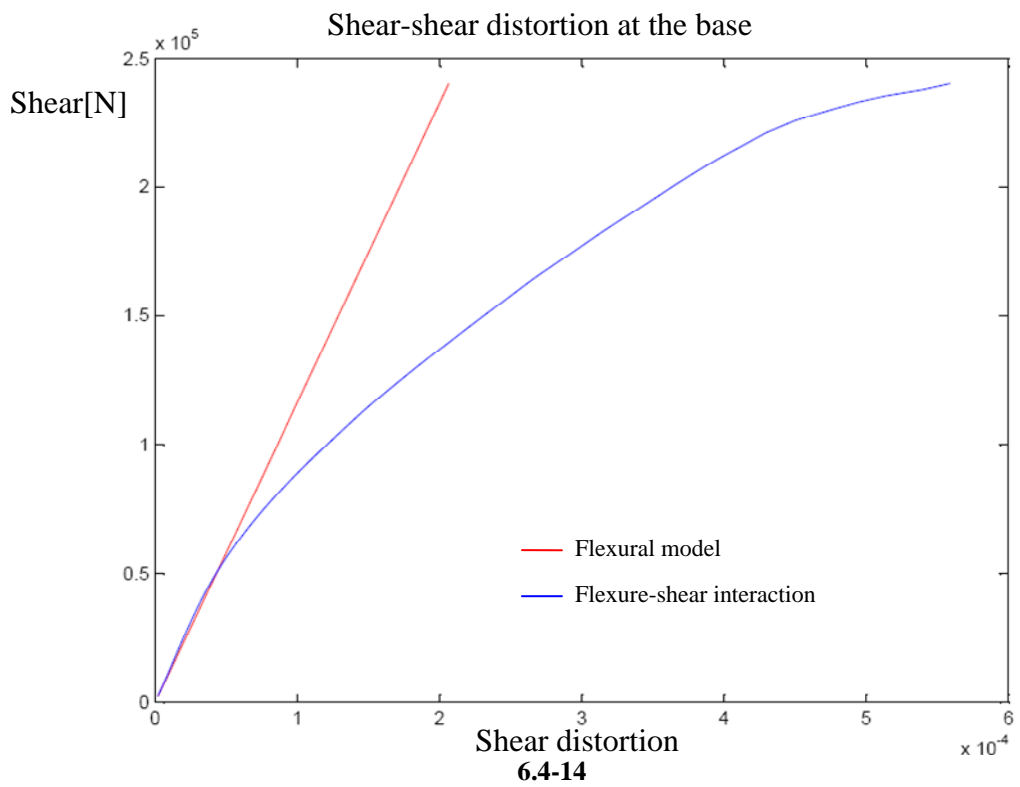
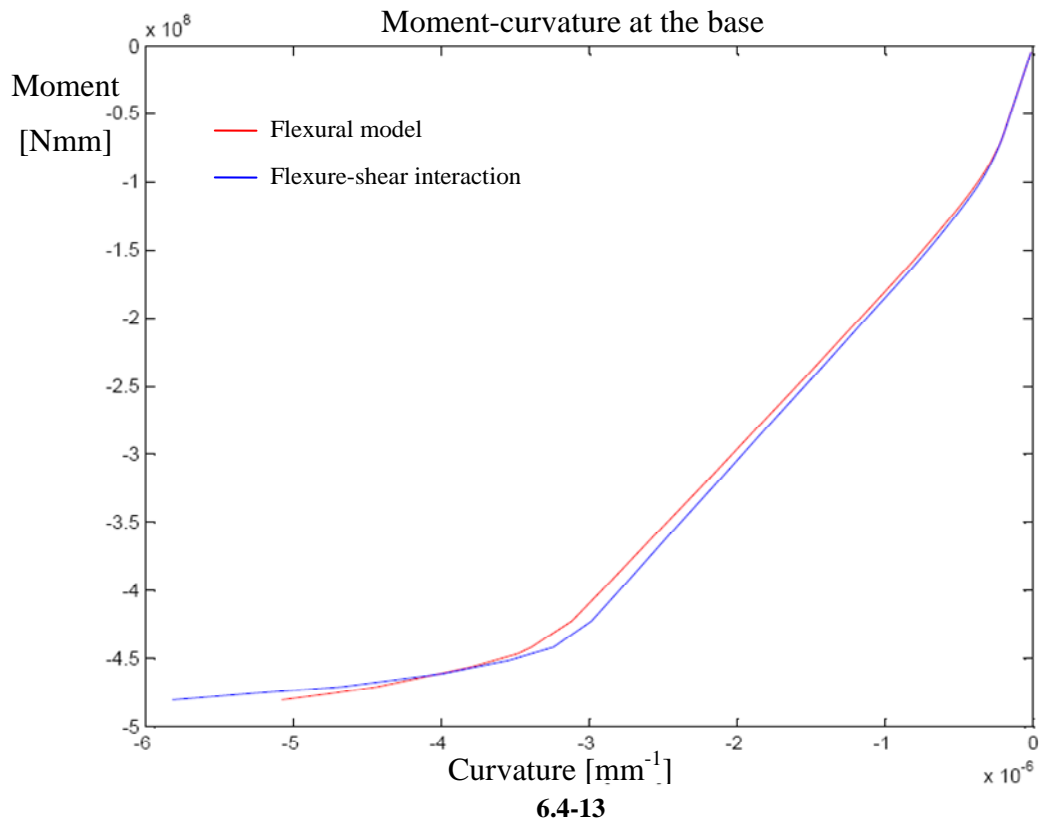


6.4-11

The results are presented in terms of pushover curve, moment curvature, shear-shear distortion in the following figures 6.4-12; 6.4-13; 6.4-14:



6.4-12

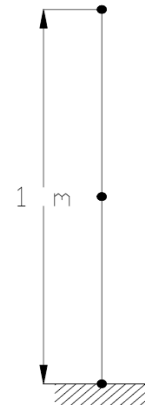


6.4.5 Analysis with the ratio $\frac{L}{d} = 1$.

In this example the wall was schematized with 3 node and 2 elements. Mechanical and geometrical parameters are represented below in fig 6.4-15:

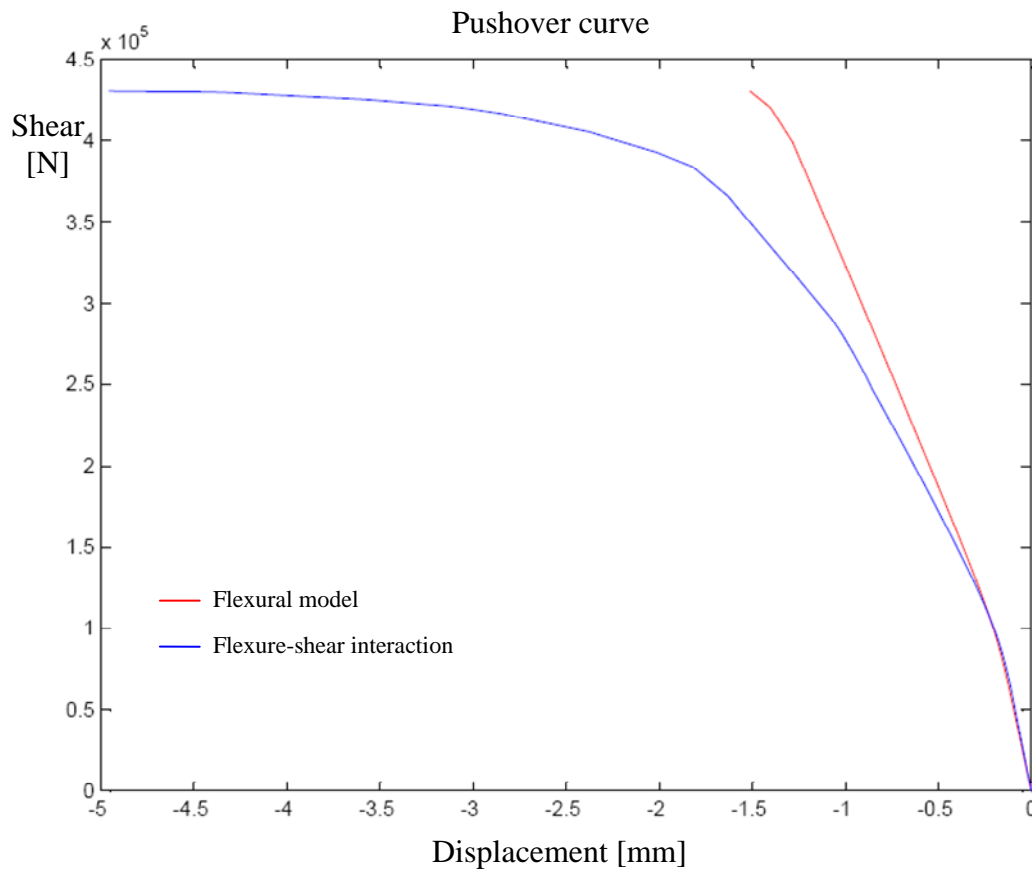
Steel	fsy [Mpa]	ft [Mpa]	ey	et	Es [Mpa]	vs
	430	540	0,002	0,1	210000	0,3

Concrete	fc [Mpa]	fct [Mpa]	ec0	ecu	Es [Mpa]	vs
	-30	3	-0,002	-0,0035	210000	0,25

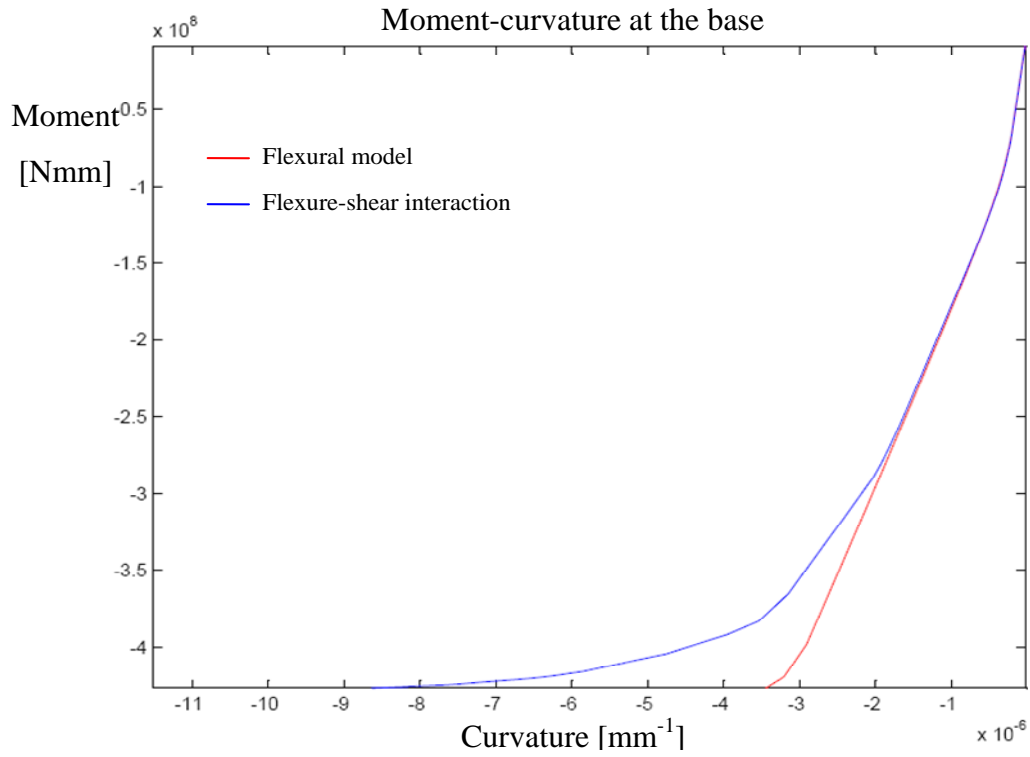


6.4-15

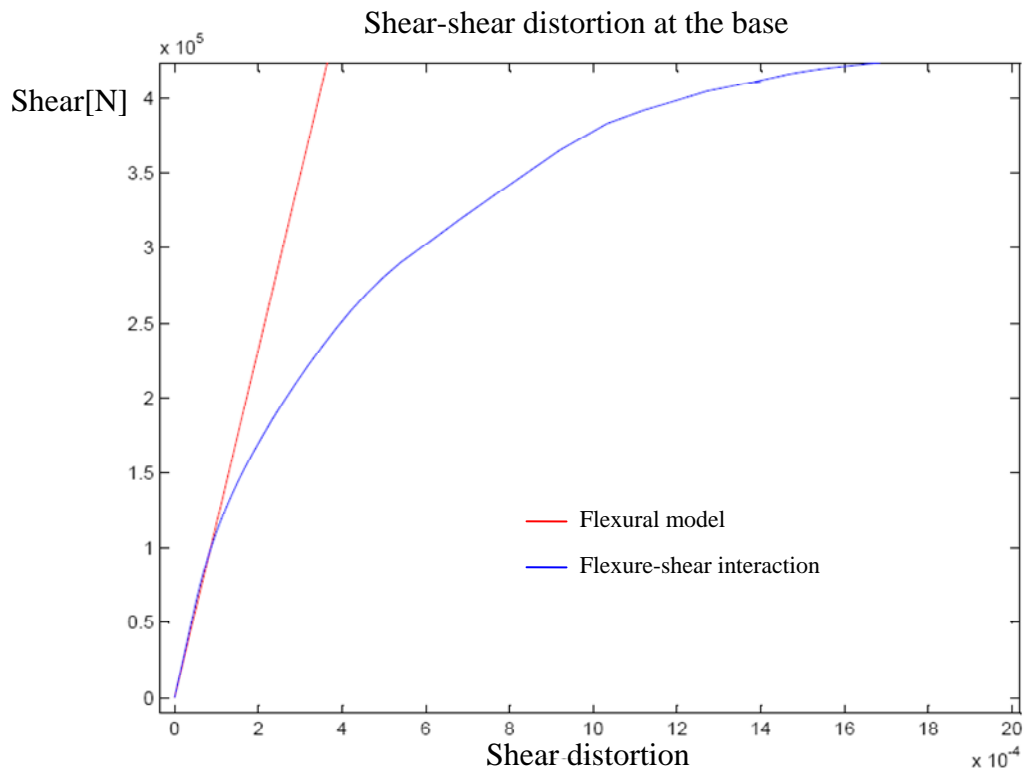
Errore. L'origine riferimento non è stata trovata.



6.4-16



6.4-17



6.4-18

It may be observed that in a squat wall much as it analyzed in latter example, the non-linear flexure-shear interaction will be decisive in determining the general behavior of the structure. It may also notice that before cracking the two models return identical results. This suggests that the model developed with flexure-shear interaction in non-linear field is an extension of the simplest flexure element.

CHAPTER 7

Alternative formulation for the shear critical beam-column element (developed in University of California Berkeley)

7.1 Sommario

Una formulazione alternativa a quella proposta fino ad ora è stata studiata presso l'Università della California di Berkeley (UCB) sotto la supervisione del professor Filip. C. Filippou. L'elemento è stato sviluppato e implementato nella piattaforma informatica FedeeasLab (Saritas, Filippou (2006)). Per quanto riguarda il campo di spostamento, l'elemento segue l'ipotesi della teoria della trave deformabile per taglio di Timoshenko, mentre per la derivazione della risposta elemento è stato utilizzato una formulazione variazionale a tre campi basata sul funzionale di Hu-Washizu. Il problema dei grandi spostamenti è considerato attraverso l'uso della formulazione corotazionale. Invece di un legame costitutivo bidimensionale per ogni fibra, è stato direttamente utilizzato un modello tridimensionale del materiale in cui è stata successivamente applicata una condensazione delle variabili attraverso l'equilibrio trasversale della sezione. Questo garantisce l'accoppiamento delle tensioni in ogni sezione di controllo. Per lo stesso elemento finito sono state introdotti due diversi legami costitutivi tridimensionali, uno per le strutture in l'acciaio ed un altro per l'analisi di strutture in cemento armato.

Per il calcestruzzo è stato implementato un modello di danno con due parametri, uno per controllare i danni in compressione e un altro parametro per il danno in trazione. Il modello di danno tridimensionale utilizzato è stato formulato da Lee e Fenves (1998). Le pagine seguenti descrivono in dettaglio la formulazione dell'elemento finito e le relazioni costitutive per il calcestruzzo e l'acciaio.

Validazioni ed analisi con il modello presentato nel seguente capitolo, sono tutt'ora in corso, in particolare si fanno svolgendo confronti tra i due modelli presentati nella tesi.

7.2 Finite element formulation

The finite element model under study is a two-dimensional beam formulated with the assumption of small displacements, but large displacements and therefore non-linear geometry can be considered and took into account in the transformation of the element response from the local to the global reference system, through the corotational formulation, as shown by Souza (2000) and Filippou and Fenves (2004).

7.2.1 Kinematic assumptions

The simplest beam theory including shear deformations in the structural response is the Timoshenko beam theory based on the following displacement field:

$$\begin{aligned} u_x(x, y) &= u(x) - y \cdot \theta(x) \\ u_y(x, y) &= w(x) \end{aligned} \quad (7.2.1)$$

Where $\theta(x)$ is the rotation of the normal to the undeformed x-axis, the normal to the section does not coincide with the axis of the deformed beam.

In a single field variational formulation, the nodal displacements are generally assumed as primary variables, and the interpolation functions of displacements are used to derive the overall response of the element. If instead, a functional approach based on a two or three fields is considered, in addition to the interpolation functions for displacements, are required interpolation functions for tension (2 fields) or tension and the deformations (3 fields). These elements are generally more accurate and numerically stable in the non-linear fields. The element presented is based on the latter approach, the element was derived from the three functional fields, also known as Hu-Washizu functional, in which was then introduced the kinematic assumption (7.2.1)

7.2.2 Hu-Washizu Functional

The mathematical formulation of the elastic element is based on the three fields, tension $\boldsymbol{\sigma}$, strain $\boldsymbol{\varepsilon}$ and displacement \mathbf{u} , and is represented by the following equation:

$$\Pi_{HW}(\boldsymbol{\sigma}, \boldsymbol{\varepsilon}, \mathbf{u}) = \int_{\Omega} W(\boldsymbol{\varepsilon}) d\Omega + \int_{\Omega} \boldsymbol{\sigma}^T [\boldsymbol{\varepsilon}^U - \boldsymbol{\varepsilon}] d\Omega + \Pi_{ext} \quad (7.2.2)$$

$W(\boldsymbol{\varepsilon})$ is the strain energy function from which stresses are derived by

$$\boldsymbol{\sigma}(\boldsymbol{\varepsilon}) = \frac{\partial W(\boldsymbol{\varepsilon})}{\partial \boldsymbol{\varepsilon}} \quad (7.2.3)$$

$\boldsymbol{\varepsilon}^U$ is the strain vector that is compatible with the displacements \mathbf{u} according to this equation:

$$\boldsymbol{\varepsilon} = \nabla^s \mathbf{u} \quad (7.2.4)$$

Under small strains it is equal to the symmetric part of the displacement gradient ∇^s . Π_{ext} is the energy associated with external forces, is expressed by the equation:

$$\Pi_{ext} = -\int_{\Omega} \mathbf{u}^T \mathbf{b} d\Omega - \int_{\Gamma_t} \mathbf{u}^T \mathbf{t}^* d\Gamma - \int_{\Gamma_u} \mathbf{t}^T [\mathbf{u} - \mathbf{u}^*] d\Gamma \quad (7.2.5)$$

Where $\mathbf{t} = \boldsymbol{\sigma} \cdot \mathbf{n}$ and \mathbf{n} is the normal to the boundary, * superscript denotes the imposed values of variables. It is assumed that the external loading is conservative so that the work depends only on the final displacement values \mathbf{u} . Ω is the domain of the free body which are associated volume forces, while $\Gamma_t \Gamma_u$ are the loaded and bounded surfaces respectively to which are associated surface forces or imposed displacements.

The formulation of the beam obtained using a three-field functional, allows for the independent specification of the strains $\boldsymbol{\varepsilon}$ from the displacements \mathbf{u} . This allow the selection of section kinematic independent from beam kinematics. Introducing the beam kinematic described in equation (7.2.1) in equation (7.2.4) the following equation can be written:

$$\begin{aligned} \varepsilon_{xx}^u &= \frac{du_x(x, y)}{dx} = u'(x) - y \cdot \theta'(x) \\ \gamma_{xy}^u &= \frac{du_x(x, y)}{dy} + \frac{du_y(x, y)}{dx} = -\theta(x) + w'(x) \end{aligned} \quad (7.2.6)$$

The section strain field is taken in accordance with the following relation.

$$\boldsymbol{\varepsilon} = \begin{Bmatrix} \varepsilon_{xx} \\ \gamma_{xy} \end{Bmatrix} = \begin{Bmatrix} \varepsilon_a(x) - y\kappa(x) \\ \phi(y, z)\gamma(x) \end{Bmatrix} \quad (7.2.7)$$

Where $\varepsilon_a(x)$ is the axial deformation along the x-axis, $\kappa(x)$ is the curvature and $\gamma(x)$ is the section shear strain. In this model can be introduced a non uniform shear strain of the section through the function $\phi(y, z)$. In this function was introduced a simplification, considering it a function of y only, instead y and z $\phi(y, z) \equiv \phi(y)$.

Writing the functional (7.2.2) for the beam, the following can be written:

$$\delta\Pi_{HW} = \int_{\Omega} \hat{\boldsymbol{\sigma}}(\boldsymbol{\varepsilon})\delta\boldsymbol{\varepsilon}d\Omega + \int_{\Omega} \delta\boldsymbol{\sigma}^T [\boldsymbol{\varepsilon}^u - \boldsymbol{\varepsilon}]d\Omega + \int_{\Omega} \boldsymbol{\sigma}^T [\delta\boldsymbol{\varepsilon}^u - \delta\boldsymbol{\varepsilon}]d\Omega + \delta\Pi_{ext} \quad (7.2.8)$$

substituting (7.2.6) and (7.2.7) in (7.2.8) results:

$$\begin{aligned} \delta\Pi_{HW} = & \int_{\Omega} \left\{ \hat{\sigma}_{xx} (\delta\varepsilon_a(x) - y\delta\kappa(x)) + \hat{\sigma}_{xy} (\phi(y)\delta\gamma(x)) \right\} d\Omega + \\ & \int_{\Omega} \left\{ \delta\sigma_{xx} [(u'(x) - \varepsilon_a(x)) - y(\theta'(x) - \kappa(x))] \right\} d\Omega + \\ & \int_{\Omega} \left\{ \delta\sigma_{xx} [w'(x) - \theta(x) - \phi(y)\gamma(x)] \right\} d\Omega + \\ & \int_{\Omega} \left\{ \sigma_{xx} [(\delta u'(x) - \delta\varepsilon_a(x)) - y(\delta\theta'(x) - \delta\kappa(x))] \right\} d\Omega + \\ & \int_{\Omega} \left\{ \sigma_{xx} [\delta w'(x) - \delta\theta(x) - \phi(y)\delta\gamma(x)] \right\} d\Omega + \delta\Pi_{ext} \end{aligned} \quad (7.2.9)$$

Section forces are defined as follow:

$$\begin{aligned} N = \int_A \sigma_{xx} dA \quad M = \int_A -y\sigma_{xx} dA \quad V = \int_A \sigma_{xy} dA \\ \text{and} \quad V = \int_A \phi(y)\sigma_{xy} dA \end{aligned} \quad (7.2.10)$$

Where N is the axial force, M is the bending moment, V is the shear force and V* that is work conjugate with the shear strain field $\phi(y, z)\gamma(x)$ of the equation (7.2.7). From equations (7.2.10), the equation (7.2.9) become:

$$\begin{aligned} \delta\Pi_{HW} = & \int_0^l \left\{ \delta\varepsilon_a(x) (\hat{N} - N) + \delta\kappa(x) (\hat{M} - M) + \delta\gamma(x) (\hat{V}^* - V^*) \right\} dx + \\ & + \int_0^l \left\{ \delta N (u'(x) - \varepsilon_a(x)) + \delta M (\theta'(x) - \kappa(x)) + \delta V (w'(x) - \theta(x)) - \delta V^* \gamma(x) \right\} dx + \\ & + \int_0^l \left\{ \delta u'(x) N + \delta\theta'(x) M + (\delta w'(x) - \delta\theta(x)) V \right\} dx + \Pi_{ext} \end{aligned} \quad (7.2.11)$$

Where

$$\begin{aligned} \hat{N} = \int_A \hat{\sigma}_{xx} dA \quad \hat{M} = \int_A -y\hat{\sigma}_{xx} dA \quad \hat{V} = \int_A \hat{\sigma}_{xy} dA \\ \text{and} \quad \hat{V} = \int_A \phi(y)\hat{\sigma}_{xy} dA \end{aligned} \quad (7.2.12)$$

The potential energy of the external loads can be written as follow:

$$\delta\Pi_{ext} = - \int_0^l \left\{ \bar{n}(x)\delta u(x) + \bar{q}(x)\delta w(x) + \bar{m}(x)\delta\theta(x) \right\} dx \quad (7.2.13)$$

Whose quantity are represented in the following figure fig.7.2-1:

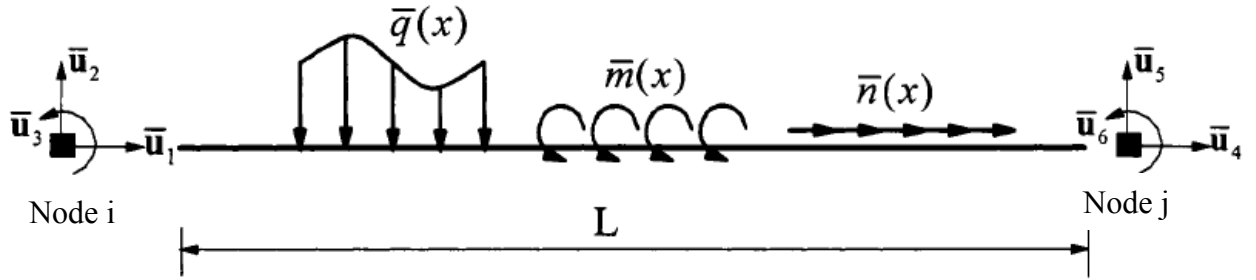


fig.7.2-1

The integration by parts of all terms with derivatives in the displacement fields in yields :

$$\int_0^l \{ \delta N u'(x) + \delta u'(x) N - \delta u(x) \bar{n}(x) \} dx = \{ \delta N u(x) + \delta u(x) N \} \Big|_0^l - \int_0^l \{ \delta N' u(x) + \delta u(x) (N + \bar{n}(x)) \} dx \quad (7.2.14)$$

$$\int_0^l \{ \delta M \theta'(x) + \delta \theta'(x) M - \delta V \theta(x) - \delta \theta(x) V \} dx = \{ \delta M \theta(x) + \delta \theta M \} \Big|_0^l - \int_0^l \{ (\delta M' + \delta V) \theta(x) + \delta \theta(x) (M' + V) \} dx \quad (7.2.15)$$

$$\int_0^l \{ \delta V w'(x) + \delta w'(x) V - \bar{q}(x) \delta w(x) \} dx = \{ \delta V w(x) + \delta w(x) V \} \Big|_0^l - \int_0^l \{ \delta V' w(x) + \delta w(x) (V' + \bar{q}(x)) \} dx \quad (7.2.16)$$

Considerate valide le seguenti equazioni di equilibrio:

$$\begin{aligned} N' + \bar{n}(x) &= 0 & M' + V &= 0 & V' + \bar{q}(x) &= 0 \\ \delta N' &= 0 & \delta M' + \delta V &= 0 & \delta V' &= 0 \end{aligned} \quad (7.2.17)$$

the integral terms on the right hand side of Equations (7.2.14), (7.2.15), (7.2.16) are zero, overcoming the need for displacement approximations u , w and θ along the beam. Consequently only the nodal displacement are necessary in the formulation.

7.2.3 Force interpolation matrix

Assuming $\bar{n}(x) = w_x$, $\bar{q}(x) = w_y$ constant along the beam length, from the simple supported beam scheme represented in figure fig. 7.2-2:

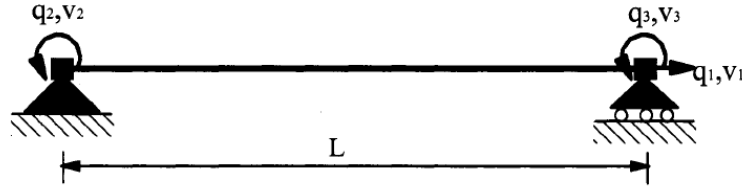


fig. 7.2-2

The following equation can be written:

$$\mathbf{s}(x) = \mathbf{b}(x)\mathbf{q} + \mathbf{s}_p(x) \quad (7.2.18)$$

Where:

$$\mathbf{s}(x) = \begin{pmatrix} N(x) \\ M(x) \\ V(x) \end{pmatrix}, \quad \mathbf{q} = \begin{pmatrix} q_1 \\ q_2 \\ q_3 \end{pmatrix} \quad (7.2.19)$$

While $\mathbf{b}(x)$ is the force interpolation function and \mathbf{s}_p represents the section stress resultants under the element loading w .

$$\mathbf{b}(x) = \begin{bmatrix} 1 & 0 & 0 \\ 0 & x/L - 1 & x/L - 1 \\ 0 & -1/L & -1/L \end{bmatrix} \quad (7.2.20)$$

$$\mathbf{s}_p(x) = \begin{bmatrix} L(1-x/L) & 0 \\ 0 & \frac{1}{2}L^2((x/L)^2 - x/L) \\ 0 & \frac{1}{2}L(1-2x/L) \end{bmatrix} \begin{pmatrix} w_x \\ w_y \end{pmatrix} \quad (7.2.21)$$

The variation of the equation (7.2.18) is:

$$\delta\mathbf{s}(x) = \mathbf{b}(x)\delta\mathbf{q} \quad (7.2.22)$$

7.2.4 Description of the shear forces

At this point it is necessary to introduce a relation between the shear forces V that satisfy the equilibrium equations (7.2.17) and the shear forces V^* described previously.

To find a relationship between V and V^* , it is assumed the hypothesis of linear elastic material, for which the following equation can be written:

$$\begin{aligned} V &= \int_A \sigma_{xy} dA = \int_A \phi(y)(G\gamma(x))dA \\ V^* &= \int_A \phi(y)\sigma_{xy} dA = \int_A \phi(y)^2(G\gamma(x))dA \end{aligned} \quad (7.2.23)$$

Therefore, this relationship can be expressed as follows:

$$V^* = \beta V \quad \text{in cui} \quad \beta = \frac{\int_A \phi(y)^2 dA}{\int_A \phi(y) dA} \quad (7.2.24)$$

Substituting (7.2.24) in the functional, combining the parameter β with the deformation $\gamma(x)$, modified deformation can be founded as follow:

$$\bar{\gamma}(x) = \beta \cdot \gamma(x) \quad (7.2.25)$$

In the functional the this equation can be written:

$$\delta\gamma(x)\hat{V}^* = \delta\bar{\gamma}(x)\hat{V} \quad (7.2.26)$$

therefore:

$$\hat{V} = \int_A \psi(y)\sigma_{xy} dA \quad \text{in cui} \quad \psi(y) = \frac{\phi(y)}{\beta} \quad (7.2.27)$$

7.2.5 Section deformation and stiffness matrix

The kinematics of the section is described by the following equation:

$$\boldsymbol{\varepsilon} = \begin{pmatrix} \varepsilon_{xx} \\ \gamma_{xy} \end{pmatrix} = \mathbf{a}_s \cdot \mathbf{e} = \begin{bmatrix} 1 & -y & 0 \\ 0 & 0 & \psi(y) \end{bmatrix} \cdot \begin{bmatrix} \varepsilon_a(x) \\ \kappa(x) \\ \bar{\gamma}(x) \end{bmatrix} \quad (7.2.28)$$

The section forces can be expressed by the following equations:

$$\hat{\mathbf{s}} = \begin{pmatrix} \hat{N} \\ \hat{M} \\ \hat{V} \end{pmatrix} = \begin{pmatrix} \int_A \hat{\sigma}_{xx} dA \\ \int_A -y\hat{\sigma}_{xx} dA \\ \int_A \psi(y)\hat{\sigma}_{xy} dA \end{pmatrix} = \int_A \begin{bmatrix} 1 & 0 \\ -y & 0 \\ 0 & \psi(y) \end{bmatrix} \cdot \begin{bmatrix} \hat{\sigma}_{xx} \\ \hat{\sigma}_{xy} \end{bmatrix} dA \quad (7.2.29)$$

The derivative of section forces, with respect to the section deformations defined in results in the section tangent stiffness matrix

$$\mathbf{k}_s = \frac{\delta \hat{\mathbf{s}}}{\delta \mathbf{e}} = \int_A \mathbf{a}_s^T \frac{\delta \hat{\boldsymbol{\sigma}}(\boldsymbol{\varepsilon})}{\delta \mathbf{e}} dA = \int_A \mathbf{a}_s^T \mathbf{k}_m \mathbf{a} dA \quad (7.2.30)$$

Where \mathbf{k}_m is the tangent modulus, defined as $\mathbf{k}_m = \frac{\delta \hat{\boldsymbol{\sigma}}(\boldsymbol{\varepsilon})}{\delta \boldsymbol{\varepsilon}}$

Considering a fibre discretization of the section, the section stiffness matrix can be obtained by the following summation.

$$\mathbf{k}_s = \sum_{i=1}^n \begin{bmatrix} k_{aa,i} & -y \cdot k_{aa,i} & \psi(y_i) k_{sa,i} \\ -y \cdot k_{aa,i} & y_i^2 k_{aa,i} & -y_i \psi(y_i) k_{sa,i} \\ \psi(y_i) k_{sa,i} & -y_i \psi(y_i) k_{sa,i} & \psi(y_i)^2 k_{ss,i} \end{bmatrix} \cdot A_i \quad (7.2.31)$$

where n is the number of fibre of the section.

Once known the section stiffness matrix, the element stiffness matrix is obtained by integration, than the structural stiffness matrix is assembled by classical method.

7.3 Constitutive relationships.

The finite element described in the formulation can be used to simulate concrete and steel structures. To catch the flexure-shear coupling, a multi axial bond must be used, at least a bidimensional relationship. For steel structures has been implemented a classical plasticity model, while for concrete a three-dimensional approach based on the damage model, proposed by Lee and Fenves (1998), is used. To adjust a three-dimensional model in a beam element has been introduced a static condensation. This procedure is carried out considering the stirrups as a translational constraint, or introducing the hypothesis of a plane stress state if stirrups are not present.

7.3.1 Steel material model

To model steel structures, was used a general J2 plasticity model as a constitutive relationship, presented by Lubliner et al. (1993) improved by Auricchio and Taylor (1995). This model, compared to the classical Prandtl-Reuss J2, has the advantage of considering the material hardening through the expansion of the yield surface.

In this plasticity model are defined two type of function, one limit function \tilde{F} and one yield function F , the latter is the same function as that used in classical plasticity theory.

The function \tilde{F} distinguishes between admissible and inadmissible states, and provides a smooth transition between elastic and inelastic states. This behaviour is much more realistic for metallic materials. Graphically, this kind of model can be represented by the following figure in case of uniaxial material.

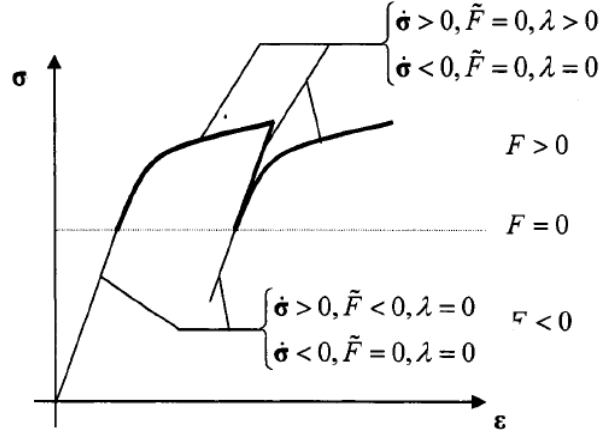


fig. 7.3-1

The function F is classically defined as:

$$F = \sqrt{J_2} - k \quad (7.2.32)$$

Where J_2 is defined as the second invariant of the deviatoric stress tensor while \tilde{F} is defined as follow:

$$\tilde{F} = h(F) \cdot \left(\frac{\delta F}{\delta \sigma} : \dot{\sigma} \right) - \lambda \quad (7.2.33)$$

where λ is called consistency parameter and must satisfies the following loading/unloading conditions:

$$\lambda \geq 0, F \leq 0 \quad e \quad \lambda F = 0 \quad (7.2.34)$$

$h(F)$ is defined as follow:

$$h(F) = \frac{F}{\delta(\varphi - F) + H\varphi}; \quad H = H_i + H_k \quad (7.2.35)$$

where φ is the distance between the current and the asymptotic radius of the yield function and δ is the rate of approaching the asymptote. Booth are the constants that define the connection between the curves.

H_i is the isotropic hardening modulus and H_k is the kinematics hardening modulus.

For further information about this plasticity model of can be found in Lubliner et al. (1993) Auricchio and Taylor (1995).

7.3.2 Concrete material model

Concrete has shown the stress-strain behavior of a plastic material as well as that of a material with damage. For this reason several models proposed to combine the two theories. Lubliner et al. (1989) developed a plastic-damage model that is easier to calibrate with experimental data. However, Lee and Fenves (1994) show that the relation between the degradation variables and the plastic strain lead to a complex and unstable algorithm.

Lee and Fenves (1998) developed a plastic-damage model with two damage variables, one for a tensile and one for a compressive damage state, and modified the yield function of the Barcelona model to include the two damage variables. Lee and Fenves (1998) plastic-damage model is the basis on which the concrete constitutive relationship is developed.

This choice arises from the fact that the concrete has the behavior of a plastic material although it is certainly subjected to cyclic damage. Compared to the model presented in Lee and Fenves's articles, the derivation of the tangent modulus of the material has been changed. In the following will be briefly explained the damage model used.

According to the plasticity theory, the strain tensor can be divided into two parts, one elastic and one plastic, as follow:

$$\bar{\boldsymbol{\sigma}} = \mathbf{C}_0 (\boldsymbol{\varepsilon} - \boldsymbol{\varepsilon}^p) \quad (7.2.36)$$

\mathbf{C}_0 is the initial elastic stiffness. The plastic strain rate is determined with a flow rule in connection with a plastic potential function Φ according to this relation:

$$\dot{\boldsymbol{\varepsilon}}^p = \dot{\lambda} \frac{\partial \Phi(\bar{\boldsymbol{\sigma}})}{\partial \bar{\boldsymbol{\sigma}}} \quad (7.2.37)$$

In the original Lee and Fenves (1998) model a single internal damage variable $\boldsymbol{\kappa}$ is introduced, which is assumed to satisfy the following damage evolution rule

$$\dot{\boldsymbol{\kappa}} = \dot{\lambda} \mathbf{H}(\bar{\boldsymbol{\sigma}}, \boldsymbol{\kappa}) \quad (7.2.38)$$

Lubliner et al. (1989) use a single damage variable, this variable is a combination of tensile and compressive damage variables. This assumption is accurate only for monotonic

loading. Lee and Fenves introduce two damage variables, one for compression and the other for tensile state. This hypothesis makes the behavior more realistic in the case of cyclic loading. The damage variables are taken as follow:

$$\boldsymbol{\kappa} = \begin{Bmatrix} \kappa_t \\ \kappa_c \end{Bmatrix} \quad (7.2.39)$$

Tensile and compression strength are functions of the damage parameters:

$$f_t = f_t(\kappa_t), \quad f_c = f_c(\kappa_c) \quad (7.2.40)$$

According to the classical damage mechanics this relation can be written:

$$\bar{\boldsymbol{\sigma}} = \frac{\boldsymbol{\sigma}}{1-D} \quad (7.2.41)$$

Where $\bar{\boldsymbol{\sigma}}$ represent the effective stress and D is a positive scalar parameter, that can assume values between 0 (undamaged material) ad 1 (broken material). From the definition the following equation can be deduced:

$$f_t = [1 - D_t(\kappa_t)] \bar{f}_t(\kappa_t), \quad f_c = [1 - D_c(\kappa_c)] \bar{f}_c(\kappa_c) \quad (7.2.42)$$

where $0 \leq D_t(\kappa_t) \leq 1$, $0 \leq D_c(\kappa_c) \leq 1$. A single damage parameter can be derived by the two parameters above:

$$D = D(\boldsymbol{\kappa}) = 1 - (1 - D_t)(1 - D_c) \quad (7.2.43)$$

The limit surfaces proposed initially by Lubliner and subsequently modified by Lee and Fenves is effective for every type of loading, as shown in numerous analysis, except for an hydrostatic loading, for which the problem of never reach the crisis.

The limit surface concerned is represented by the following equation:

$$F(\boldsymbol{\sigma}) = \frac{1}{1-\alpha} \left(\alpha I_1 + \sqrt{3J_2} + \beta \langle \hat{\sigma}_{\max} \rangle \right) - c_c \quad (7.2.44)$$

Where $\hat{\sigma}_{\max}$ is the algebraically largest principal stress, I_1 is the first invariant of the hydrostatic stress tensor and J_2 is the second invariant of the deviatoric stress tensor, α is a dimensionless parameter, expressed in terms of the initial uniaxial compressive yield stress f_{c0} and the initial biaxial compressive yield stress f_{b0} , according to:

$$\alpha = \frac{f_{b0} - f_{c0}}{2f_{b0} - f_{c0}} \quad (7.2.45)$$

β is the Barcellona constant, which is found in the homonymous model (Lublimer (1989)). Lee and Fenves have changed the parameter β as follows:

$$\beta = \beta(\mathbf{\kappa}) = \frac{C_c(\mathbf{\kappa})}{C_t(\mathbf{\kappa})}(\alpha - 1)(1 + \alpha) \quad (7.2.46)$$

Where $C_c = -\bar{f}_c(\mathbf{\kappa}_c)$, $C_t = \bar{f}_t(\mathbf{\kappa}_t)$ are cohesion values in tension and compression, respectively.

An important aspect to consider is the static condensation of the stiffness matrix, obtained for a three-dimensional material, on a beam column element. To this end, the constraints have been imposed considering the effect of shear reinforcement (stirrups), according to the following equilibrium equation:

$$\mathbf{R} = \begin{Bmatrix} R_y \\ R_z \end{Bmatrix} = \begin{Bmatrix} \sigma_{yy} + \rho_y f_y \\ \sigma_{zz} + \rho_z f_z \end{Bmatrix} = \begin{Bmatrix} 0 \\ 0 \end{Bmatrix} \quad (7.2.47)$$

Where, without shear reinforcement $\rho_y = \rho_z = 0$ the equation (7.2.47) returns the case of plane stress state condition. Linearizing (7.2.47) with respect to an initial strain $\boldsymbol{\varepsilon}_0$ in the y direction gives:

$$\begin{aligned} & \sigma_{yy}(\boldsymbol{\varepsilon}_0) + \rho_y f_y(\boldsymbol{\varepsilon}_{y,0}) + \frac{\partial \sigma_{yy}}{\partial \varepsilon_{xx}} \Delta \varepsilon_{xx} + \frac{\partial \sigma_{yy}}{\partial \varepsilon_{yy}} \Delta \varepsilon_{yy} + \frac{\partial \sigma_{yy}}{\partial \varepsilon_{zz}} \Delta \varepsilon_{zz} + \\ & + \frac{\partial \sigma_{yy}}{\partial \gamma_{xy}} \Delta \gamma_{xy} + \frac{\partial \sigma_{yy}}{\partial \gamma_{yz}} \Delta \gamma_{yz} + \frac{\partial \sigma_{yy}}{\partial \gamma_{xz}} \Delta \gamma_{xz} + \rho_y \frac{\partial f_y}{\partial \varepsilon_{yy}} \Delta \varepsilon_{yy} = 0 \end{aligned} \quad (7.2.48)$$

In z direction similarly:

$$\begin{aligned} & \sigma_{zz}(\boldsymbol{\varepsilon}_0) + \rho_z f_z(\boldsymbol{\varepsilon}_{z,0}) + \frac{\partial \sigma_{zz}}{\partial \varepsilon_{xx}} \Delta \varepsilon_{xx} + \frac{\partial \sigma_{zz}}{\partial \varepsilon_{yy}} \Delta \varepsilon_{yy} + \frac{\partial \sigma_{zz}}{\partial \varepsilon_{zz}} \Delta \varepsilon_{zz} + \\ & + \frac{\partial \sigma_{zz}}{\partial \gamma_{xy}} \Delta \gamma_{xy} + \frac{\partial \sigma_{zz}}{\partial \gamma_{yz}} \Delta \gamma_{yz} + \frac{\partial \sigma_{zz}}{\partial \gamma_{xz}} \Delta \gamma_{xz} + \rho_z \frac{\partial f_z}{\partial \varepsilon_{zz}} \Delta \varepsilon_{zz} = 0 \end{aligned} \quad (7.2.49)$$

In writing the linearized equations, it was considered that for a planar beam, the shear deformations are zero $\gamma_{yz} = 0$, $\gamma_{xz} = 0$ as well as their increments $\Delta \gamma_{yz} = 0$, $\Delta \gamma_{xz} = 0$.

The equations (7.2.48) and (7.2.49) can be written in matrix form as follow:

$$\begin{bmatrix} C_{yyyy} + \rho_y E_y & C_{yyzz} \\ C_{zzyy} & C_{zzzz} + \rho_z E_z \end{bmatrix} \begin{Bmatrix} \Delta \varepsilon_{yy} \\ \Delta \varepsilon_{zz} \end{Bmatrix} = - \begin{Bmatrix} R_{y,0} \\ R_{z,0} \end{Bmatrix} - \begin{bmatrix} C_{yyxx} & C_{yyxy} & C_{yyxz} \\ C_{zzxx} & C_{zzxy} & C_{zzxz} \end{bmatrix} \begin{Bmatrix} \Delta \varepsilon_{xx} \\ \Delta \gamma_{xy} \\ \Delta \gamma_{xz} \end{Bmatrix} \quad (7.2.50)$$

The incremental stress-strain relation, can be written separating the normal strains in the transverse direction:

$$\begin{bmatrix} \Delta\sigma_{xx} \\ \Delta\sigma_{xy} \\ \Delta\sigma_{xz} \end{bmatrix} = \begin{bmatrix} C_{xxxx} & C_{xxxy} & C_{xxxz} \\ C_{xyxx} & C_{xyxy} & C_{xyxz} \\ C_{xzxx} & C_{xzxy} & C_{xzzz} \end{bmatrix} \begin{Bmatrix} \Delta\varepsilon_{xx} \\ \Delta\gamma_{xy} \\ \Delta\gamma_{xz} \end{Bmatrix} + \begin{bmatrix} C_{xxyy} & C_{xxzz} \\ C_{xyyy} & C_{xyzz} \\ C_{xzyy} & C_{xzzz} \end{bmatrix} \begin{Bmatrix} \Delta\varepsilon_{yy} \\ \Delta\varepsilon_{zz} \end{Bmatrix} \quad (7.2.51)$$

substituting the (7.2.51) in (7.2.50) for the converged state $\mathbf{R}=\mathbf{0}$ (transverse equilibrium), the condensed material stiffness matrix can be obtained

$$\mathbf{k}_m = \begin{bmatrix} C_{xxxx} & C_{xxxy} & C_{xxxz} \\ C_{xyxx} & C_{xyxy} & C_{xyxz} \\ C_{xzxx} & C_{xzxy} & C_{xzzz} \end{bmatrix} - \begin{bmatrix} C_{xxyy} & C_{xxzz} \\ C_{xyyy} & C_{xyzz} \\ C_{xzyy} & C_{xzzz} \end{bmatrix} \left(\begin{bmatrix} C_{yyyy} + \rho_y E_y & C_{yyzz} \\ C_{zzyy} & C_{zzzz} + \rho_z E_z \end{bmatrix} \right)^{-1} \begin{bmatrix} C_{yyxx} & C_{yyxy} & C_{yyxz} \\ C_{zzxx} & C_{zzxy} & C_{zzxz} \end{bmatrix} \quad (7.2.52)$$

The same procedure can be used considering only two stress components σ_{xx} e σ_{xy} .

CONCLUSION

This thesis illustrates the attempt to introduce a model that can accurately reproduce the nonlinear behavior of structures where shear deformation is critical for the overall behaviour. In a fibre beam-column element based on flexibility formulation a constitutive relationship that allows to reproduce the nonlinear flexure-shear interaction was introduced for the purpose. Indeed in this category of elements there aren't still models, of proven accuracy, able to reproduce the squat structures behaviour. The main characteristics of the beam-column element are substantially two:

- The flexibility formulation, based on the two-fields mixed method
- The constitutive relationship based on the MCFT, in which a rotating smeared-crack bidimensional model is assumed for the concrete.

While the fibre model considered is based on the incremental load approach and tangent stiffness matrix, the modified compression field theory on which the constitutive relation is based, considers a total load approach and secant stiffness matrix for the iterations.

In particular was chosen to adapt the original MCFT to an algorithm based on the incremental load approach and the tangent stiffness matrix to take advantage of the more fast convergence resulting from this approach. The algorithm includes an element state determination, well established for flexibility based elements, and a new section state determination, with iterations at the fibre level for the determination of the stress and strains in concrete and steel according to the constitutive model.

The proposed model was implemented in an original computer code and then calibrated and validated through comparisons with available experimental results.

The verification regarded in particular some tests conducted by Osterle et al(1979) on RC walls for which the different contributions to the deflected shape due to flexure and shear were available. The results shown that The model was able to simulate accurately these contributions at different levels of excursion in the inelastic range. The results were carried out in terms of Pushover curve, moment-rotation, shear- shear deformation and deformed shape.

A further test was carried out through numerical comparisons with the computer program VecTor2, based on bi-dimensional finite elements and on MCFT constitutive law. The analysis was carried out on a shear wall fixed at the base and loaded by a force on top.

Although the two codes are based on two different types of finite elements, the results obtained in global terms, that is in terms of pushover curve are comparable. Even numerical comparisons have shown that the proposed model can be effectively used, in the monotonic loading, for the analysis of squat structures.

Various numerical analyses were then performed in order to study the influence of flexure-shear interaction. First of all a bridge pier with circular cross section was analyzed to investigate this kind of influence, the analyses were repeated changing the height of the pier and maintaining the same section diameter, in order to keep the slenderness as the control parameter of the analysis. Then a similar analysis was carried out on a shear wall in which the slenderness range was between one and ten. From these analyses it is evident the influence of the nonlinear shear deformation, especially for the elements characterized by a ratio of length to section dimension lower than 4. The observed variation along the element of the shear response, associated to the variation of bending moment, highlights the influence of flexure-shear interaction in the inelastic range and the capability of the model in reproducing this effect.

The implementation of the MCFT constitutive relationship in a fibre beam-column model seemed to be a proper solution for the simulation of shear dominated elements in the nonlinear range. The inclusion of shear response however involved a significant increase of the complexity of the algorithm of the fibre model. The presented applications of the model regard analyses in presence of monotonic loading. More research work is required at the date to extend the applications for cyclic loading.

As regards to the model studied in the University of California Berkeley has been reported the finite element formulation based on a three fields functional and the constitutive laws for concrete and steel structures. Between the two models presented are still in progress studies and comparisons, which will be reported in future papers.

With regard to the first model presented in this thesis, the following future developments can be highlighted:

- Implementation of a cyclic analysis, changing from a load control to a displacement control. This allows to capture effects such as softening, fundamental in nonlinear analysis of reinforced concrete structures

- Simplification of the constitutive relationship, with the aim of reducing the levels of iteration and therefore the computational time.
- The future extension of the model should account for a more accurate distribution of shear strains over the section, until now assumed constant.
- Finally The beam finite element model can be extended to include the interaction of axial force, biaxial bending moment, biaxial shear and torsion through the 3d coupling of normal and shear stresses. A warping function for torsion must be added to the kinematic assumptions.

As regard to the second model studied at University of California Berkeley, the following developments are underway:

- Numerical validation and comparisons between the two models, first in monotonic than in cyclic loading
- Implementation of Biaxial constitutive relationship as Modified Compression Field theory, in the Timoshenko beam element formulated on three-field Hu-Washizu variational.

REFERENCES

- Bairan, J.M. (2005). "A Nonlinear Coupled Model for the Analysis of Reinforced Concrete Sections Under Bending, Shear, Torsion and Axial Forces.", *Ph.D. thesis*, Technical University of California, Barcelona, Spain.
- Banon, H., Biggs, J. e Irvine, M.(1981). "Seismic Damage in Reinforced Concrete Frames". *Journal of Structural Engineering*, ASCE, 107(ST9), p.p. 1713-1729.
- Bentz, E.C. (2000). "Sectional Analysis of Reinforced Concrete Member.", *Ph.D. thesis*, Technical University of Toronto, Canada.
- Brancaleoni, F., Ciampi, V. e Di Antonio, R (1983). "Rate Type Models for Nonlinear Hysteretic Structural Behaviour." *EUROMECH Colloquium*, Palermo Italia
- Ceresa P., Petrini L., Pinho R. (2007). "Flexure-shear fibre beam-column elements for modelling frame structures under seismic loading - state of the art." *Journal of Earthquake Engineering*, Vol. 11, Special Issue 1.
- Ceresa P., Petrini L., Pinho R. e Auricchio F.(2007). " Development of a Flexure-Shear Fibre Beam-Column Elements for Modelling of Frame Structures Under Seismic Loading." *First European Conference on Earthquake Engineering and Seismology*, Geneva, Switzerland 2006, paper number 1425
- Cervenka, V. (1985). "Constitutive Models for Cracked Reinforced Concrete." *ACI journal*, 82(6),877-882.
- Cloug , R. e Benuska, L. (1966). "Nonlinear Earthquake Behaviour of Tall Buildings." *Journal of Mechanical Engineering*, ASCE, 93(EM3), 129-146.
- Clough, R. and Johnston, (1967). "Effect of Stiffness Degradation on Earthquake Ductility Requirements." *Transactions of Japan Earthquake Engineering Symposium*, Tokyo, p.p. 195-198.
-

- Crisfield, M.A. (1986). “Snap-Through and Snap-Back response in concrete structure and the danger of under-interaction”, *International Journal of Numerical Methods in Engineering*, 22, 751-767.
- Darvall, L.P. e Mendis, P. (1985). “Elastic-Plastic- Softening Analysis of Plane Frames”, *Journal of Structural Engineering*, ASCE, 11 (STA4), 871-888.
- Filippou, F.C. e Issa, A. (1988). “Nonlinear Analysis of Reinforced Concrete Frames under Cyclic Load Reversal”, *EERC Report 83-19, Earthquake Engineering. Research Centre*, Berkeley.
- Taucer F.F. , Spacone E. e Filippou F.C., (1991). “A Fiber Beam-Column Element for Seismic Response Analysis of Reinforced Concrete Structures”, *EERC Report 91-17, Earthquake Engineering Research Centre*, Berkeley.
- Spacone, E. e Taucer, F.F., Filippou, F.C. (1996). “A Fiber Beam-Column Model for Nonlinear Analysis of R/C Frames: Part.1 Formulation” *Earthquake Engineering and Structural Dynamics* 25, 711-725
- Giberson, M. (1967). “The Response of Nonlinear Multi-Story Structures Subjected to Earthquake Excitation”. *Earthquake Engineering Research Laboratory*, Pasadena.
- Guedes, J. e Pinto, A.V. (1997). “A Numerical Models for Shear Dominates Bridges Piers”, *Proceedings of the Second Italy-Japan Workshop on Seismic Design and Retrofit of Bridges*, Rome, Italy.
- Guedes , J., Pegon, P. e Pinto, A.V.(1994-1997). “A Fiber-Timoshenko Beam Element in CASTEM 2000”, *Special publication Nr. 1.94.31 Applied Mechanics Unit*, Safety Technology Institute, Commission of European Communities, Joint Research Centre, Ispra Establishment, Italy

References

- Guner S, Vecchio FJ. Pushover Analysis of Shear-Critical Frames: Formulation. *ACI Structural Journal* 2010; 107: 63-71.
- Lai, S. Will, G. e Otani, S. (1984). “Model for Inelastic Biaxial Bending of Concrete Members”. *Journal of Structural Engineering*, ASCE, 110(ST11), 2563-2584.
- Mander, J.B., Priestley, M.J.N. e Park, R. (1988). “Theoretical Stress-Strain Model for Confined Concrete”. *Journal of Structural Engineering*, ASCE, 114(ST8), 1804-1826.
- Martinelli, L. (1998-2002) “Modellazione di Pile da Ponte in C.A. a travata soggetti ad eccitazione sismica”, Phd. thesis, Dipartimento di Ingegneria Strutturale, Politecnico di Milano, Milano, Italy
- Mazars, J. Kotronis, P., Ragueneu, F. e Casaux, G. et al. (2006). “Using Multifiber Beams to Account for Shear and Torsion. Application to Concrete Structural Element”, *Computer Methods in Applied Mechanics and Engineering* 195(52), 7264-7281.
- Meyer, C., Roufaiel, M.S. and Arzoumanidis, S.G.(1983). “Analysis of Damaged Concrete Frames for Cyclic Loads”, *Earthquake Engineering and Structural Dynamics*, vol.11, 207- 228.
- Meyer, C., Roufaiel, M.S. (1987). “Analytical Modelling of Hysteretic Behaviour of R/C Frames”, *Journal of Structural Engineering*, ASCE, 113(ST3), 429-444.
- Otani, S. (1974). “Inelastic Analysis of R/C Frame Structure”, *Journal of the Structural Division*, ACSE, 100(ST7).
- Oesterle G, Fiorato AE, Johal LS, Carpenter JE, Russell HG,(1974) Corley WG. Earthquake resistant structural walls – Tests of isolated walls. Report to National Science Foundation, 1976, Submitted by Research and Construction Technology Laboratories, Portland Cement Association, Illinois.

- Petrangeli, M, Pinto, P. e Ciampi, V.(1996,1999). “Fiber Element for Cyclic Bending and Shear of R/C Structures. I: theory”, *Journal of Engineering and Mechanics* 125(9), 994,1001.
- Ranzo, G. e Petrangeli, M. (1998). “A Fiber Beam Element with Section Shear Modelling for Seismic Analysis of R/C Structures “, *Journal of Earthquake Engineering* 2, 443-473
- Remino, M. (2004). “Shear Modelling of Reinforced Concrete Structures”, Phd. Thesis, Dipartimento di Ingegneria civile, Università degli studi di Brescia, Brescia, Italia.
- Rose, B.W. (2001). “A Constitutive Model for the Analysis of reinforced concrete beams-columns subjected to lateral loads”, Phd. Thesis, CEAE Dept., University of Colorado, Boulder, Colorado.
- Saiidi M., Sozen M. A. (1981) “Simple Nonlinear Seismic Analysis of R/C Structures”, *Journal of the Structural Division, ASCE*, 107 (ST5)
- Saritas A, Filippou FC. (2009) “Inelastic axial-flexure–shear coupling in a mixed formulation beam finite element.” *International Journal of Non-Linear Mechanics*; 44: 913-922.
- Selby, R.G., Vecchio, F.J. (1991). “Towards Compression-Field Analysis of Reinforced Concrete Solids” *Journal of Structural Engineering, ASCE*, 117(6), 1740-1758.
- Soleimani, D., Popov, E.P. e Bertero, V.V. (1979). “Nonlinear Beam Model for R/C Frame Analysis”, *7th ASCEE Conference of Electronic Computation*, St. Louis.
- Takayanagi, T. e Schnobrich, W. (1979) . “Nonlinear Analysis of Coupled Wall Systems”, *Earthquake Engineering and Structural Dynamics*, vol.7, 1-22.

References

- Takeda, T., Sozen, M.A. e Nilsen, N. (1970). “Reinforced Concrete Response to Simulated Earthquakes”, *Journal of Structural Engineering*, ASCE, 96(ST12), 2557-2573.
- Takizawa, H. e Aoyama, H. (1976). “Biaxial Effects in Modelling Earthquake Response of R/C Structure”, *Trans. of Arch. Inst. of Japan* , 240, Part.1 in Feb. 1976, pp. 51-62, Part. 2 in March 1976, pp. 65-77.
- Vecchio, F.J., Collins, M.P. (1986). “ The Modified Compression Field Theory for Reinforced Concrete Element Subjected to Shear”, *Journal of American Concrete Intitute*, 83(2), 219-231.
- Vecchio, F.J., Collins, M.P. (1988). “Predicting the Response of Reinforced Concrete Beams Subjected to Shear Using the Modified Compression Field Theory”, *ACI Structural Journal*, 85,258-268.
- Vecchio, F.J.(2000). “Disturbed Stress Field Model of Reinforced Concrete: Formulation”, *Journal of Structural Engineering*, ASCE, 126(9), 1070-1077.
- Vecchio, F.J.(2001). “Disturbed Stress Field Model of Reinforced Concrete: Implementation”, *Journal of Structural Engineering*, ASCE, 127 (1), 12-20.
- Walraven, J. C. (1981). “Fundamental analysis of aggregate interlock.” *Journal of Structural Engineering*, ASCE, 107(11), 2245–2270.
- Wong P, Vecchio FJ. (2003) VecTor2 and Formworks Manual. <http://www.civ.utoronto.ca/vector/>, .
- Zeris, C.A. e Mahin, S.A. (1988). “Analysis of Reinforced Concrete Beam-Column under uniaxial Excitation”, *Journal of Structural Engineering*, ASCE, 114(ST4), 804-820.

References

Zienkiewicz, O.C. e Taylor, R.L (1989). **The Finite Element Method**. Vol. I. Basic Formulation and Linear Problems. Fourth Edition, McGraw Hill, London.

Zienkiewicz, O.C. e Taylor, R.L (1989). **The Finite Element Method**. Vol. II. Solid and Fluid Mechanics, Dynamics and Non-Linearity. Fourth Edition, McGraw Hill, London.